A STUDY OF LIGHT CURVE VARIATIONS IN ECLIPSING CONTACT BINARY STARS

BY

ANALIZE JOOSTE

submitted in accordance with the requirements

for the degree of

MASTER OF SCIENCE (ASTRONOMY (98973))

in the subject of

ASTRONOMY

at the

UNIVERSITY OF SOUTH AFRICA

SUPERVISOR: Prof DP Smits

YEAR OF FINAL REGISTRATION: 2021

STUDENT NUMBER 0669-373-3

I declare that

A STUDY OF LIGHT CURVE VARIATIONS IN ECLIPSING CONTACT BINARY STARS

is my own work and that all the sources that I have used or quoted have been acknowledged by means of complete references.

I further declare that I submitted the dissertation to originality checking software and that it falls within the accepted requirements for originality.

I further declare that I have not previously submitted this work, or part of it, for examination at Unisa for another qualification or at any other higher education institution.

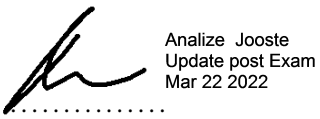

.....
Analize Jooste

.....
Date

Acknowledgements

It is appropriate that all Glory and Honour goes to God for such a wonderful creation and the ability to study such beauty and splendour.

I would also like to thank my supervisor Prof. D. P. Smits for his guidance, encouragement and support throughout the course of this study and through so many years, even post retirement. I am highly indebted and know I would not have achieved this submission without him.

To my family: Thank you for your love and support throughout my studies. I also dedicate this work to my special 4-legged friend, Rupert. Thank you for your love, patience and being at my side every step of the way until your untimely passing.

The Python routine was provided by Ms Patricia Skelton as well as assistance on how to use it, with lots of patience and guidance. Thanks for also being a good friend and know I miss you.

I also wish to thank Ms Andri Prozesky for her help when I got stuck in navigating around administrative processes and her encouragement throughout these.

Thanks are due to the following individuals:

- The anonymous referees for their comments on the paper by Jooste & Smits (2021).

I would like to thank the SuperWASP team for granting access to their database.

This research has made use of the ASAS database, SIMBAD database, operated at CDS, Strasbourg, France and the SAO/NASA Astrophysics Data Stream and B.R.N.O database.

Summary

The study of light curves of W UMa (W Ursa Majoris type) eclipsing contact binary stars can provide insight into their physical dimensions as well as their evolution. By making use of different data sets, including from the All Sky Automated Survey (ASAS) and the Wide Angle Search for Planets (SuperWASP), light curves were modelled to assess if there is a trend regarding their mass-ratios q and the inclination angles i of these systems in relation to the appearance of the light curves. A selection of stars were also subjected to period variation analysis and the results thereof presented. Period changes that are fore-casted with a degree of certainty are indicative of evolutionary changes in these systems. An area of future study is to analyse amongst others the underlying causes that contribute to the variations observed. To do so requires quality data spanning decades. Results of the analysis of the appearance of light curves with regards to secondary minima in relation to q and i are presented as well as improved periods for a selection of 14 stars by making use of SuperWASP data.

KEYWORDS: stars: binaries: eclipsing − stars: fundamental parameters − binaries: close − stars: contact − stars: variables: other − stars: individual: DY Cet; EE Cet; ER Ori; AH Aur; XY Leo; Y Sex; XX Sex; VY Sex; AM Leo; AP Leo; AG Vir; Ou Ser; VZ Lib; V2612 Oph.

Contents

Chapter 1

Introduction

There are many binary or even multiple star systems in the Universe. Depending on their nature, different methods of observation can be used to identify them. These stars are all gravitationally bound and orbit a common centre of mass (Shu, 1982; Bowers & Deeming, 1984; Percy, 2007).

There are binary stars that can be viewed as two separate stars, which are known as visual, or wide, binaries (Shu, 1982; Percy, 2007). Some binary stars show their nature through the "wobble" of their orbits which indicate the presence of a companion star that is not visible; these are called astrometric binary stars. Some systems can only be identified through spectroscopy and, depending on whether one or both stars' spectra are detected, these systems are classified as single-lined or double-lined spectroscopic binaries, respectively (Shu, 1982).

However, when the two companion stars' separations are too close to resolve them individually, then their double nature can be established through eclipses as observed from their light curve (Shu, 1982; Hilditch, 2001; Percy, 2007). The geometry of such systems impacts on the probability of these eclipses being detected (Percy, 2007). The likelihood of observing eclipses is especially high if their orbital inclination is almost aligned relative to the viewer's line-of-sight (Percy, 2007).

Of particular interest are eclipsing contact binary stars which share a convective envelope. These stars have both companions close to the main sequence of the Hertzprung-Russel (HR) diagram (Hilditch, 2001). The most common type of these contact binaries are the W UMa type stars that have spectral types between early A and late K. The prototype of this class of variable stars, W UMa, was discovered in 1903, and at the time had unique properties for a variable star. After much research on these stars with the advent of technological advancements, and the ever improving processing power of computers, physical models have evolved that can explain many of the observed features associated with their light curves (Wilson, 1994). However, there is still much that is not understood about W UMa stars, in particular, the evolutionary path that has led them to where they currently are, and what will happen to them in the future.

Data collected through automated sky surveys has led to the discovery of thousands of these systems, but many of them have yet to be studied in detail. Rucinski (1993) and Hambálek & Pribulla (2013) have pointed out that the shape of a light curve depends mainly on three parameters: the mass ratio q of the two components, the inclination angle i of the orbital plane to the observer's line-of-sight, and the degree of contact f between the two components. The mass ratio can be determined by detailed spectroscopic measurements but, as of yet, many of the W UMa systems have not been subjected to this level of investigation. Once the mass ratio has been determined it is possible to model the

parameters of these systems reliably using available software packages, such as Binary Maker 3.0 (BM3), PHysics of Eclipsing binariEs (PHOEBE) and the Wilson-Devinney code.

As mentioned previously, the evolution of W UMa systems is still open to much debate. One of the easily observed properties of these stars is the period of the system. The period can be accurately measured using relatively inexpensive telescopes equipped with photometers. The multitude of sky surveys that make their data available online these days provide a useful resource to determine their period. Of particular interest for studying the evolution of these systems is any changes that might be occurring in the periods of these binary stars. Period changes can indicate a loss of angular momentum, the redistribution of mass between the components, the presence of magnetic fields, or there could be a third component gravitationally bound to the binary system.

In this report, data from the All Sky Automated Survey (ASAS) and the Wide Angle Search for Planets (SuperWASP) online databases are used to investigate some of the properties of a sample of W UMa stars. Using the known parameters of the binary stars from the literature, models have been run to see how the light curves are affected as different parameters are varied. Then, using WASP data, the periods of the stars are determined to look for any changes that might be occurring.

The layout of the dissertation is as follows:

Chapter 2 describes how light curves can be used to categorize eclipsing binary stars, followed by a brief mathematical derivation of the Roche model and how it can be used to explain the light curve shapes in terms of a physical model. The common convective envelope model is described, and how this can be disrupted by the thermal relaxation model. The properties of W UMa, the prototype of the contact binaries discussed in this dissertation, are then described, followed by the general properties of the class as a whole.

Chapter 3 looks at the parameters that are required to model W UMa type stars, and the software package called Binary Maker 3.0 that has been used to simulate light curves. Details of the observational data and how they are collected end up this chapter.

Chapter 4 starts off by describing how the data from the All Sky Automated Survey are processed and how synthesized light curves are generated using this data. The parameters used for the modelling are based on a set of stars listed by Deb & Singh (2011) that are fitted to the All Sky data. Some of the parameters are then varied to see what changes occur in the light curves. Both quantitative and qualitative results of this analysis are detailed.

Chapter 5 makes use of data from the SuperWASP database. The analysis of these data is described, including how they are used to check up on the parameters from the Deb & Singh (2011) sample. These data contain many more points than the ASAS data and so they can be used to measure the periods of these stars very accurately. The types of period changes that could occur are discussed and the mechanisms that could produce these changes. The observed minus calculated, or O–C method, is described together with the programmes that have been used to perform this analysis.

Chapter 6 looks at the results obtained for 14 stars whose periods have been investigated using the O–C method.

Chapter 7 provides a summary of the key findings of these investigations, and the future outlook regarding these studies.

In this dissertation, the photometric convention is used of referring to the primary minimum as the deeper of the two photometric minima.

An appendix provides diagrams of the synthesized light curves that were used for the analysis in Chapter 4.

Chapter 2

Binary Stars

It is said that approximately 50% to 90% of the Local Group consists of binary stars (Dryomova & Svechnikov, 2006; Avvakumova & Malkov, 2014) with the term *binary star* being accredited to J. Herschel who first made use of it in 1802 (Hilditch, 2001).

In this chapter, methods of classifying close binary stars are discussed. Because the main focus of this work is contact binaries, a review of the prototype of contact eclipsing binaries, W Ursae Majoris (W UMa), is presented, followed by the general properties of the class of contact binaries as a whole. Processes that can lead to changes in the light curve are then presented.

2.1 Classification Methods for Eclipsing Binary Stars

The General Catalogue of Variable Stars (GCVS)[1] lists 18 categories of eclipsing binary systems. Some of the categories are not relevant to the contact binary stars discussed in this dissertation so the descriptions will be limited to categories of interest only.

The earliest method of classifying eclipsing binary stars was based on the shape of their light curves (Kopal, 1955; Percy, 2007). An alternative classification scheme that takes into account the physical attributes of the system makes use of the Roche model. The details of the Roche model are discussed in §2.1.2, and leads to binary stars being classified as detached, semi-detached or contact systems.

A colour-absolute magnitude or luminosity calibration was developed by Rucinski & Duerbeck (1997) using *Hipparcos* parallax data of 40 contact binary systems. The relation makes use of the colour index $(B-V)_0$ and the period P of the system to derive the absolute magnitude M_V as follows

$$M_V = -4.44 \log P + 3.02(B-V)_0 + 0.12 \, . \tag{2.1}$$

2.1.1 Light Curve Classification

According to Kopal (1955), it has been the practice to classify the stars into three categories based on the shape of their light curves. The prototypes for this classification scheme are the light curves of Algol, β Lyrae, and W Ursae Majoris; stellar systems with light curves similar to these prototypes are also referred to as types EA, EB and EW. Note that this classification scheme lacks physical

[1] https://http://www.sai.msu.su/gcvs/gcvs/

substantiation as it is based entirely on the shape of the light curve, and not on the underlying physical processes of the systems.

EA

The EA (Algol) type systems in the GCVS system have profiles with almost flat light curves between eclipses, the beginning and end of which can be clearly identified. Variability of the light curve may extend over several magnitudes from maxima to minima; secondary minima may not be present. Periods of EA systems vary from 0.2 d up to or even exceeding 10 000 d (GCVS, 2020).

A typical EA light curve is presented in Fig. 2.1. It is for the star RV Crt using ASAS data.

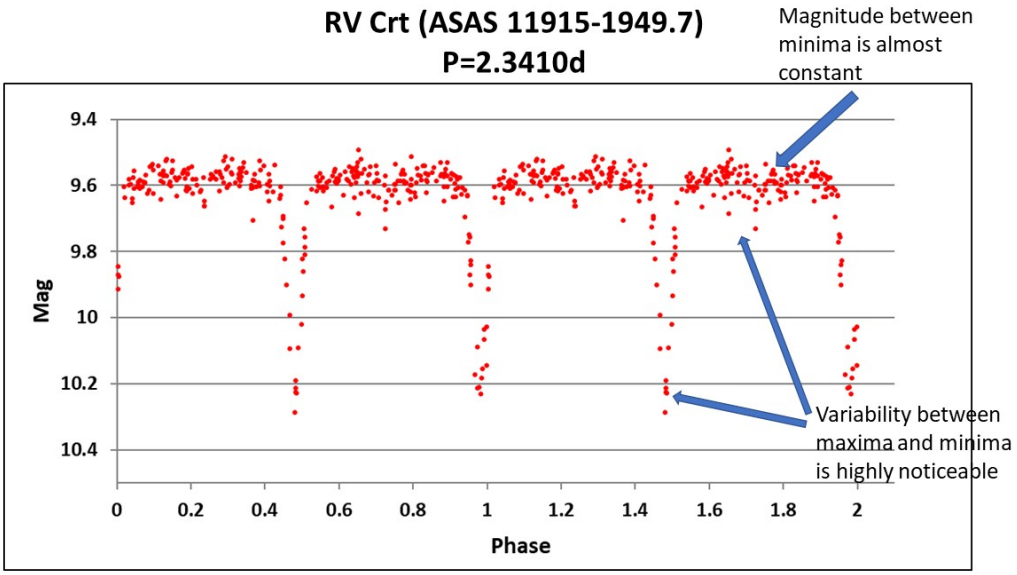

Figure 2.1: The ASAS light curve of RV Crt as an example of an EA system.

Note that although the Algol light curve is the protostar of a detached system, Algol itself is no longer considered to be a detached system; it is now regarded as a semi-detached system (Percy, 2007).

EB

EB or β-Lyr systems have light curves that vary continuously as the phase changes. Rounded maxima and distinct minima occur but the start and end of eclipses cannot be discerned. A secondary minimum is always present with a significantly smaller depth than the primary minimum. These star systems are often associated with stars of spectral types B to A (GCVS, 2020).

An example of an EB light curve is that of HS Aqr shown in Fig. 2.2 that uses ASAS data.

EW

EW or W UMa systems have light curves that vary continuously over the orbital period, displaying distinct maxima and minima. It is not possible to determine from their light curve the beginning or end

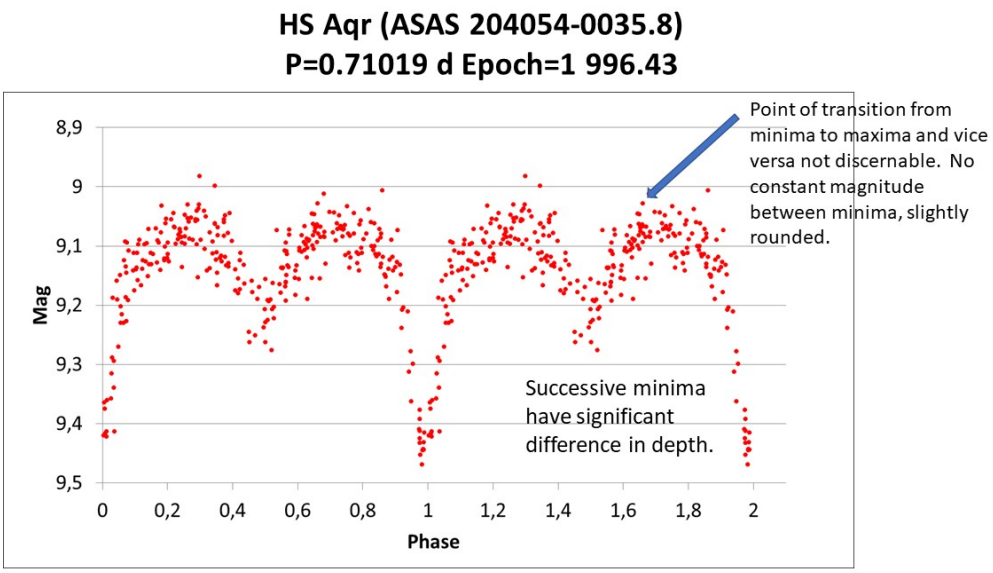

Figure 2.2: The light curve of HS Aqr using ASAS data with $P = 0.71019$ d.

of eclipses. The primary and secondary minima have almost equal depths (sometimes it is difficult to determine which is the deeper of the two). The difference between maximum and minimum is

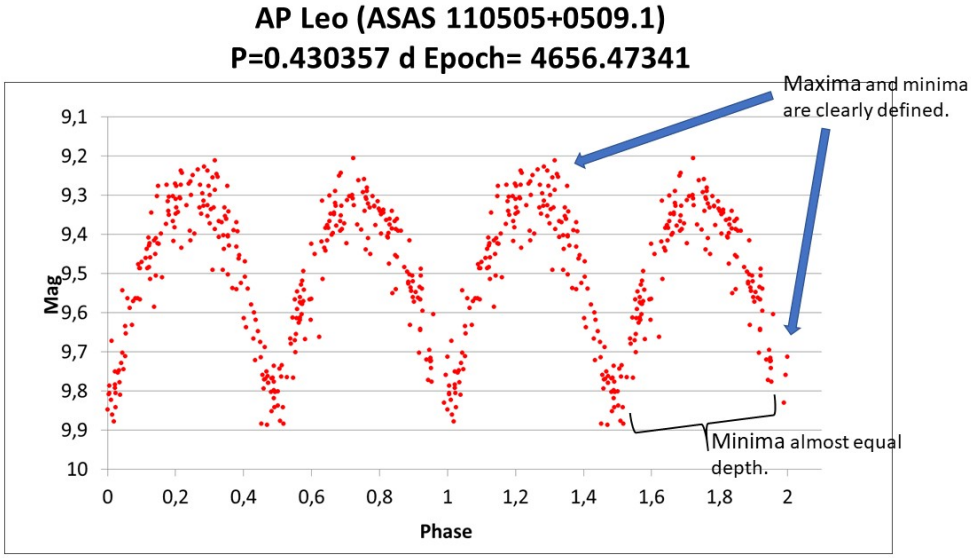

Figure 2.3: The light curve of AP Leo using ASAS data is an example of a W UMa system.

typically less than 0.8 mag in the V-band. The periods of EW systems are usually less than 1 d with the smallest period $P > 0.20$ d. Spectral types for EW systems typical range from F – K or even later (GCVS, 2020).

The light curve of AP Leo shown in Fig. 2.3 using ASAS data is an example of an EW system.

2.1.2 The Roche Model

Consider a binary system consisting of two masses M_1 and M_2, with $M_1 > M_2$, separated by a distance R rotating about their centre of mass at an angular velocity ω. According to Newton's formulation of Kepler's third law, ω is related to the separation R of the two masses and their total mass $M_1 + M_2$ by

$$\omega^2 = G\frac{M_1 + M_2}{R^3} \tag{2.2}$$

where G is the gravitational constant and SI units are used.

Transform the system so that the two stars are at rest in a Cartesian coordinate system with the mass M_1 at the origin as shown in Fig. 2.4. The system now rotates about the origin at an angular velocity ω. The total potential Ψ at an arbitrary point $P(x, y, z)$ is given by Kopal (1959) as

$$\Psi = G\frac{M_1}{r_1} + G\frac{M_2}{r_2} + \frac{\omega^2}{2}\left\{\left(x - \frac{M_2 R}{M_1 + M_2}\right)^2 + y^2\right\}, \tag{2.3}$$

where

$$r_1^2 = x^2 + y^2 + z^2 \qquad \text{and} \qquad r_2^2 = (R - x)^2 + y^2 + z^2\ . \tag{2.4}$$

The first and second terms in eqn. (2.3) represent the gravitational potentials of the masses M_1 and M_2 respectively, while the third term is the centrifugal potential of the system due to its rotation about

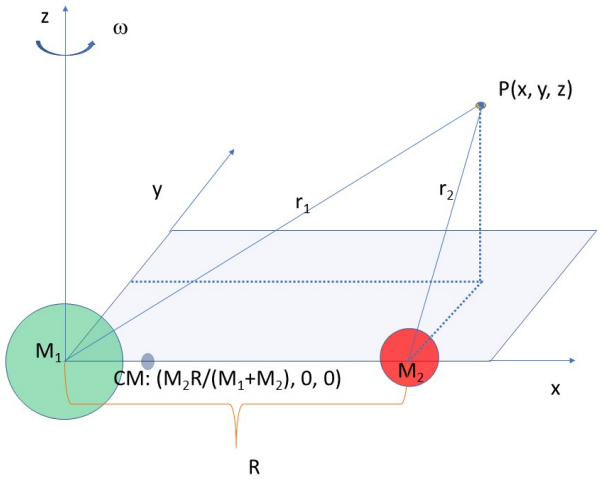

Figure 2.4: Diagrammatic layout of two masses M_1 and M_2 and the point $P(x, y, z)$ at which the potential Ψ is determined.

the origin. Converting eqn. (2.3) into spherical coordinates and setting

$$\Omega = \frac{R\Psi}{GM_1} - \frac{M_2^2}{2M_1(M_1+M_2)} \tag{2.5}$$

it can be shown that

$$\Omega = \frac{1}{r_1} + q\left\{\frac{1}{\sqrt{1-2\lambda r_1 + r_1^2}} - \lambda r_1\right\} + \frac{q+1}{2} r_1^2(1-\nu^2), \tag{2.6}$$

where the mass ratio $q = M_2/M_1$ has been introduced, and the parameters λ and ν are given by

$$\lambda = \cos\phi \sin\theta \qquad \text{and} \qquad \nu = \cos\theta \ . \tag{2.7}$$

When Ω is set to a constant value, surfaces having a fixed potential are produced which are referred to as Roche equipotentials. There are five points in the plane of the two masses where the potential goes to zero. These points are referred to as Lagrange points and are labelled L_1 to L_5. Examples of contours of constant potential are shown in Fig. 2.5, together with the five Lagrangian points L_1 to L_5. The surface potential depicted by the slightly elongated figure "8" that passes through the L_1 point, also known as the inner Lagrangian point, in Fig. 2.5 contains the volumes referred to as the Roche lobes. The L_1 point is the position where the two Roche lobes make contact.

Because the potential at the Lagrangian points is zero, so too is the net force acting on mass at these points. This means that at L_1 matter can flow from one lobe to the other. Similarly, at point L_2, matter can flow out of the system and escape from the gravitational clutches of the binary system, as indicated by the arrows in Fig. 2.5.

In eqn. (2.6) if r_1 and $r_2 = \sqrt{1-2\lambda r_1 + {r_1}^2}$ are small, then Ω will have a large value, and will result in two almost-spherical surfaces around the masses. In Fig. 2.5 these would be the surfaces passing through the two inner circles surrounding M_1 and M_2. This indicates that if all the stellar mass lies close to each mass-point, it will occupy a spherical lobe around the particular mass-point.

As r_1 and r_2 increase, the shape of the equipotentials deviate from a spherical shape, becoming more ellipsoidal until the Roche limit is reached. The Roche lobes define a maximum volume that a star in a binary system can occupy so that all its mass is under its own gravitational control. The equipotential surfaces that lie beyond the Roche limit define the shape taken by a contact binary system. In these systems the two stars are physically connected by a narrow neck in the region of the L_1 point and are surrounded by a common envelope filling the region between the Roche lobe and the appropriate equipotential surface of the system.

The shape of the star in a binary system is influenced by the associated effective equipotential, and can be non-spherical, particularly if the components are close. A spherical radius of a Roche lobe r_L has been developed by Eggleton (1983) which is given by

$$r_{L1,2} = \frac{0.49q^{\frac{2}{3}}}{0.69q^{\frac{2}{3}} + \ln(1+q^{\frac{1}{3}})}, \quad 0 < q < \infty \ . \tag{2.8}$$

If the primary component radius is to be determined $q = \frac{M_1}{M_2}$, while for the secondary component $q = \frac{M_2}{M_1}$ is used (Hambálek & Pribulla, 2013).

Following Kopal (1959), the ratio of the axial rotation of the star to the Keplarian angular velocity of the orbital motion of the system can be defined as n where

$$n^2 = \frac{\omega^2 R^3}{G(M_1+M_2)}, \tag{2.9}$$

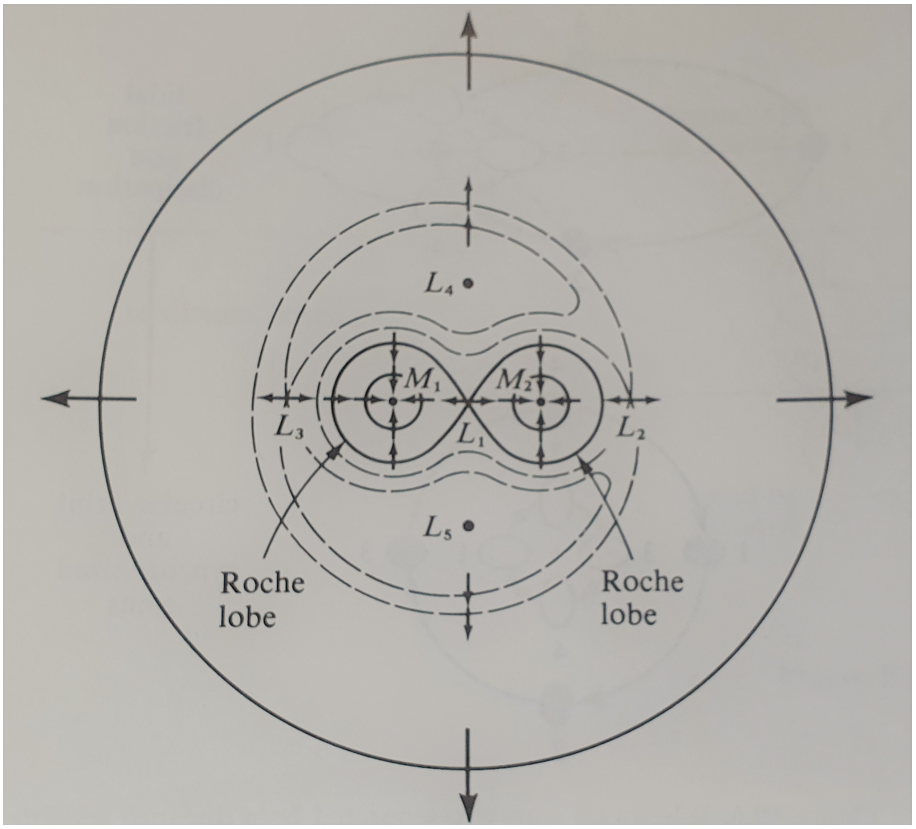

Figure 2.5: Equipotential contours around a system with $q = \frac{2}{3}$ with zero effective gravity at the various Lagrangian points shown as L_i. This diagram is taken from Shu (1982).

and a normalised surface potential C can be defined as

$$C = \frac{2R\Psi_{1,2}}{G(M_1 + M_2)}. \tag{2.10}$$

The critical surface labelled C_0 defines the Roche lobes and is dependent on n and the mass ratio q. For each $C > C_0$ the system will result in two detached equipotentials, while $C < C_0$ produces a contact system. Using the criterion for C, Kopal (1959) devised a classification system based on the Roche-lobe model.

2.1.3 Roche model classification

Detached systems

If the surface of both stars of a binary system lie well below their Roche lobes, then the stars will have nearly spherical surfaces, and there will be no mass transfer between the two stars. The stars are detached and generate a light curve corresponding to that of EA systems. The system is regarded as detached if $C_1 > C_0$ and $C_2 > C_0$.

Semi-Detached systems

If one star fills its Roche lobe while the surface of its companion lies below the Roche lobe, then matter can flow from the Roche lobe-filling star to its companion through the L_1 point, creating a system that is referred to as semi-detached. Kopal (1959) defined a system as semi-detached if either of $C_{1,2} < C_0$ with the remaining element $C_{2,1} = 0$.

The Roche lobe-filling star is no longer spherical so its observed surface area changes as the stars rotate, producing a continuously varying light curve in which it is not possible to see the start and end of eclipses. The light curves produced by semi-detached systems have the characteristics of binaries classified as EB.

Contact systems

If the surface of both stars in a binary lie above the Roche lobe, then the outer material from both stars forms a common envelope around the two masses. Neither star has a spherical shape so the surface area seen by an observer is continuously changing and the start and end of eclipses cannot be determined. If the common convective envelope transfers energy between the two stars then the temperature of the surface will not vary much over a rotation cycle and the two eclipse minima will have almost equal depths, leading to EW type light curves. The system will be in contact when $C_1 < C_0$ and $C_2 < C_0$.

In Fig. 2.6 a rendition of the common envelope surrounding the contact binary RW Dor is shown. The neck around the L_1 point can be seen, allowing matter to flow around the two stars.

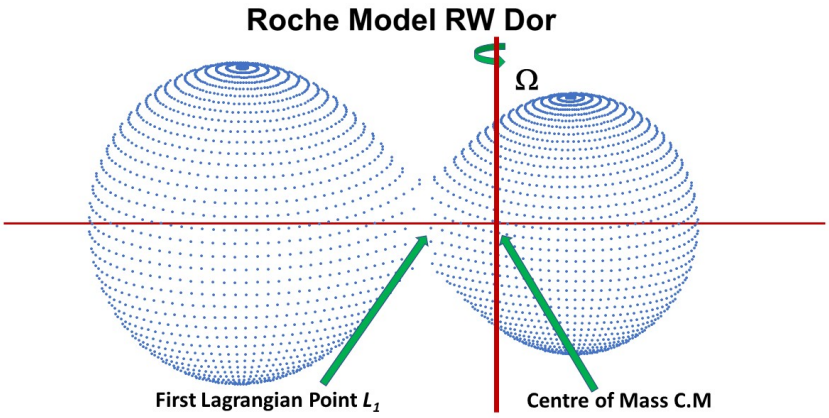

Figure 2.6: A depiction of the common envelope model of RW Dor using parameters from Deb & Singh (2011), produced using Binary Maker 3.

2.2 Common Convective Envelope Model (CCE)

The use by Kopal (1955) of the Roche model to explain detached, semi-detached and contact systems had a fair amount of success, but could not explain the almost constant temperature observed in the contact systems during an orbital cycle. In particular, (Kuiper, 1941) had pointed out that zero age

systems of unequal mass could not exist unless they satisfied the condition given by

$$\frac{R_2}{R1} = \left(\frac{M_2}{M_1}\right)^{0.42}. \tag{2.11}$$

The introduction by Lucy (1968a,b) of a common convective envelope solved many of the problems of the Roche model contact systems, and was able to provide a good model for the interpretation of light curves for systems with a primary star that is more massive than the secondary star. Because the contact binaries share a convective envelope and their masses differ substantially, the more massive component is considerd to be contributing the larger portion of the nuclear energy (Paczyński et al., 2006) as shown in Fig. 2.7). Although the model has had a lot of success, there is still some on-going discussion relating to how precisely this common envelope is created (Podsiadlowski, 2001).

2.3 Thermal Relaxation Oscillation Model

The Thermal Relaxation Oscillation Model, (TRO) (Lucy, 1976; Robertson & Eggleton, 1977), was developed to explain definite light curve fluctuations that were often observed as well as period changes occurring in W UMa systems. The model assumes that the system is not in thermal equilibrium, although, because of their low angular momentum, they will be in thermal contact (Robertson & Eggleton, 1977). The model allows mass to flow between the components, resulting in cyclical states of being either semi-detached or in marginal contact (Qian, 2001b; Paczyński et al., 2006) in instances when mass and angular momentum are both conserved. Mass transfer occurs from the secondary star to the primary star and energy flows from the primary component to the secondary. The process is explained qualitatively and numerically by Lucy (1976) through mass-radius relations for a certain fixed adiabatic constant K and different values of $\log K$. A slow expansion of the secondary star following a compressed state, will imply a mass transfer to the primary star with a corresponding adjustment (decrease) in q. This change in q will impact the period P and separation between the two companion stars in order to retain both total angular momentum and mass. The separation will lead to a situation of being in marginal contact.This model was introduced by Lucy (1976) to account for stars that had a primary star that was less massive but hotter than its secondary star.

2.4 W Ursae Majoris

W UMa is the prototype of the EW contact binary stars. In this section the properties of W UMa are reviewed before looking at the general class of eclipsing contact binaries.

The W UMa star system was first observed by Muller & Kempf (1903) in January 1903 using the Potsdam Observatory photometer. They reported variability of the light curve with a period P that ranged between $3^{\mathrm{h}}\,59^{\mathrm{m}}$ and $4^{\mathrm{h}}\,01^{\mathrm{m}}$ corresponding to $P \sim 0.17\,\mathrm{d}$. This period was very small compared to other known binary stars, so they concluded that it could not be an Algol-type system, but postulated that it consisted of two ellipsoids that may be in contact. Further investigations conducted during 1906 by Parkhurst & Jordan (1906) determined a period $P = 0.126\,\mathrm{d}$. These early measurements are not consistent with the present value of $P = 0.3336368\,\mathrm{d}$, probably due to the technological constraints imposed by using photographic methods to determine the period. Russell (1912) reported that the spectrum was of class G and made an attempt to determine some values for the orbital parameters of the system. Following spectrographic analysis, it was found that lines in the spectrum are broadened by the rapid rotation of the two stars (Struve & Horak, 1950). Radial velocity curves were constructed using the Fe I $\lambda 4046$ line which produced values for the radial velocity of the system centre-of-mass with respect to the Sun of $-50\,\mathrm{km\,s^{-1}}$, and Doppler velocities of the individual stars

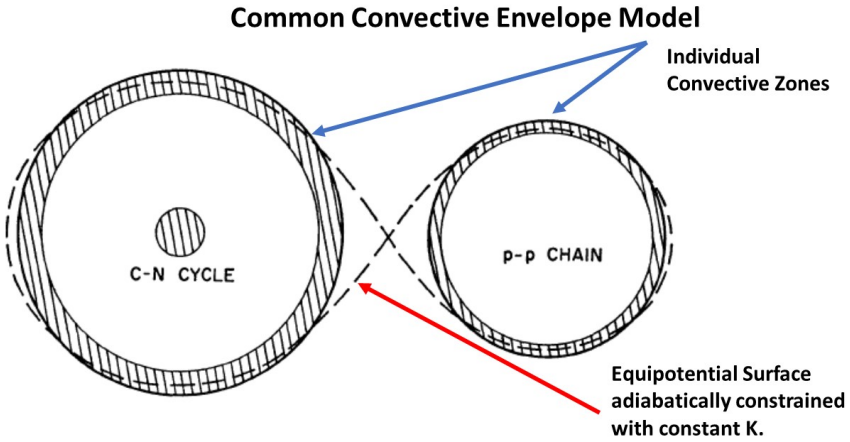

Figure 2.7: Adapted from the model for a Zero Aged W UMa system provided by Lucy (1968a), the dashed areas are showing convective zones, the relevant nuclear cycle for the particular star and then the common convective envelope.

with respect to the centre-of-mass of $K_1 = 125\,\mathrm{km\,s^{-1}}$ and $K_2 = 250\,\mathrm{km\,s^{-1}}$ where $K_j = \omega r_j \sin i$ and i is the inclination of the system. This analysis leads to a mass ratio $q = K_2/K_1 = 2.0$ which they found to be inconsistent with the mass-luminosity (M-L) relationship. This is known as the light curve paradox and is a general problem with EW stars in that they do not follow the normal M-L relationship for main-sequence stars.

Further studies of W UMa were conducted by Mochnacki (1972); Hutchings & Hill (1973); Whelan et al. (1974) which led to a discrepancy being found between the mass ratio q determined photometrically, $q_{\mathrm{ph}} \approx 0.43$, and spectroscopically, $q_{\mathrm{sp}} \approx 0.54$. Through various model iterations Hilditch (1981) showed that the difference between q_{ph} and q_{sp} is lowered if the value of the gravity darkening element is $\beta = 0$. (The gravity darkening concept will be elaborated on in subsection 3.0.7.) Measurements by McLean (1981) determined a value of $q_{\mathrm{sp}} = 0.48$ and Rucinski et al. (1993) obtained $q_{\mathrm{sp}} = 0.479$. The most accurate determination to date is that of Pribulla et al. (2007a) who determined a value of $q = 0.484(3)$.

The measured centre-of-mass velocity V_0 of W UMa shows a range of values between 0 and $-43\,\mathrm{km\,s^{-1}}$ Pribulla et al. (2007a). This matter is not settled but the value does seem to have improved with refined observations and technology. Rucinski et al. (1993) measured $V_0 = -29.6 \pm 4.9\,\mathrm{km\,s^{-1}}$ and Pribulla et al. (2007a) determined $V_0 = -28.4 \pm 0.5\,\mathrm{km\,s^{-1}}$. It has been suggested that some of these changes, that also impact the period, may be ascribed to various mass and angular momentum transfer processes that are not yet well understood.

Variations in the orbital period of W UMa have been recognized for many years. Whelan et al. (1974) proposed that a third body with $M_3 = 0.2 M_\odot$ may be responsible for a quasi-sinusoidal variation of the period. However, mass exchange, mass loss through the L_2 Lagrangian point or apsidal motion could not be ruled out as the cause of the period changes. A recent O–C diagram generated using B.R.N.O data (B.R.N.O., 2020) is shown in Fig. 2.8 which clearly shows that the period is changing. An analysis of period changes in W UMa by Nelson et al. (2016), showed that the period of the system was changing by $dP/dt = -0.287 \times 10^{-7}\ \mathrm{d\,yr^{-1}}$. From the shape of the O–C curve it is clear

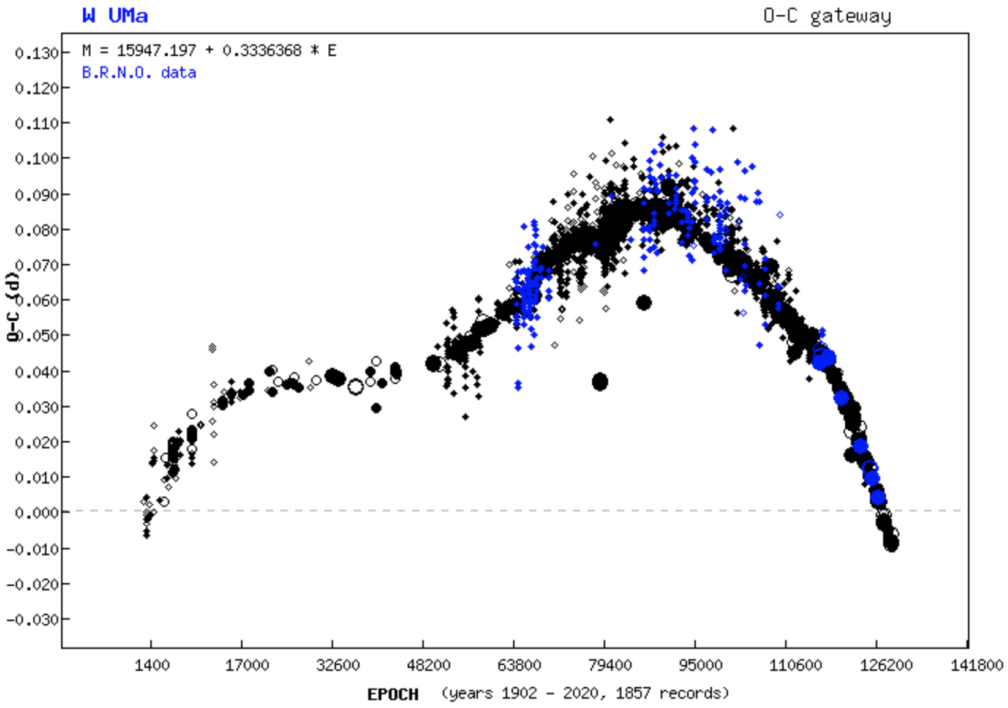

Figure 2.8: The non-linear shape of the O–C graph for W UMa indicates that its period is changing.

that neither a linear nor a quadratic fit is appropriate to describe the long term behaviour of the period. Using a linear fit to recent B.R.N.O. data, the period is presently $P = 0.3336368$ d.

2.5 W UMa type systems

W UMa stars are low mass contact eclipsing binary systems that have continuously varying light curves, minima with nearly equal depths ($\Delta m_V \sim 0.1$ mag) and periods ranging between 0.2 and 1 d. The light amplitude ranges from 0.1 to 1 mag in V (5500Å) with spectral types from F to K (Hilditch, 2001).

Colour variations across the orbital cycle are small, suggesting an almost uniform temperature over an optically thick envelope. The small difference in depth of the minima corresponds to a difference of less than 1000 K between the lobes, thereby supporting the nearly uniform temperature model. The spectral types of W UMa stars are associated with stars with convective photospheres, suggesting that the common envelope is convective (Webbink, 2003).

Rotationally broadened lines are present in the spectra, as well as blended absorption lines, consistent with a model in which the two stars of the system are close together and rotating rapidly. The two masses have spins that are phase locked with their orbital motion, producing extremely rapidly rotating stars for their spectral types. In common with single stars, this rapid rotation produces substantial chromospheric emission (Eaton, 1983), but magnetic activity levels appear to be lower than for single rapidly rotating stars. This suggests that the convective envelope suppresses dynamo action.

According to the geometry of the Roche model, the two halves of the light curves of W UMa stars

should be symmetric. However, in many light curves there are asymmetries present. The O'Connell effect refers to light curves that show unequal heights of successive maxima. It was formerly known as the periastron effect in close binaries, but O'Connell (1951) showed that there is a wavelength dependence associated with the maximum height, and hence concluded that it could not be due to the orbital eccentricity of the system. For contact binaries, the orbits are circular which supports O'Connell's observations. The O'Connel effect in W UMa-type stars is now attributed to star spots on the surface of one of the stars which, because the star spot has a lower temperature than the surrounding stellar photosphere, reduces the flux from that star at certain phases of the orbit. In single stars, star spots are associated with high levels of magnetic activity induced by rapid rotation. Contact binaries, because they are phase locked to the orbital period are very fast rotators for their spectral types, but star spot activity on contact binaries is not excessive, suggesting that the common convective envelope suppresses magnetic activity in some way.

The W UMa stars were classified by Binnendijk (1970) into two sub-groups labelled A type and W type. For type A systems, the primary eclipse occurs when the more massive star is eclipsed by the smaller, cooler component. For W-type systems, the less massive companion is hotter than its more massive companion and is eclipsed at primary minimum. This is contrary to the properties of main sequence stars. This phenomenon, known as the light curves paradox, was first noticed by Struve & Horak (1950) in the protoype system, W UMa, which is a W-type system. van Hamme (1982) pointed out that for all contact binaries, their masses and radii are too large and not aligned to their observed spectral types compared to single main sequence stars.

Lucy & Wilson (1979) introduced another class of EW system called B-type. These are contact systems but the members of the binaries have poor thermal contact, leading to large temperature differences between the components. Their light curves resemble semi-detached (EB) systems, hence the B for the subtype classification. Csizmadia & Klagyivik (2004) refined this classification to stars with $\Delta T \geq 1000\,\mathrm{K}$ which is the definition used here. B-type systems will not be considered in this work.

The formation and evolution of contact binary systems is not properly understood and still hotly debated. Do contact binaries start off as single stars and merge later, or are they born as a binary system and evolve together? Are type A and W binaries formed in the same way with one type being more evolved than the other? Angular momentum losses via magnetic braking (Lucy, 1976; van't Veer & Maceroni, 1989; Rovithis-Livaniou, 2006; Liu et al., 2018) or third body interactions are popular candidates for mechanisms leading to the formation of close binary systems. Once formed, it is possible that contact systems may become semi-detached via the TRO mechanism, but there is no conclusive evidence yet of this being an evolutionary process.

For a single rotating star, angular momentum loss (AML) through a process of magnetic braking is governed by the braking law which is given in the form of $\dot{\omega} = c_3 \omega^{c_4}$ (van't Veer & Maceroni, 1989) where $\omega = \frac{2\pi}{P}$. Here c_3 and c_4 are constants that determine the strength of braking.

Gazeas & Stępień (2008) found that though the orbital angular momentum does increase with increasing period, the correlation is low. They describe in detail through model calculations how binary stars lose mass and angular momentum through a magnetic stellar wind, that leads consequentially to a smaller orbit. As the stellar mass reduces, and with the primary near or about to be a terminal age main sequence star (TAMS), the Roche lobe will reach its surface. The mass transfer will continue until the process reverses, the process only stopping when the Roche lobe becomes larger than the stellar mass of the mass transferring component.

For A-type systems, the companion stars were believed to be on or close to the TAMS with mass ratios that can be as low as $q = 0.07$. The companion stars of W-type systems are not as evolved

and could still be Zero Age Main Sequence stars (ZAMS), having mass ratios ranging between 0.4 to 0.6 $M_\odot$ (Lucy & Wilson, 1979; Wilson, 1994; Li et al., 2008; Nelson et al., 2014).

However, there is some disagreement with the suggestion that A type systems are more evolved than W type due to contradictory results regarding total mass and angular momentum (Maceroni & van't Veer, 1996; Yakut & Eggleton, 2005; Gazeas & Stępień, 2008). There is support for the TRO model (Nelson et al., 2014), suggesting that the importance of period variation determination may lend insight into the state of the binary system.

Yıldız & Doğan (2013) used a modelling code called MESA[2] to determine the initial masses of the contact binary components based on the observed masses and luminosities of the secondary components. They found that the secondary star started off as the more massive component of the pair and then transferred matter to its less massive companion. Only about one third of the mass is transferred from the more massive to the less massive star, with the remaining mass lost from the system, leaving the initially more massive star with less mass than its companion. The initial masses of the stars are $M_{1i} = 0.2 - 1.5\,M_\odot$ and $M_{2i} = 1.3 - 2.6\,M_\odot$, where M_1 is the mass of the current more massive star, and M_2 the less massive component. If the system's secondary star had a mass $M_{2i} > 1.8 \pm 0.1\,M_\odot$ it evolved into an A-type system, while for a lower mass it becomes a W-type system. Yıldız (2014) extended the work of Yıldız & Doğan (2013) to determine the age of A- and W-type as 4.4 and 4.6 Gyr respectively.

Zhang et al. (2020) agrees with the evolution of A-type systems as described by Yıldız & Doğan (2013), but suggest that W-type systems are not as evolved. They propose that the less massive star also started off as the more massive component and has expanded and transferred matter to the other component and lost some of the mass out of the system, leaving behind a hot core that has a higher surface temperature than the component that is now more massive.

2.6 Light Curve Changes

The shape of the light curve in the W UMa system has remained constant over the years, but as shown in Fig. 2.8 the period of the system is changing over time. Variations in periods are indicative of dynamic changes in the system and can be monitored easily using modest equipment. Models that explain the observed period changes can provide insight into physical processes occurring in contact binaries.

There are essentially two types of changes impacting light curves: those that are apparent or geometrical changes, such as through the presence of third bodies, and those that are evolutionary in nature (Kalimeris et al., 1994a; Rovithis-Livaniou, 2006).

The presence of a third body that is in orbit with a W UMa-type system, will introduce a sinusoidal term into its O–C diagram via a light travel time effect as it moves about the centre-of-mass of the three-body system (Kalimeris et al., 1994b). The existence of tertiary bodies influence the appearance of the light curve and thus alignment of physical to modelled light curves. The presence of a third light may change the depth of the minimum as well as the slopes of the light curve branches (Binnendijk, 1960).

Recent studies suggest that some W UMa stars may have been formed from or even have third bodies impacting on their evolution (Eggleton & Kiseleva-Eggleton, 2001; Paczyński et al., 2006). As many as 40% of contact binary stars are estimated to have a third or more bodies influencing the system (Nelson et al., 2016). The third body introduces a perturbation on the orbit which may include

[2] http://mesa.sourceforge.net/

precession of the orbital plane in which both the orbital plane and the inclination may vary periodically. These oscillations are referred to as Kozai cycles by Eggleton & Kiseleva-Eggleton (2001) who were the first to propose this mechanism as influencing binary stars. Tidal forces may also play a role (Eggleton & Kiseleva-Eggleton, 2001).

van't Veer & Maceroni (1989) proposed a CCE-dominated mechanism to explain period changes in contact binary systems. They report a correlation of changes in orbital periods, P, with fill-out factors, f, with f being associated with a measure of the CCE thickness and thus mass transfer process in situations where the mass ratios, q, are large. The evolution of binaries will be from high to low mass ratios and increasing fill-out factors. According to their model, a short P is associated when f is large at high q. In this regard it is noteworthy that A-type stars are usually associated with larger fill-out factors (Nelson et al., 2014). The fill-out factor influence would impact the width of the minimum of the light curve, given that it is related to the radius of the system for a particular mass ratio (Hambálek & Pribulla, 2013).

Magnetic activity or the dynamo effect (Applegate, 1992; Hilditch, 2001; Rovithis-Livaniou, 2006) of fast rotating stars, may also be responsible for period changes in light curves. Applegate (1992) pointed out that the orbital period of contact systems is related to their internal structure. Consequently, any changes to the internal structure will impact on the period. Applegate proposed that a structural change due to magnetic activity would affect the hydrostatic equilibrium of the system. The change could be either a contraction or expansion of the system. In responding to such changes, the orbit inevitably may reflect this through changes in the angular momentum, and, consequently, translate into small period changes that are cyclical in nature. In essence the internal structure of the star is affected by a subsurface magnetic field B of a few kilogauss that could have a variability of $\Delta L/L \approx 0.1$. This leads to a change in period on the order of $\Delta P/P \approx 10^{-5}$ on the time scale of decades (Applegate, 1992). The Applegate phenomenon is expected to cause a sinusoidal influence on the O–C diagram.

The impact of star spots on the shape of O–C plots has been investigated by Ogloza (1997); Rovithis-Livaniou et al. (2003); Watson & Dhillon (2004). The general conclusion is that the overall slope of O–C residuals are not influenced by spots, but that temporary changes may be noticeable over short time lines. The presence of spots will thus have a different result compared to the Applegate phenomenon and other systemic changes that impact long term period as revealed by O–C diagrams.

A period-colour relationship has been reported by Rucinski & Maceroni (2001) wherein a typical contact binary would become hotter as its period lengthens which may be due to the age of the system as it matures along the main-sequence stars.

Lanza & Rodonò (1999) suggest that orbital period variation may also be a consequence of gravitational quadrupole moment changes (due to the non-spherical nature of the surface) of the active star.

Chapter 3

Software Solutions and Sources of Data

To generate a synthetic light curve certain key parameters are required. There exist several programmes of various complexity and sophistication that can perform this task. The modelling reported in this work was done predominantly using Binary Maker 3[1] (BM3), so the parameters input into this programme will be described in this chapter. BM3 also facilitates the depiction in three dimensions of close binary stars showing how they orbit around their common centre-of-mass. BM3 was created by Bradstreet & Steelman (2002).

3.0.1 Period P

The period P of the system is the time between two successive primary minima and can be determined by observation. For contact binaries, periods lie in the range $0.2 < P < 1.0$ d. The period is not needed as an input in BM3 unless observed radial velocity data is used, but to generate phase-amplitude data from observations, the period is required. Phase varies between 0 and 1 over a complete cycle. For contact binaries, which have circular orbits, the primary minimum occurs at phase 0 and the secondary minimum at phase 0.5. The maxima occur at phases of 0.25 and 0.75. Over time (or equivalently, after many cycles), period changes may occur.

3.0.2 Mass ratio q

The mass ratio q is usually defined as $q = M_2/M_1$ where M_1 is the mass of the more massive star, and M_2 the less massive star, and, therefore, q is usually less than 1. However, for W-type systems which have M_2 hotter than M_1, it is necessary to invert the mass ratio so that $q > 1$ to make the primary eclipse occur at phase 0.

3.0.3 Inclination angle i

The inclination angle i is the angle between an Earth-bound observer and the orbital plane of the binary system. When looking down on the poles of the binary, the inclination is 0°, while an $i = 90^\circ$ corresponds to the orbital plane lying along the observers line-of-sight. In Fig. 3.1 the diagram on the left hand side shows a view of the system with $i = 0^\circ$, and on the right hand side i is close to 90°.

[1] Licence number 2NGGK-VHKK5-A26X9-BWLXU-PNMJY

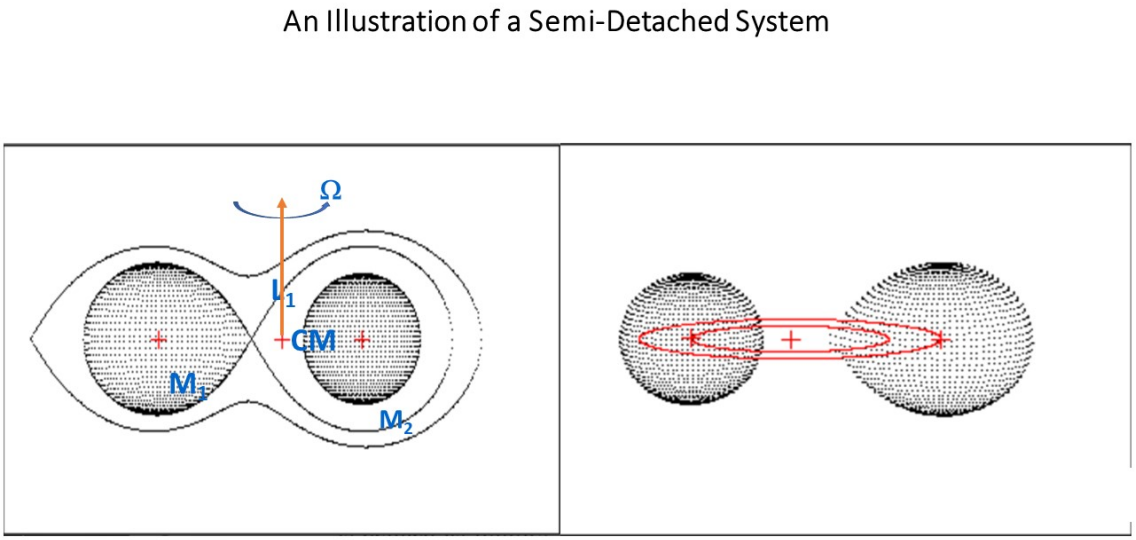

Figure 3.1: Depictions of a detached system at inclinations of 0° (left) and close to 90° (right).

If the inclination is small, the stars will not eclipse each other; for $i > 50°$ eclipses can start to be detected. If i is close to 90° total eclipses can occur which can produce flat minima. These flat minima provide additional information on the physical size of the stars and, hence, help with modelling by constraining solutions.

3.0.4 Temperature of the stars $T_{1,2}$

The temperature of star 1, T_1 will often be the temperature of the star with the higher temperature, but this does depend to some extent on how the subscripts 1 and 2 are defined. The temperature of the stars can be determined observationally from spectra which are used to estimate the spectral type of the stars.

Both stars' temperatures are required when modelling synthetic light curve. The small difference between the depths of minima in EW stars indicates that the temperature of the stars are similar and therefore cannot be separated by spectral typing. Let $\Delta m_{1,2}$ denote the depth of the minima of EW stars. Brancewicz & Dworak (1980) used the Stefan-Boltzmann law and mass-luminosity relationship to derive the following formula

$$\frac{T_2}{T_1} = \sqrt[4]{\frac{1+0.4\Delta m_2}{1+0.4\Delta m_1}}$$

to calculate the temperature of the two components. Limb-darkening is not included in this expression, and therefore it has some limitations.

3.0.5 Omega surface potential Ω

The Omega potential is defined in section 2.1.2 by eqn. (2.6) as

$$\Omega = \frac{1}{r_1} + q\left\{\frac{1}{\sqrt{1-2\lambda r_1 + r_1^2}} - \lambda r_1\right\} + \frac{q+1}{2} r_1^2 (1-\nu^2)$$

where the parameters λ and ν are given by (see eqn. (2.7))

$$\lambda = \cos\phi \sin\theta \qquad \text{and} \qquad \nu = \cos\theta \ .$$

For a given value of Ω an equipotential surface exists, which along with a specified mass ratio, completely describes the surface structure of the stars. BM3 defines an inner critical Roche potential when the stars just come into contact as Ω_{inner}, and an outer limit where the gravitational acceleration goes to zero (and hence matter can escape from the system) as Ω_{outer}.

Each Roche equipotential surface can be defined by a constant C, as discussed in section 2.1.2. In BM3, the C potential is defined by

$$C = \frac{2\Omega}{1+q} + \left(\frac{q}{1+q}\right)^2 .$$

3.0.6 Fill-out factor f

BM3 makes use of a fill-out parameter f that is a modification of a parameter defined by Lucy & Wilson (1979) to specify equi-potentials in contact binaries. It represents the degree of contact and is defined by

$$f = \frac{\Omega_{\text{inner}} - \Omega}{\Omega_{\text{inner}} - \Omega_{\text{outer}}}.$$

For contact systems the fill-out factor lies in the range $0 \leq f \leq 1$, i.e. from contact at the critical inner surface when $f = 0$ to the outer critical surface when $f = 1$.

3.0.7 Gravity brightening (darkening) exponent $\alpha_{1,2}$

For radiative stars von Zeipel (1924) showed that the surface flux is directly proportional to the gravitational acceleration g at the stellar surface. BM3 determines the local temperature T_{local} on the star's surface using

$$T_{\text{local}}^4 = T_{\text{eff}}^4 \left(\frac{g}{g_p}\right)^{\alpha}$$

where T_{eff} is the mean effective temperature at the surface of the star, g is the local gravity at a specific area and g_p is the value of g at the poles.

Gravity darkening exponents will have values of either $\alpha_1 = \alpha_2 = 0.32$ for convective envelopes or $\alpha_1 = \alpha_2 = 1.0$ in the case of radiative envelopes. Whether a star is convective or radiative depends on its effective temperature such that stars with $T < 7200\,\text{K}$ are convective, while for $T > 7200\,\text{K}$ they are radiative (Lucy, 1967).

3.0.8 Limb darkening coefficient $x_{1,2}$

The flux from a star depends on the temperature of the material which is being looked at. In the centre of the star, it is possible to see down to deeper layers of the photosphere where the effective temperature is higher than on the edge of the star where surface layers are not as hot. This produces a dimming of the brightness as one looks from the centre of the star towards the edge.

The limb darkening formula used by BM3 is

$$\frac{I}{I_0} = 1 - x - x\cos\theta \tag{3.1}$$

where $\theta \in [0^\circ, 90^\circ]$. At the centre of the stellar disc $\theta = 0^\circ$, while at the limb it will be $\theta = 90^\circ$. The limb darkening coefficients are dependent on both the wavelength and temperature. Although the data used in this study are not strictly speaking taken in the V-band, they are close enough to take the central wavelength at $\lambda = 5500$ Å. The limb darkening coefficients used in BM3 are estimated by linear interpolation of the relevant temperature ranges from the van Hamme tables (van Hamme, 1993). The van Hamme tables provide data for various gravity coefficients; a gravity coefficient factor $\log g = 4.5$ has been used for the purposes of this project.

3.0.9 Bolometric albedo $A_{1,2}$

In contact binaries, the two stars are close to each other and interact with each others radiation. The flux emitted by one star will strike the surface of its companion, heating up the surface. This energy can be re-radiated, thereby affecting the overall flux from the stars. The bolometric albedo is also referred to as the reflection coefficient. The reflection element is needed to account for flux from the close companion that is absorbed and re-emitted (reflected). This effect is prominent particularly before the primary minimum. For radiative stars the coefficient is assumed to be 1.00 whereas for convective stars Ruciński (1969) showed that surface convection will carry away some of the radiation and re-radiate it in regions away from where it was incident, and hence the albedo is assumed to be 0.50. The reflection element $A_{1,2}$ for each star will be either $A = 0.5$ or $A = 1.0$ depending on whether the stars are convective ($T < 7200$ K) or radiative ($T > 7200$ K).

3.0.10 Third light

When measuring the light curve of a contact binary, light may be included that does not belong to the contact system (Binnendijk, 1960; Walker, 1993). This additional light comes from other stars in the field, whether they are gravitationally bound to the system or background objects. The third light, l_3 reduces the amplitude of a light curve but leaves the shape unaltered, (Hambálek & Pribulla, 2013).

The third light contribution to the observed magnitude of the system is given by $l_3 = \frac{F_3}{F_1+F_2}$ where F_i is the flux of the binary components $i = 1, 2$ and the third component. The true amplitude A_{true} of the binary can be determined from the observed amplitude A_{obs} using (Hambálek & Pribulla, 2013)

$$A_{\text{true}} = -2.5\log[10^{-0.4A_{\text{obs}}}(1+l_3) - l_3] \ .$$

3.1 Modelling light curves with Binary Maker 3.0

An example of the typical user interface and views from BM3 is shown in Fig. 3.2. In this example the data of the contact binary ASAS 234718-0805 are used.

Observed data (red) is read into the programme and then the synthesised light curve (blue) is generated by the software based on the parameters input into the appropriate fields. The parameters such

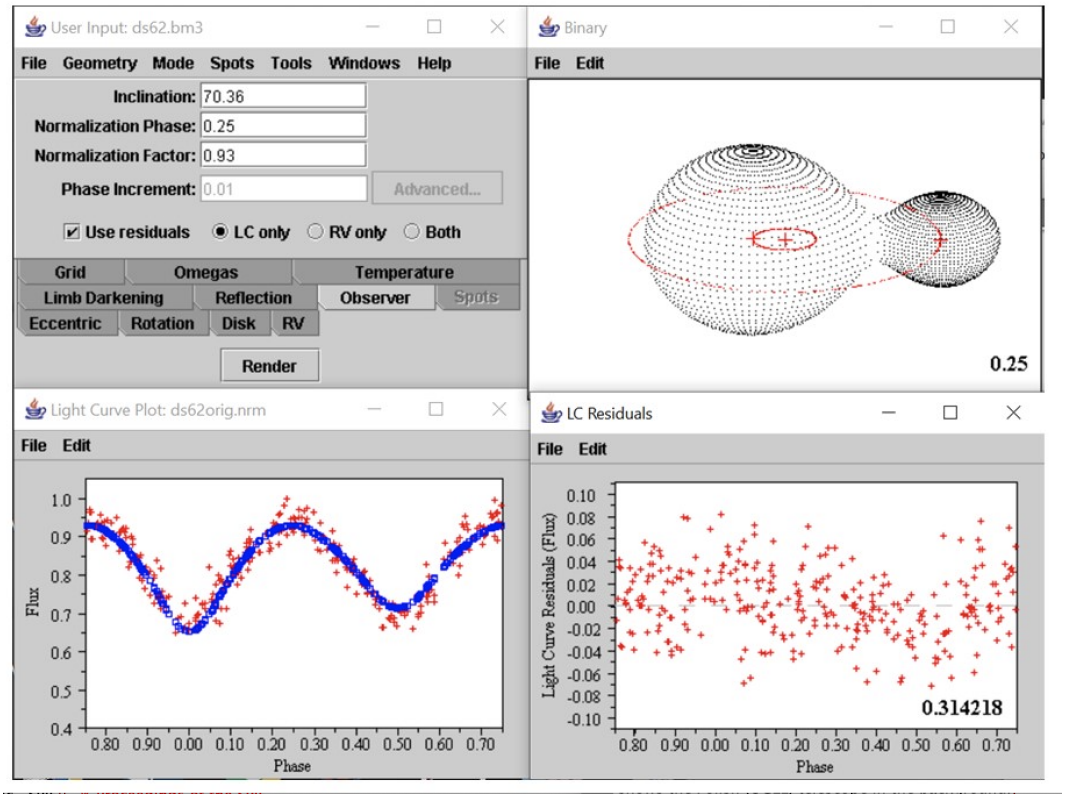

Figure 3.2: Binary Maker 3.0 user interface showing the process of modelling the contact binary ASAS 234718-0805.2.

as inclination, temperature and fillout factor are then adjusted iteratively until a best fit solution is obtained. The bottom right plot is of the residuals obtained by subtracting the synthesised light curve from the observed data. The top right panel shows the Roche-lobe configuration for this particular system.

3.2 Data

For this project, two different data sets were used: The All Sky Automated Survey (ASAS), and the Wide Angle Search for Planets (WASP) which was upgraded after a few years to what is now called SuperWASP. The equipment and data files produced by each facility will be described briefly below.

3.2.1 ASAS

ASAS is a project designed to detect star variability in the range from 8 – 14 mag. The telescopes for the ASAS-3 data are located at the Las Campanas Observatory in Chile. The robotic observatory is shown in the foreground of Fig. 3.3. ASAS-3 used two small wide-field telescopes each making use of a 200 mm f/2.8 lens connected to a CCD camera fitted with standard $V-$ and $I-$band filters. It also made use of a narrow-field 750/3.3 telescope and a super-wide 50/4 scope. The telescopes systematically take 3 min exposures of the night sky on clear nights, and then move to a neighbouring

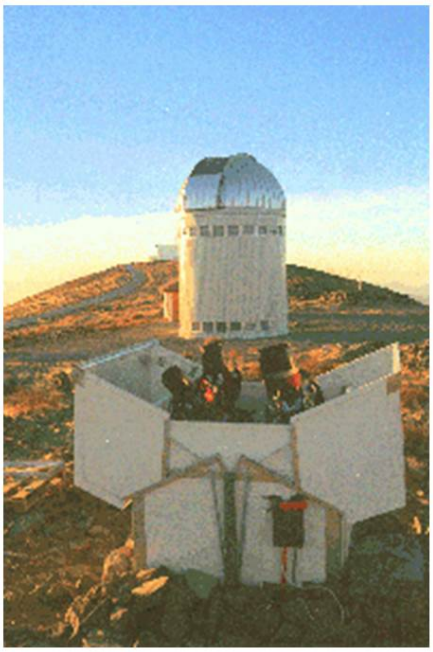

Figure 3.3: The ASAS-3 enclosure with 4 instruments which became operational in 2002 (ASAS, 2005).

field for the next exposure. ASAS has been observing the whole sky south of $+28^{\circ}$ since 2000. In this way, each patch of sky gets observed about every three days.

The ASAS Catalog of Variable Stars provides information on colour, variability type and periods of variable stars it has detected. The data is publicly available and can be downloaded from the ASAS[2] website (ASAS, 2005; Pojmanski & Maciejewski, 2004).

Each row of data from the files downloaded from the website consisted of 13 fields. These fields are as follows:

1. HJD which is the Heliocentric Julian Date of the particular observation.
2. MAG_0 – MAG_4 are the measured magnitudes for each of five different apertures.
3. MER_0 – MER_4 are the magnitude uncertainties for each aperture measurement.
4. FRAME is the camera frame number for the particular observation.
5. GRADE indicates the quality of the datum point ranging from A to D, where A indicates a good quality observation, B a mean observation, C a low grade observation and D a poor quality observation.

Only grade A and B data points have been retained, producing, typically, between 300 to 500 useable data points per star. In a few exceptional cases, more than 500 data points are available. For the sake of consistency in this project, MAG_0 data were used throughout the analysis. When data from

[2]http://www.astrouw.edu.pl/asas/?page=acvs

ASAS have been used, the ASAS designation of the file is used which is labelled as ASAS followed by the abbreviated Right Ascension and Declination of the star.

3.2.2 SuperWASP

WASP was established by UK-based astronomers during 2000. Following the success of this first venture, an improved multi-detector SuperWASP camera project was initiated. One of the instruments is located in La Palma, at the Observatorio del Roque de los Muchachos, (SuperWASP-N), and the other (SuperWASP-S) in Sutherland at the South African Astronomical Observatory (SAAO). A good overview of the WASP and SuperWASP systems and subsequent developments is given by Smith & WASP Consortium (2014). The SuperWASP telescope consists of eight cameras mounted on an equatorial mount, as shown in Fig. 3.4. The SuperWASP cameras make use of Canon 200 mm f/1.8 telephoto lenses. A total field of view of 482 square degrees per system is available with sensitivity down to 15th magnitude, with an average night's data being about 50 Gb (Smith & WASP Consortium, 2014). The SuperWASP V magnitude system is defined by the TYCHO-2 V_t bandpass (Pollacco et al., 2006). This is wider than the Johnson-Cousins system V-band filter. More details regarding the equipment are available on the SuperWASP [3] website (Pollacco et al., 2006; SuperWASP, 2018).

Figure 3.4: SuperWASP-S with its 8 Camera arrangement (Pollacco et al., 2006).

Because SuperWASP is designed to search for transiting exoplanets, its mode of observing is different to that of ASAS. The SuperWASP telescopes also take 3 min exposures, but track a field for several hours before moving on to the next field. During the course of one night, it is possible to obtain significant parts of EW light curves, in particular, there are several observations made across minima which can be used to time when the minima occur. Because SuperWASP stays on one field for several hours per night, they do not attempt to cover the whole sky. Crowded fields such as the Galactic bulge and Milky Way are avoided, concentrating instead on areas where the stars are more sparsely spread.

[3] http://www.superwasp.org/technical.htm

The number of data points in SuperWASP files contain from 3000 to over 100 000 points.

Chapter 4

Modelling light curves

The physical properties of binary systems can be determined by using models to synthesize light curves that can then be compared with observed data. Many eclipsing binary light curves have been measured photometrically, but, unless the mass ratio q is known, solutions from photometric data often produce results that are not reliable. To solve this problem, spectroscopic radial velocity measurements can be used to determine the mass ratio, which can then be fixed when synthesizing models using photometric data. Deb & Singh (2011) searched for eclipsing binaries in the ASAS online data base that have well-determined mass ratios q from radial velocity measurements. They used the Wilson Devinney light curve modelling package to determine the geometrical and physical parameters of their sample, finding good agreement with parameters determined in the literature. The W UMa systems from the Deb & Singh (2011) sample are used here to look for patterns in synthesized models using BM3.

The modelling discussed in this chapter uses data from ASAS, and the parameters determined mostly by Deb & Singh (2011). The ASAS data had some spurious data points that needed to be cleaned as described below. The parameters were then entered in BM3 and tweaked to fit the ASAS light curves. Some problems with the parameters are noted. The parameters are then used to synthesize light curves with a range of inclinations. Patterns emerging from these models are analysed and discussed.

4.1 Processing of ASAS data

Of the 62 systems listed in Deb & Singh (2011), five are B-type systems, six are semi-detached (EB) systems, and two are detached (EA) systems. Only A- and W-type contact binaries are studied here, which leaves a sample of 49 EW systems to work with. This sample, listed in Table 4.1, were used for synthetic light curve modelling.

The data for each W UMa star was retrieved as outlined in Section 3.2.1. ASAS provides a suggested period P for these stars on their web page which Deb & Singh (2011) checked and refined in some cases. The ASAS data were imported into Excel and then folded on the period P_{ME} and the epoch $T_0 =$ JD – 245 0000 from Table 1 in Deb & Singh (2011) to determine the phase Φ of each data point, where

$$\Phi = \mathrm{mod}\left[\frac{\mathrm{HJD} - T_0}{P}\right] .$$

Table 4.1: Data of 49 W UMa stars of types A and W extracted from Deb & Singh (2011). The star number in column 1 refers to the serial number of the stars in the Deb & Singh (2011) article which are arranged in order of increasing Right Ascension.

Star No.	ASAS ID	GCVS ID	q	Type	i (°)	$\Omega_1 = \Omega_2$	T_1 (K)	T_2 (K)	Fillout	$f(M)/M_\odot$
1	003628+2132.3	DZ Psc	0.136	A	79.88	1.985	6381	6294	0.85	1.471
2	011638–3942.S	AD Phe	0.370	W	74.00	6.096	5940	5717	0.19	1.435
3	012104+0736.3	AQ Psc	0.226	A	69.06	2.253	6250	6024	0.35	1.659
5	014854–2053.6	TW Cet	0.750	A	81.18	3.308	5865	5753	0.06	1.625
6	023833–1417.9	DY Cet	0.356	A	82.48	2.529	6650	6611	0.24	1.898
7	024952+0856.3	EE Cet	0.315	W	63.50	6.710	6250	5989	0.02	1.704
9	030953–0653.6	UX Eri	0.373	W	75.70	6.065	6093	6006	0.18	1.776
10	033459+1742.6	V1123 Tau	0.279	W	68.10	7.251	5940	5906	0.18	1.435
11	034814+2218.9	EQ Tau	0.442	A	82.33	2.711	5790	5711	0.09	1.747
12	034928+1254.7	V1128 Tau	0.534	W	74.50	5.057	6250	6082	0.03	1.666
14	041209–1028.2	BV Eri	0.401	W	80.44	5.547	5712	5411	0.16	1.428
16	051114–0833.4	ER Ori	0.656	W	82.08	4.430	6250	5931	0.25	2.288
17	051832–6813.6	RW Dor	0.630	W	76.32	4.556	5560	5272	0.20	1.242
18	062605+2759.9	AH Aur	0.169	A	76.28	2.081	6381	6416	0.66	1.789
21	073246–2047.5	TY Pup	0.250	A	84.47	2.121	6881	6801	0.71	1.671
22	073338–5007.4	HI Pup	0.190	A	79.47	2.134	6514	6662	0.57	1.408
23	073905–0239.1	V868 Mon	0.373	A	72.14	2.512	7000	6584	0.49	2.507
24	084002+1900.0	TX Cnc	0.455	W	62.19	5.427	6250	6121	0.23	1.331
26	100141+1724.5	XY Leo	0.729	W	68.63	4.214	5150	4742	0.25	1.190
27	100234+1702.8	XZ Leo	0.348	A	77.16	2.471	7300	7265	0.40	2.245
28	100248+0105.7	Y Sex	0.195	A	79.12	2.146	6650	6448	0.52	1.665
29	101602–0618.5	XX Sex	0.100	A	74.88	1.928	6881	6378	0.42	1.288
30	104033+1334.0	UZ Leo	0.303	A	84.05	2.374	7148	7158	0.83	2.577
31	105030–0241.7	VY Sex	0.313	W	65.53	6.720	5960	5877	0.20	1.392
32	110211+0953.7	AM Leo	0.459	W	73.85	5.400	6650	6616	0.18	1.884
33	110505+0509.1	AP Leo	0.297	A	79.66	2.404	6250	6247	0.37	1.775
34	120103+1300.5	AG Vir	0.382	A	72.54	2.547	8180	7542	0.40	2.566
35	121206+2232.0	CC Com	0.527	W	90.58	4.982	4546	4399	0.04	1.084
36	123300+2642.9	RW Com	0.471	W	72.43	5.319	4830	4517	0.15	1.053
39	141726+1234.1	VW Boo	0.428	A	77.29	2.698	5560	5099	0.12	1.373
40	141937+0553.8	NN Vir	0.491	A	65.52	2.696	7148	7201	0.60	1.994
41	143504+0906.8	CK Boo	0.111	A	60.87	1.924	6250	6234	0.91	1.173
43	152243+1615.7	OU Ser	0.173	A	50.47	2.090	5940	5759	0.68	0.639
44	153152–1541.1	VZ Lib	0.330	A	90.35	2.479	5790	5974	0.29	1.413
45	155649+2216.0	AU Ser	0.709	A	83.85	3.157	5636	5320	0.46	1.499
46	164121+0030.4	V502 Oph	0.335	W	69.77	6.397	5940	5739	0.22	1.681
47	165717+1059.8	V2357 Oph	0.231	A	47.05	2.261	5560	5440	0.21	0.560
48	171358+1621.0	AK Her	0.277	A	88.69	2.374	6765	6130	0.30	1.500
49	173356+0810.0	V2377 Oph	0.395	W	44.06	5.954	5940	5418	0.14	0.487
51	180921+0909.1	V839 Oph	0.305	A	80.19	2.363	6381	6424	0.61	2.035
52	182913+0647.3	V2612 Oph	0.286	W	66.36	6.991	6381	6273	0.56	1.281
54	193524+0550.3	V417 Aql	0.362	W	82.47	6.160	6381	6252	0.24	1.871
55	194813+0918.5	OO Aql	0.846	A	93.81	3.384	6093	5871	0.24	1.956
57	204628–7157.0	MW Pav	0.228	A	84.81	2.147	6881	6837	0.52	1.843
58	205710+1939.0	LS Del	0.375	W	45.25	6.051	6250	6192	0.09	0.617
59	222257+1619.4	BB Peg	0.360	W	87.96	6.142	6381	6076	0.32	1.860
60	233655+1548.1	V407 Peg	0.256	A	71.11	2.240	7300	6438	0.81	2.044
61	234535+2528.3	V357 Peg	0.401	A	73.23	2.640	7000	6438	0.10	2.115
62	234718–0805.2	EL Aqr	0.203	A	70.36	2.177	6881	6137	0.48	1.663

A phase-magnitude diagram (PMD) was then plotted from these data. In many instances there are points that deviate considerably from the mean light curve. Through the application of filters and conditional statements in the Excel spreadsheet, these outlying points were removed. The resulting "cleaned" data, consisting of phase Φ and ASAS V-band magnitudes were imported into BM3. BM3 converts this phase–magnitude data into phase–normalised flux data and displays it graphically. Synthesised data produced by BM3 can then be compared with the observed data and the model parameters tweaked until the residuals are at a minimum.

Using the model parameters provided by Deb & Singh (2011), BM3 synthesised models were compared with the ASAS data. The following caveats regarding the ASAS data and the parameter values were noted:

DS18 = ASAS 062605+2759.9 = AH Aur There are gaps in the data at certain phases, which can be seen in Fig. A.4.

DS21 = ASAS 073246–2047.5 = TY Pup Using a fillout factor $f = 0.71$ in BM3 gives $\Omega = 2.240968$ which differs from the value $\Omega = 2.121$ given in Table 4 of Deb & Singh (2011). The inclination angle $i = 84.47^\circ$ does not align the synthetic light with the ASAS light curve; a better fit is obtained using $i = 74.47^\circ$. Zhou et al. (2015) noted this discrepancy and proposed a third light to solve this problem, or alternatively to use $i = 78.52^\circ$. Further discussion based on SuperWASP data is presented in section 5.2.5.

DS26 = ASAS 100141+1724.5 = XY Leo There is a gap in the ASAS data around phase $\Phi = 0.8$, which can seen in Fig. A.47.

DS28 = ASAS 100248+0105.7 = Y Sex The period $P_{\rm ME} = 0.487736$ d listed in Deb & Singh (2011) is incorrect. The ASAS Period $P_{\rm ASAS} = 0.41982$ d was amended to $P = 0.41982105$ d for use in BM3. The adjustment was made when folding the data to get a light curve with the least amount of scatter. An improved period of P=0.419 8258(4) d was subsequently reported in Table 6.2 following a regression analyis of SuperWASP data.

DS29 = ASAS 101602–0618.5 = XX Sex The coordinates provided by Deb & Singh (2011) in their Table 1 are incorrect. The correct coordinates, which are in agreement with the ASAS naming convention, are $\alpha(2000) = 10:16:02.1$ and $\delta(2000) = -6:18:26.3$.

DS31 = ASAS 105030–0241.7 = VY Sex The data is spread unevenly in phase, particularly in the region $0.1 < \Phi < 0.3$ as can be seen in Fig. 4.1. The parameters provided by Deb & Singh (2011) for this star show a poor fit to the data between phases from 0.6 to 0.7 as indicated by the arrow in Fig. 4.1.

DS35 = ASAS 121206+2232.0 = CC Com Use the f value rather than the Ω value in Table 4 of Deb & Singh (2011). Furthermore, using $T_2 = 4599$ K rather than 4399 K gives an improved fit to the light curve.

DS36 = ASAS 123300+2642.9 = RW Com Use the f value rather than the Ω value in Table 4 of Deb & Singh (2011).

DS48 = ASAS 171358+1621.0 = AK Her An inclination of $i = 78.69^\circ$ gives a better fit to the ASAS data than the value $i = 88.69^\circ$ in Table 4 of Deb & Singh (2011). Other inclinations were also tested using BM3. This is probably a typing mistake by Deb & Singh (2011)

DS57 = ASAS 204628–7157.0 = MW Pav Use the f value rather than the Ω value in Table 4 of Deb & Singh (2011).

DS59 = ASAS 222257+1619.4 = BB Peg A lower light curve residual is obtained by setting $T_2 = 6400$ K rather than the value $T_2 = 6076$ K given in Table 4 of Deb & Singh (2011).

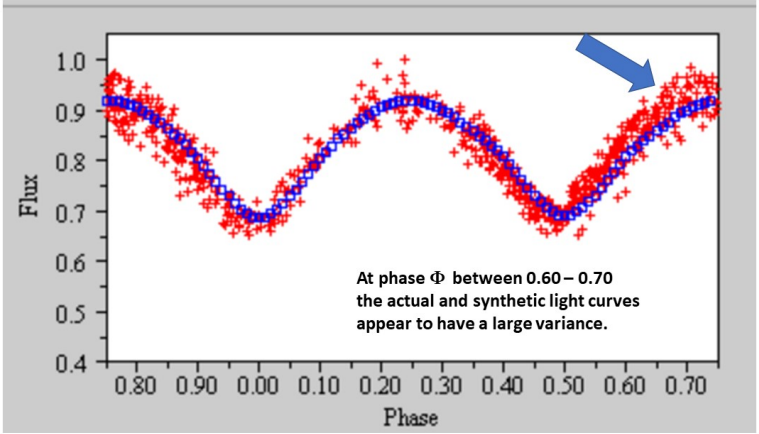

Figure 4.1: The data for ASAS 105030–0241.7 are less dense between phases 0.1 to 0.3. A significant difference between the ASAS data and the synthesized light curve is indicated by the arrow.

Considering the above findings, it is not clear why these discrepancies exist. Some errors reported here appear to be typos in the tables of the Deb & Singh (2011) article. Because the focus of this investigation was to determine if there is a relationship between the light curve appearance when varying q and i, these findings were not pursued further.

Although there are only 49 systems, making it a small statistical sample, it was noted that there is no clustering of the parameters around any particular values, as indicated in Fig. 4.2. This means that all the parameters are randomly distributed, arguing against an evolutionary trend towards any particular configuration. However, there are certain changes that occur in the light curves as the parameters are varied. In particular, if the inclination of a binary system is too low, an eclipse will not be seen; as the inclination increases the depth of the eclipses increase and the shape of the eclipse changes. In the next section, changes in the depth and shape of the eclipsing light curve are examined using the parameters from the sample of known systems as the starting point.

4.2 Synthesised light curves

A modelled light curve was created using the parameters provided by Deb & Singh (2011) for each star. The i values were taken from Table 4.1. The inclination angle was then adjusted in intervals of 5° ranging from 70° up to 90° and new synthetic light curves were generated. In total six modelled light curves were generated for each star. The original inclination was not used, only the stepped inclination light curves were used for further analysis.

Each of the six synthetic light curve files generated by BM3 was imported into Excel and these were plotted on one graph to note trends emerging for that star. Each graph thus shows an original inclination that appears in red, followed by the five plots for the inclinations at $70^\circ, 75^\circ, 80^\circ, 85^\circ$ and 90°. So as not to clutter the text here with excessive figures, the light curves of the 49 stars are presented in Appendix A. For 14 sources, the original inclinations, which are plotted in red, have a value less than 70° and therefore have a smaller amplitude than the modelled curves.

Note also that the figures have been plotted in order of increasing mass ratio q rather than by right

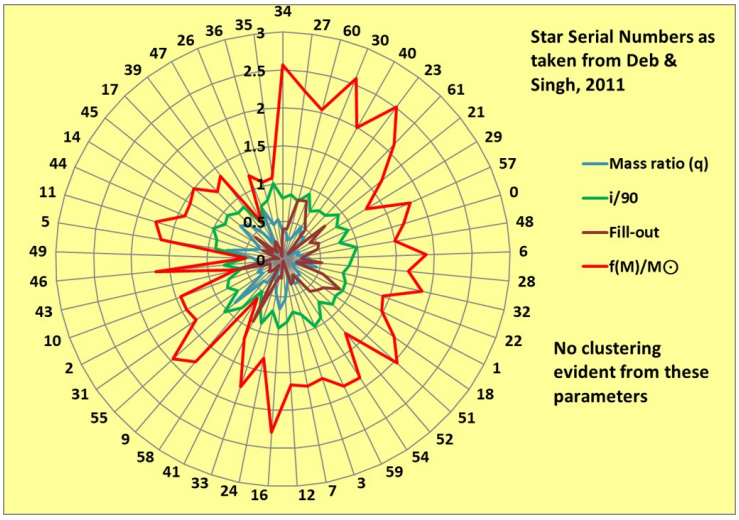

Figure 4.2: Spider diagram showing no clustering of the sample around particular values of the parameters.

ascension. Most plots have a normalised flux scale between 0.4 and 1.0 (a few of the high mass ratio systems start at 0.3). From a quick scan of the figures it can be seen that as the mass ratio increases, so too do the depths of the minima. This is just a general trend, it is not a hard and fast condition. Because the depth of the minima does not always increase as the mass ratio increases, this indicates that the depth of the minima depend on parameters other than just the mass ratio and inclination. For example, a third light could cause such changes.

The next step entailed creating another spreadsheet in which each of the 49 stars' light curves were separately evaluated quantitatively. The depths and widths of both primary and secondary minima at various heights above each minimum were measured for each of the inclination angles.

In BM3, normalised fluxes are calculated according to the brightest (smallest magnitude) data point in the observed data. The mean light curves are therefore offset from 1.0 by some amount δ in normalised flux. The depth of the minima relative to the maximum needs to be determined so the light curves need to be corrected for this offset. An example of how these corrections are applied is shown in Table 4.2 for the synthesised light curves of DS62 = ASAS 234718–0805.2 which are shown in Fig. 4.3. The normalisation offset in this case is $\delta = 0.0700$ which is added to all measured quantities to shift the curves up by this amount. In all further calculations, shifted values are used.

Table 4.2: Data for the secondary minima across five inclination angles for DS62 = ASAS 234718–0805.2. For DS62 the normalisation offset is $\delta = 0.0700$.

DS 62	Inclination Angle				
	70°	75°	80°	85°	90°
Secondary Minimum value s_i in normalised flux	0.7160	0.6973	0.6944	0.6930	0.6923
Secondary Min. corrected for normalisation factor δ	0.7860	0.7673	0.7644	0.7630	0.7623
Minima depth difference between i and $i = 90°$	0.0237	0.0050	0.0021	0.0007	0.0000
Minima depth relative to 90°.	1.0313	1.0066	1.0027	1.0009	1.0000

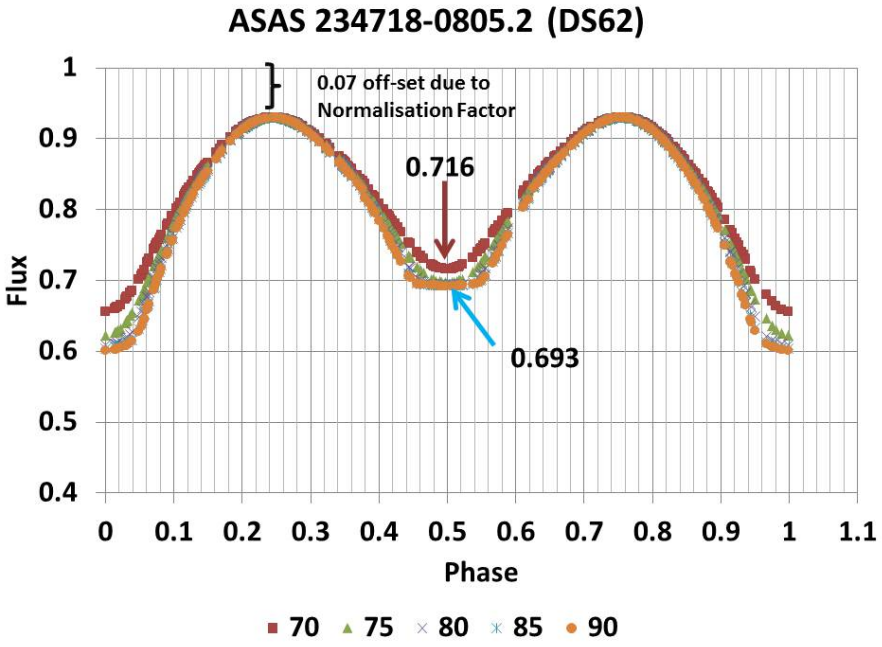

Figure 4.3: The modelled light curves for various inclination angles for DS62 = ASAS 234718–0805.2 showing the secondary minima at $i = 70°$ and $i = 85°$.

4.3 Results

4.3.1 Qualitative observations

It is a well known feature of W UMa light curves that as the inclination increases so too do the depths of the primary and secondary eclipses. This is a geometrical effect caused by more of each star's surface area being blocked by the foreground star during eclipse. This can be seen particularly clearly for stars whose initial inclination is way below the modelled values from $i = 70°$ to $i = 90°$, as can be seen, for example, in Figs. A.48 and A.37.

Totally eclipsing systems, i.e. those with inclinations close to 90°, are particularly convenient to study because flat eclipses can occur which help to constrain modelled parameters, and therefore provide better solutions. The light curve of DS62 shown in Fig. 4.3 has a flat secondary eclipse, whereas the primary eclipse, which is shown more clearly in Fig. A.8, does not appear flat, even at an inclination of $i = 90°$. Although the primary eclipse is total at this inclination, limb darkening of the eclipsed star gives the light curve a rounded appearance rather than appearing flat.

The trend noted here, that does not appear to have attracted attention in the literature, is that the secondary eclipse tends to flatten out before the primary eclispe, and does so faster than the primary eclipse. It has been noted that for low q values the secondary minima will have a flat appearance for a larger range of i than for high q values. Rucinski (1997) has mentioned that there is some correlation between the light amplitudes and how these may vary depending on q but has not expanded on it.

These qualitative observations, based on the synthesized light curves in Appendix A, have been analysed quantitatively, as discussed in the next section.

4.3.2 Quantitative analysis

From the analysis shown in Table 4.3 it is evident that the larger the value of q the higher the deviation to be expected between $s_{70^\circ}/s_{90^\circ}$ and $s_{90^\circ}/s_{90^\circ} = 1$. The value of $s_{90^\circ}/s_{90^\circ} = 1$ is not shown in Table 4.3.

To analyse this situation further, Table 4.4 was developed. Two trends are noticeable. The one trend is that for each star as i increases, the ratio of the difference between two successive minima decreases. This happens from left to right in each row of Table 4.4 (see columns 4 to 7). In addition to this, for increasing values of q the trend becomes more pronounced, as can be seen by examining the last column of the table.

When the ratios of the depths of secondary minima in Table 4.4 for successive 5° intervals fall below 0.005 (for example $\frac{s_{80^\circ}-s_{85^\circ}}{s_{90^\circ}} < 0.005$), it has been noted that the secondary minima start to appear flat. The mass ratio q has an influence on the inclination that the secondary minimum starts to appear flat. The first point to note is that if $i \leq 75^\circ$ then regardless of the value of q, light curves will not appear flat. This is illustrated in Fig. 4.4. In Fig. 4.5, Fig. 4.6 and Fig. 4.7 the influence of q on the inclination at which flatness occurs is shown. From these plots it can be seen that the secondary minimum will appear flat if the inclination lies between 75° and 80° for $q < 0.21$, whereas for $q < 0.63$ a flat secondary minimum will only occur if the inclination lies between 85° and 90°. These results are summarised in Table 4.5.

Table 4.3: Depth of secondary minimum s_i expressed as a fraction with respect to s_{90°. The stars are presented in order of increasing mass ratio q to demonstrate the influence of this parameter.

Star No.	ASAS ID	q	Type	$s_{70^\circ}/s_{90^\circ}$	$s_{75^\circ}/s_{90^\circ}$	$s_{80^\circ}/s_{90^\circ}$	$s_{85^\circ}/s_{90^\circ}$
29	101602–0618.5	0.100	A	1.0072	1.0042	1.0019	1.0006
41	143504+0906.8	0.111	A	1.0110	1.0053	1.0026	1.0008
1	003628+2132.3	0.136	A	1.0186	1.0054	1.0020	1.0000
18	062605+2759.9	0.169	A	1.0422	1.0093	1.0022	1.0007
43	152243+1615.7	0.173	A	1.0277	1.0048	1.0024	1.0007
22	073338–5007.4	0.190	A	1.0403	1.0054	1.0027	1.0009
28	100248+0105.7	0.195	A	1.0320	1.0047	1.0023	1.0007
62	234718–0805.2	0.203	A	1.0313	1.0066	1.0027	1.0009
3	012104+0736.3	0.226	A	1.0498	1.0105	1.0029	1.0009
57	204628–7157.0	0.228	A	1.0491	1.0096	1.0024	1.0007
47	165717+1059.8	0.231	A	1.0539	1.0119	1.0029	1.0007
21	073246–2047.5	0.250	A	1.0718	1.0200	1.0034	1.0011
60	233655+1548.1	0.256	A	1.0676	1.0248	1.0064	1.0017
48	171358+1621.0	0.277	A	1.0625	1.0199	1.0030	1.0010
10	033459+1742.6	0.279	W	1.0778	1.0241	1.0028	1.0008
52	182913+0647.3	0.286	W	1.0862	1.0295	1.0035	1.0010
33	110505+0509.1	0.297	A	1.0897	1.0309	1.0028	1.0007
30	104033+1334.0	0.303	A	1.1011	1.0371	1.0032	1.0010
51	180921+0909.1	0.305	A	1.1125	1.0416	1.0037	1.0011
31	105030–0241.7	0.313	W	1.0937	1.0342	1.0030	1.0009
7	024952+0856.3	0.315	W	1.0638	1.0235	1.0021	1.0006
44	153152–1541.1	0.330	A	1.0987	1.0392	1.0027	1.0009
46	164121+0030.4	0.335	W	1.0993	1.0397	1.0033	1.0011
27	100234+1702.8	0.348	A	1.1610	1.0725	1.0075	1.0015
6	023833–1417.9	0.356	A	1.1268	1.0546	1.0046	1.0011
59	222257+1619.4	0.360	W	1.1083	1.0474	1.0046	1.0008
54	193524+0550.3	0.362	W	1.1217	1.0546	1.0054	1.0009
2	011638–3942.S	0.370	W	1.1133	1.0511	1.0060	1.0010
9	030953–0653.6	0.373	W	1.1256	1.0566	1.0059	1.0007
23	073905–0239.1	0.373	A	1.1106	1.0517	1.0067	1.0010
58	205710+1939.0	0.375	W	1.1340	1.0606	1.0066	1.0009
34	120103+1300.5	0.382	A	1.1339	1.0654	1.0103	1.0015
49	173356+0810.0	0.395	W	1.1053	1.0492	1.0076	1.0010
14	041209–1028.2	0.401	W	1.1159	1.0554	1.0091	1.0009
61	234535+2528.3	0.401	A	1.1180	1.0569	1.0091	1.0010
39	141726+1234.1	0.428	A	1.1179	1.0581	1.0115	1.0009
11	034814+2218.9	0.442	A	1.1667	1.0862	1.0202	1.0007
24	084002+1900.0	0.455	W	1.1748	1.0930	1.0234	1.0010
32	110211+0953.7	0.459	W	1.1919	1.1130	1.0426	1.0066
36	123300+2642.9	0.471	W	1.1379	1.0733	1.0183	1.0011
40	141937+0553.8	0.491	A	1.2402	1.1433	1.0469	1.0007
35	121206+2232.0	0.527	W	1.1973	1.1104	1.0351	1.0011
12	034928+1254.7	0.534	W	1.2194	1.1296	1.0445	1.0009
17	051832–6813.6	0.630	W	1.2244	1.1425	1.0630	1.0038
16	051114–0833.4	0.656	W	1.2659	1.1721	1.0817	1.0080
45	155649+2216.0	0.709	A	1.2637	1.1734	1.0851	1.0141
26	100141+1724.5	0.729	W	1.2617	1.1712	1.0848	1.0153
5	014854–2053.6	0.750	A	1.3433	1.2333	1.1243	1.0264
55	194813+0918.5	0.846	A	1.3761	1.2698	1.1543	1.0509

Table 4.4: Difference in secondary minima depth relative to s_{90°. Columns 4 to 7 list values for incremental changes of 5°, while column 8 is for the overall difference between 70° and 90°.

Star No.	ASAS ID	q	$\frac{s_{70^\circ}-s_{75^\circ}}{s_{90^\circ}}$	$\frac{s_{75^\circ}-s_{80^\circ}}{s_{90^\circ}}$	$\frac{s_{80^\circ}-s_{85^\circ}}{s_{90^\circ}}$	$\frac{s_{85^\circ}-s_{90^\circ}}{s_{90^\circ}}$	$\frac{s_{70^\circ}-s_{90^\circ}}{s_{90^\circ}}$
29	101602–0618.5	0.100	0.0031	0.0022	0.0013	0.0006	0.0072
41	143504+0906.8	0.111	0.0058	0.0026	0.0018	0.0008	0.0110
1	003628+2132.3	0.136	0.0132	0.0034	0.0020	0.0000	0.0186
18	062605+2759.9	0.169	0.0329	0.0071	0.0015	0.0007	0.0422
43	152243+1615.7	0.173	0.0229	0.0024	0.0017	0.0007	0.0277
22	073338–5007.4	0.190	0.0349	0.0027	0.0019	0.0009	0.0403
28	100248+0105.7	0.195	0.0273	0.0025	0.0015	0.0007	0.0320
62	234718–0805.2	0.203	0.0247	0.0039	0.0018	0.0009	0.0313
3	012104+0736.3	0.226	0.0393	0.0077	0.0020	0.0009	0.0498
57	204628–7157.0	0.228	0.0394	0.0073	0.0017	0.0007	0.0491
47	165717+1059.8	0.231	0.0420	0.0090	0.0022	0.0007	0.0539
21	073246–2047.5	0.250	0.0518	0.0166	0.0023	0.0011	0.0718
60	233655+1548.1	0.256	0.0427	0.0185	0.0047	0.0017	0.0676
48	171358+1621.0	0.277	0.0426	0.0169	0.0020	0.0010	0.0625
10	033459+1742.6	0.279	0.0537	0.0213	0.0020	0.0008	0.0778
52	182913+0647.3	0.286	0.0568	0.0259	0.0025	0.0010	0.0862
33	110505+0509.1	0.297	0.0588	0.0282	0.0021	0.0007	0.0897
30	104033+1334.0	0.303	0.0641	0.0339	0.0022	0.0010	0.1011
51	180921+0909.1	0.305	0.0709	0.0379	0.0026	0.0011	0.1125
31	105030–0241.7	0.313	0.0596	0.0312	0.0021	0.0009	0.0937
7	024952+0856.3	0.315	0.0403	0.0214	0.0015	0.0006	0.0638
44	153152–1541.1	0.330	0.0595	0.0365	0.0018	0.0009	0.0987
46	164121+0030.4	0.335	0.0596	0.0364	0.0023	0.0011	0.0993
27	100234+1702.8	0.348	0.0886	0.0649	0.0060	0.0015	0.1610
6	023833–1417.9	0.356	0.0722	0.0500	0.0035	0.0011	0.1268
59	222257+1619.4	0.360	0.0609	0.0428	0.0037	0.0008	0.1083
54	193524+0550.3	0.362	0.0671	0.0492	0.0044	0.0009	0.1217
2	011638–3942.S	0.370	0.0622	0.0451	0.0050	0.0010	0.1133
9	030953–0653.6	0.373	0.0690	0.0507	0.0052	0.0007	0.1256
23	073905–0239.1	0.373	0.0589	0.0449	0.0057	0.0010	0.1106
58	205710+1939.0	0.375	0.0734	0.0540	0.0057	0.0009	0.1340
34	120103+1300.5	0.382	0.0684	0.0552	0.0088	0.0015	0.1339
49	173356+0810.0	0.395	0.0561	0.0416	0.0066	0.0010	0.1053
14	041209–1028.2	0.401	0.0605	0.0463	0.0082	0.0009	0.1159
61	234535+2528.3	0.401	0.0611	0.0479	0.0081	0.0010	0.1180
39	141726+1234.1	0.428	0.0599	0.0466	0.0106	0.0009	0.1179
11	034814+2218.9	0.442	0.0805	0.0660	0.0195	0.0007	0.1667
24	084002+1900.0	0.455	0.0817	0.0696	0.0224	0.0010	0.1748
32	110211+0953.7	0.459	0.0789	0.0705	0.0360	0.0066	0.1919
36	123300+2642.9	0.471	0.0646	0.0551	0.0172	0.0011	0.1379
40	141937+0553.8	0.491	0.0969	0.0963	0.0462	0.0007	0.2402
35	121206+2232.0	0.527	0.0869	0.0753	0.0340	0.0011	0.1973
12	034928+1254.7	0.534	0.0898	0.0850	0.0436	0.0009	0.2194
17	051832–6813.6	0.630	0.0819	0.0794	0.0593	0.0038	0.2244
16	051114–0833.4	0.656	0.0938	0.0904	0.0737	0.0080	0.2659
45	155649+2216.0	0.709	0.0904	0.0883	0.0709	0.0141	0.2637
26	100141+1724.5	0.729	0.0904	0.0864	0.0695	0.0153	0.2617
5	014854–2053.6	0.750	0.1100	0.1090	0.0979	0.0264	0.3433
55	194813+0918.5	0.846	0.1064	0.1155	0.1034	0.0509	0.3761

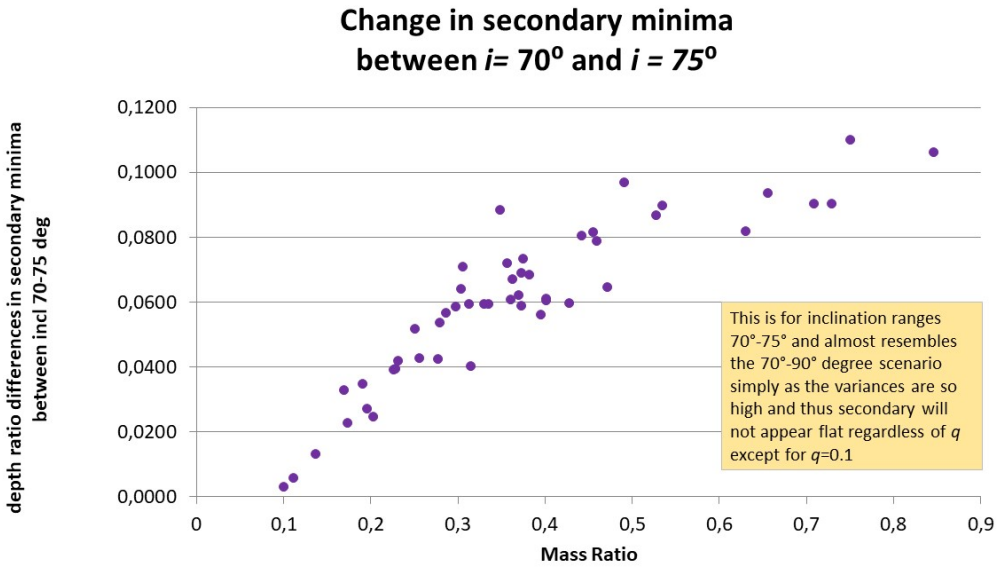

Figure 4.4: For almost all q there will be some variance in secondary minima when $70^\circ \leq i \leq 75^\circ$ and therefore profiles will usually appear rounded for secondary minima

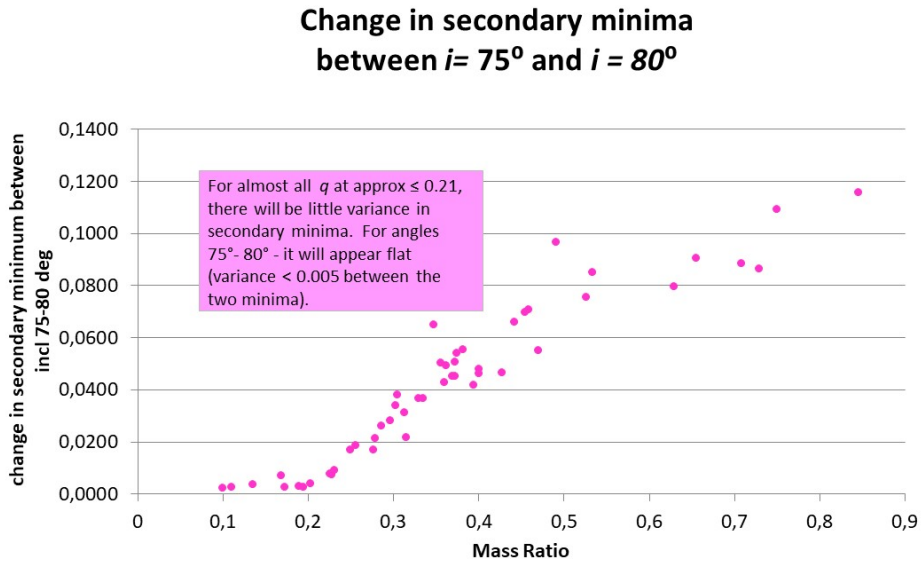

Figure 4.5: For values of $q \leq 0.21$, there will be little variance in secondary minima for $75^\circ \leq i \leq 90^\circ$ and will thus appear flat.

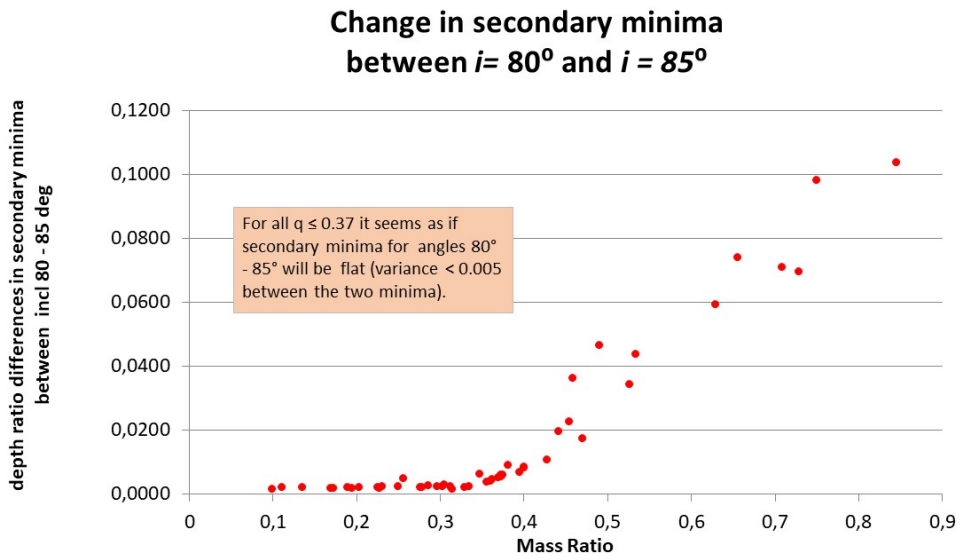

Figure 4.6: It can be seen that for all $q \leq 0.37$, the secondary minima for inclination $80^\circ \leq i \leq 90^\circ$ may appear flat as the percentage difference between successive secondary minima is below 0.005.

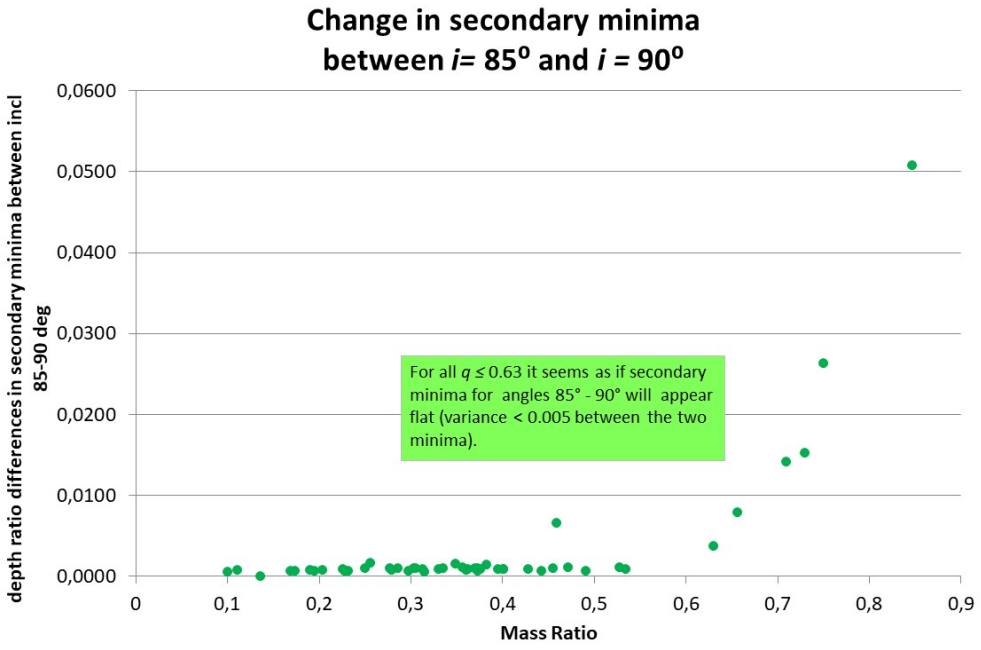

Figure 4.7: It is evident that for all $q \leq 0.63$ the secondary minima for inclination $85^\circ \leq i \leq 90^\circ$ may appear flat as the percentage difference is below 0.005. Conversely for $q > 0.63$ the secondary minima will have a larger variance between amplitudes at $i = 85^\circ$ and $i = 90^\circ$ and thus the profile will appear rounded.

Table 4.5: The cut-off values for i and q and the appearance of the secondary minima in the sample of 49 W UMa stars. The values for i and q may need refinement or small adjustments as the sample size is too small to allow for more precise values.

q	Range of i	Appearance of Secondary Minimum	Relevant Figures
All q	$< 75^\circ$	Rounded	A.1 to A.49
$q \leq 0.21$	$75^\circ - 90^\circ$	Flat	A.1 to A.8
$q \leq 0.37$	$80^\circ - 90^\circ$	Flat	A.1 to A.28
$q \leq 0.63$	$85^\circ - 90^\circ$	Flat	A.1 to A.44
$q > 0.63$	$0^\circ - 90^\circ$	Rounded	A.45 to A.49

Therefore depending on how low the q value is, the range of possible inclinations for which the secondary minima will appear "flat" and not have a large variation can be established. Given that the size of the sample is limited to 49 binary stars, which is somewhat skewed towards low q values, precise cut-off values for q where the secondary minima will have a flat appearance, cannot be established. A few small deviations have been noted so a larger sample will be necessary to improve on the precision. Furthermore, the cut-off values are determined for values of i and q only. It is possible that other factors such as fillout factor f could also influence the shape of the secondary minimum, as could the presence of a third light. Figures in the Appendix that illustrate the effect of each range of parameters are indicated in the last column of Table 4.5.

4.4 Conclusion

It has been found through both qualitative and quantitative assessments that the appearance of light curves for W UMa types A and W stars are influenced by q and that discreet cut-off for q emerged as to when the secondary minimum may have a flat rather than rounded appearance. This phenomena of appearing flat is more pronounced in the secondary minima than primary minima. The findings of this project do not imply that there is a physical relationship between q and i since these are distinct physical variables, but only that they tend to influence the appearance of the light curves, in particular the secondary minima. If the secondary minimum appears to be flat, and either i or q is known, the range for the other parameter (q or i, respectively) can be estimated. This trend was observed regardless of whether the system was of W or A type.

Depending on the extent of the variance between successive i in increments of 5° it is possible to confine the range of possible q values. If the q value is known, the range of i where the secondary minima will appear flat, can be estimated. The trend is not clearly noticeable for $i \leq 75^\circ$, but for higher inclination angles it has been found from modelling using known parameters of binary systems. These results are preliminary given the limited sample size, but can be investigated further when a larger sample becomes available.

Chapter 5

SuperWASP data

As noted earlier, the SuperWASP data usually contains many more points per source than the ASAS data. This data allows complete light curves to be constructed out of only a few nights of data, unlike ASAS which only collects one data point every third night. The SuperWASP data contains several points around the minima of the light curves which allows the timing of the minimum to be determined. Given a sufficiently long set of timing intervals makes it possible to determine the period of the system very accurately and can show whether the period is changing with time.

In this chapter, some technical details of the SuperWASP data are described and then some tests of the Deb & Singh (2011) parameter set on the SuperWASP light curves are discussed. Some possible causes of period variations are explained and then the observed minus calculated (O–C) method of period analysis is described, followed by a short description of the programme used to do the calculations. The stars analysed and the results obtained are presented in a separate chapter.

5.1 Analysis of SuperWASP data

Of the 49 stars listed in Table 4.1, data for 46 of them were found in the SuperWASP database. FITS files containing both raw and detrended data were retrieved. Using FITS Viewer 5.3[1] the data were sorted and four selected fields were converted into ASCII text files so they could be imported into other applications, such as Excel and Python programmes. The fields of interest were TMID, the time at the midpoint of the observation, TAMFLUX2, the detrended flux of the source, $\text{TAMFLUX2}_{\text{ERR}}$, the estimated error on the flux, and CAM, the camera used to collect the data for each point.

TMID was converted into HJD by applying

$$\text{HJD} = \text{TMID}/86400 + \text{Epoch}_{\text{Header}} - 2450000 \ .$$

The magnitude, Mag, was determined from the TAMFLUX2 flux values using

$$\text{Mag} = 15 - 2.5 \times \log_{10}(\text{TAMFLUX2}) \ .$$

Similarly, the uncertainty in the flux $\text{TAMFLUX2}_{\text{ERR}}$ was converted into Mag_{ERR} using

$$\text{Mag}_{\text{ERR}} = 1.08574 \times \text{TAMFLUX2}_{\text{ERR}}/\text{TAMFLUX2} \ .$$

[1] https://heasarc.gsfc.nasa.gov/docs/software/ftools/fv/

The data were then cleaned by removing outlying points, and then imported into BM3 to see how the synthesized curves compared with the observed data. Note that the SuperWASP data is recorded through a filter that is wider than a standard V-band filter, and therefore it would not be unreasonable to find slight differences between the observed and synthesized light curves.

5.2 Synthetic light curve using SuperWASP data

Following the same procedure as was done for the ASAS data, SuperWASP data were downloaded, cleaned and folded on the period. The phase-magnitude data were then imported into BM3, and parameters from Table 4.1 used to synthesize light curves. The stars for which the SuperWASP light curves presented some form of significant deviation, such as having large light curve residuals, will now be discussed briefly.

5.2.1 DS3 = AQ Psc = ASAS 012104+0736.3

The light curve of this star showed clear magnitude shifts. These shifts tend to be real, but are not unique to this star. Such shifts in amplitude are seen in several of the light curves. This could be a problem introduced into the TAMFLUX2 data by the SysRem algorithm that generates the detrended data. The general profile of the light curve is maintained, and the timing of the minima is not affected by these amplitude shifts. About 13 700 data points have been used.

The PMD is shown on the left hand of Fig. 5.1 while the synthetic curve rendered by BM3 (in blue) superimposed on the actual PMD (in red) is displayed on the bottom left hand side. The PMD residuals are also shown.

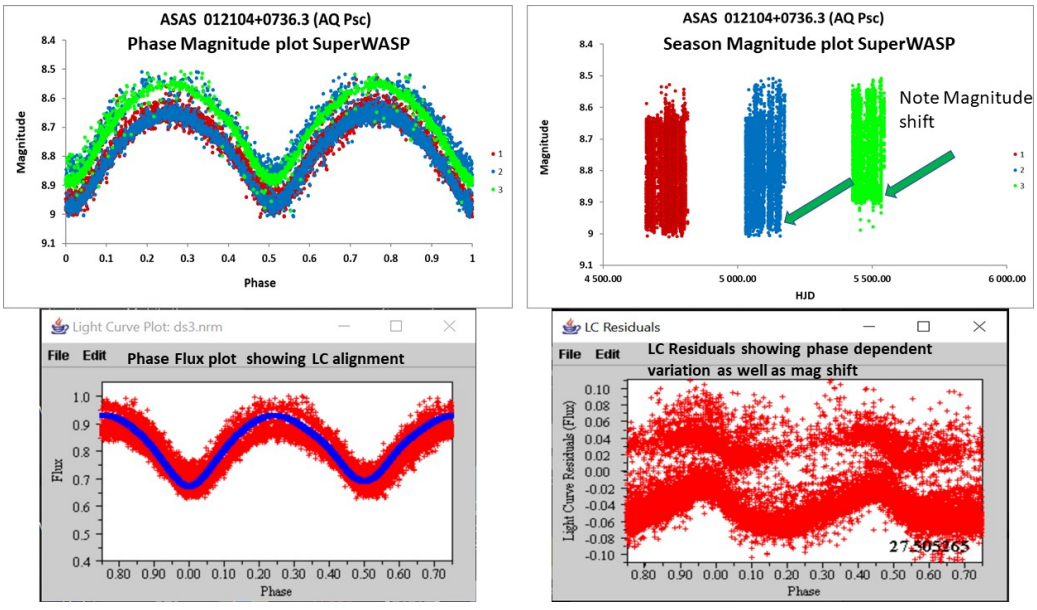

Figure 5.1: SuperWASP PMD of DS3 = AQ Psc = ASAS 012104+0736.3. Magnitude shits are evident in both the plotted and synthetic light curves, light curve residuals and season magnitude diagram.

5.2.2 DS10 = V1123 Tau = ASAS 033459+1742.6

From the light curves modelled by BM3 shown in Fig. 5.2 a misalignment of the synthetic light curve compared to the actual light curve is visible at the maxima. This may need further investigation.

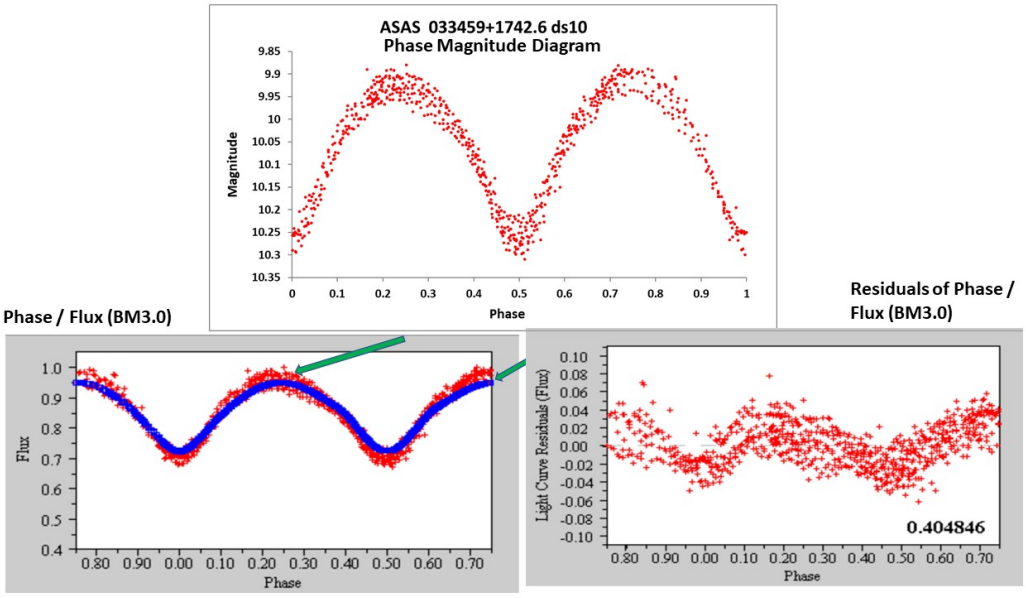

Figure 5.2: SuperWASP PMD of DS10 = V1123 Tau = ASAS S033459+1742.6 compared to its synthesized data, showing a misalignment of the maxima.

5.2.3 DS14 = YY Eri = ASAS 041209-1028.2

The SuperWASP data for this star was immensely problematic to clean compared to other stars. There are about 62 000 data points. The light curve shows many amplitude shifts, the cause of which is not clear. A PMD of the folded light curve is shown in Fig. 5.3, which clearly shows how the amplitude varies dramatically during certain portions of the time series.

The shifts suggest regular magnitude changes which are not related to the data seasons. There are instances where the amplitude increases and others where it decreases. Kim et al. (1997) studied the variation of V and $B-V$ light variations and reported a sinusoidal variation of (MaxII – MaxI) in V which they propose is due to the Applegate mechanism (Applegate, 1992) (which will be discussed in subsection 5.4).

Because this star has been well studied, further analysis of the SuperWASP data was not done at this point. To explain the differences in maxima, Yang & Liu (1999); Liu & Yang (2003) suggest YY Eri is subject to the O'Connell effect.

5.2.4 DS16 = ER Ori = ASAS 051114-0833.4

The temperatures for the two stars in this system are given in Table 4.1 as $T_1 = 6250\,\mathrm{K}$ and $T_2 = 5931\,\mathrm{K}$, indicating a temperature difference of $\Delta T = 269\,\mathrm{K}$. Other studies (see for example, Kim et al. (2003)) have found the temperatures are much closer in value. The period has shown erratic changes, and the system appears to have a third light (Pribulla et al., 2009). Revised modelling

by Lame'E et al. (2010) using their U, B, V data support almost equal temperatures of $T_1 = 5554$ K and $T_2 = 5557$ K.

SuperWASP contains almost 30 000 data points for this star. The light curve generated from this data looks similar to the U, B, V data of Lame'E et al. (2010). In particular, the SuperWASP light curve has minima with approximately equal depths, which is contrary to the light curve synthesized using the data from Table 4.1. Note that the ASAS data, which consists of only 560 points, does show a difference between the two minima.

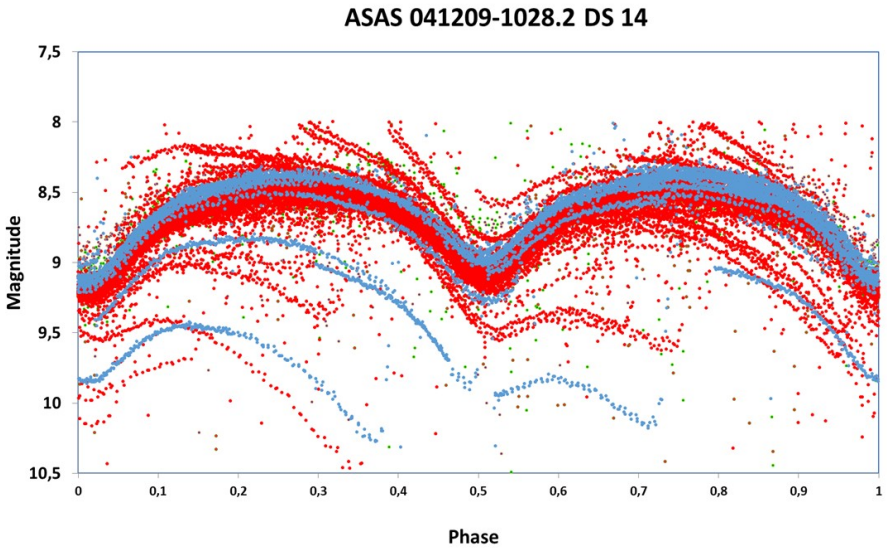

Figure 5.3: SuperWASP PMD of DS14 = YY Eri = ASAS 041209-1028.2 showing the erratic amplitude variations of the light curve.

5.2.5 DS21 = TY Pup = ASAS 073246-2047.5

The Deb & Singh (2011) parameters for this star were noted as being a problem when fitting to ASAS data. SuperWASP data contain ~ 2400 points which also do not present a good fit when using the parameters in Table 4.1. In the radial velocity studies of Duerbeck & Rucinski (2007) a mass ratio $q \approx 0.246$ was proposed. However, a recent study by Sarotsakulchai et al. (2018) reports that this value is incorrect and ought to be $q = 0.184$. When using this value in the synthesized models a good fit to the data is obtained, as shown in Fig. 5.5. It is not clear why the radial velocity method employed by Duerbeck & Rucinski (2007) produces a q_{sp} that does not fit the data as well as the value of q_{ph} obtained by Sarotsakulchai et al. (2018) using photometric data.

5.2.6 DS23 = V868 Mon = ASAS 073905–0239.1

If the inclination from Table 4.1, $i = 72.14°$, is replaced by $i = 67°$ the synthesized data produces an improved fit to the SuperWASP data.

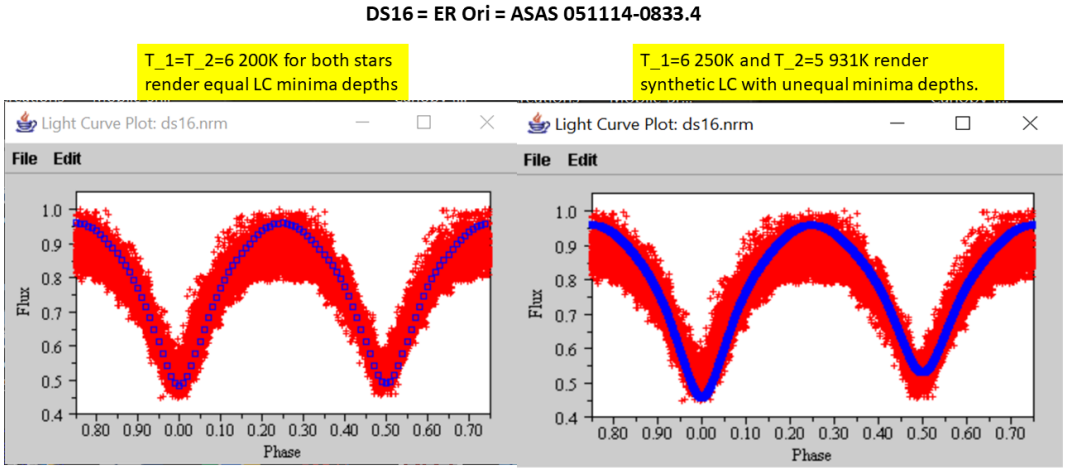

Figure 5.4: SuperWASP data of DS16 = ER Ori with synthesized fit for temperatures $T_1 = T_2 = 6200$ K (left) and $T_1 = 6250$ K and $T_2 = 5931$ K (right). The synthesized fit on the left gives a better fit to the primary minimum than that on the right.

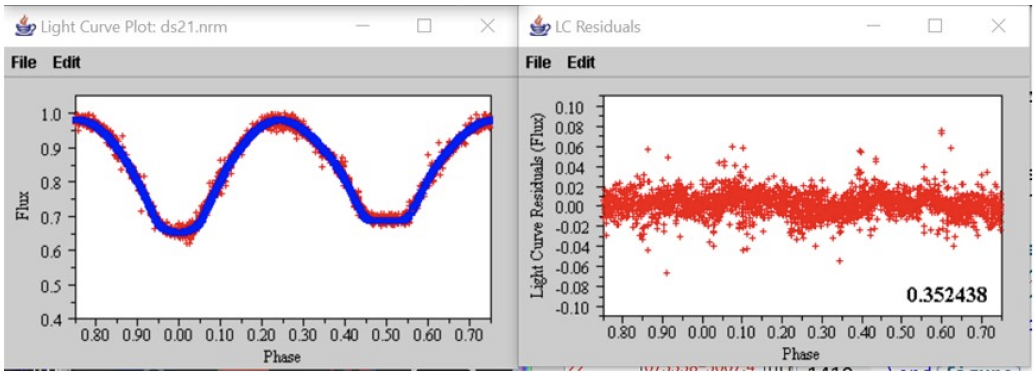

Figure 5.5: SuperWASP data (red) of DS21 = TY Pup = ASAS 073246–2047.5 synthesized (blue) using $q = 0.18$ on the left. The residuals on the right show that the synthesized model is a good fit to the data.

Zhou et al. (2015) used B,V,R_c,I_c observations to model V868 Mon using the WD code, constraining their models with the mass ratio $q = 0.373$ determined by Pribulla et al. (2009). They determined temperatures for the two components of $T_1 = 7400\,\mathrm{K}$ and $T_2 = 6446\,\mathrm{K}$ which are higher than in Table 4.1, and $i = 78.52^\circ$ or $i = 83.67^\circ$ depending on whether it is a binary or triple system.

Clearly, further modelling is required to match the synthesized model with the SuperWASP data, and to see if it supports a third light or not.

5.2.7 DS43 = OU Ser = ASAS 152243+1615.7

The synthesized light curve produced using the Deb & Singh (2011) parameter does not give a good fit to the SuperWASP data. An improved model was obtained using $i = 49.83^\circ$, $T_1 = 5421\,\mathrm{K}$, $T_2 = 5619\,\mathrm{K}$ and $\Omega_1 = 2.09$, but even this model has large residuals. Adding spots to the solution did not yield any improvement. There is not sufficient data to suggest the presence of a third body.

5.3 Period changes

To study the possible causes of orbital period changes, a process of comparing the observed period of the binary star system to that of the calculated period has been developed which is known as the O–C method. Nelson et al. (2014) have suggested calling this analysis method an "eclipse timing diagram" or ET because O–C can refer to any observation where a calculated value can be subtracted from an observed value, and is not restricted to eclipse timings. In this dissertation, the term O–C will be retained for referring to eclipse timing analysis, although the term ET is indeed appropriate.

In this regard the period P is the time for the system to make a complete orbit. The unit of measure is usually expressed in days. The measurement for a cycle is made from the time of minimum light when the light curve is at its primary eclipse (primary minimum), to the next primary minimum. This is the measured period. Usually, the period is measured over more than one cycle, in which case the number n of cycles between primary minima need to be counted. After many such period measurements, slight changes in phase may be detected, indicating small changes in period. These changes can be detected by comparing the measured period to the calculated period. Thus we have the following situation:

$$T_n - T_0 = nP \tag{5.1}$$

where T_n is the time of minimum after n cycles and T_0 is the epoch of the first minimum in this set of measurements. The phase φ of an orbital cycle is defined as (Sterken, 2005):

$$\varphi = \frac{T - T_0}{P} - E(t) \tag{5.2}$$

where T is a time measured at any arbitrary time and E(t) is the integer element of $\frac{T-T_0}{P}$ and thus $\varphi \in [0,1]$.

In the literature, it is common practice to represent the cycle number by E rather than n, which therefore leads to the expressions for observed O, and calculated times, C, of minimum light as

$$\mathrm{O} = T_0 + P \times E \tag{5.3}$$

$$\mathrm{C} = T_0 + P_{\mathrm{calc}} \times E \tag{5.4}$$

$$\mathrm{O–C} = (P - P_{\mathrm{calc}}) \times E \tag{5.5}$$

where P_{calc} is the calculated period.

If the period P is constant, then the O–C graph takes the form of a straight line. If $P_{\rm calc}$ is different to P then the straight line has a non-zero value for its slope. $P_{\rm calc}$ can then be adjusted until the slope is zero, and then $P = P_{\rm calc}$. Time is usually measured in Heliocentric Julian Days (HJD) so that at any future time $T = T_0 + P * E$ the light curve will be at the phase of E.

If the period is not constant, then the O–C plot will not be a straight line. It could have a polynomial form, a sinusoidal form, or a combination of a polynomial and sinusoidal terms. The simplest polynomial after a straight line is a second order equation (parabola) which takes the form

$$\text{O–C} = (P - P_{\rm calc})E = aE^2 + bE + c \ . \tag{5.6}$$

Differentiation of eqn. (5.6) with respect to E gives

$$\frac{d}{dE}(P - P_{\rm calc}) \times E = \frac{dP}{dE} \times E + (P - P_{\rm calc}) = 2aE + b \tag{5.7}$$

This shows that the rate of period change in d cycle^{-1} is

$$\frac{dP}{dE} = 2a \ .$$

A more conventional unit for the rate of change of period is d yr^{-1} which is given by

$$\dot{P} = \frac{365.24 \times 2a}{P_0} \ .$$

Some period changes may be a combination of linear, parabolic and sinusoid in form. These tend to be additive and depend on the various contributing circumstances of the eclipsing binary system. An example of a star with a sinusoid variation in its period is XY UMa (Pojmanski & Geyer, 1990), whose primary minimum (Min I) is given by

$$\text{Min I} = T_0 + P_0 \times E + a_s \sin\left(\frac{2\pi(E - T_s)}{P_s} - \frac{\pi}{2}\right) \ . \tag{5.8}$$

The amplitude of the sinusoid is a_s which has a period P_s. T_s is an epoch at which the sinusoid is a minimum. It is important to note that there are thus two different periods at stake that have an influence on the timing of the the minimum as observed in the light curve. It turns out that the sinusoidal term is due to a third body perturbing the orbit of the binary so that the amplitude term can be written as $a_s = a \sin i$ and T_s is the epoch when periastron is passed (Pojmanski & Geyer, 1990). After applying these concepts, the ephemeris can be written as

$$\text{Min I} = T_0 + P_0 \times E + \Delta T \tag{5.9}$$

where

$$\Delta T = \frac{r}{c} \sin i \sin(\nu + \omega) = \frac{a \sin i}{c}(1 - e^2)\frac{\sin(\nu + \omega)}{1 + e\cos\nu} \ . \tag{5.10}$$

The variables in this equation are associated with the orbit of the third body and are described in Pojmanski & Geyer (1990).

5.4 The Significance of Period Variation Analysis

Period variations can signify evolutionary changes in the binary eclipsing system, whether they are geometrical or structural in nature (Kalimeris et al., 1994a; Sterken, 2005; Nelson et al., 2016). A high degree of accuracy is required when analysing the data. Quadratic changes in the period may arise from mass-transfer or overall mass loss from the system, leading to a reduction in angular momentum. A light time effect due to the presence of a 3$^{\text{rd}}$ body (also called apsidal effects), can give rise to a sinusoidal term in the O–C residuals as discussed above for XY UMa .

The Applegate phenomenon (Applegate, 1992), is also expected to create a sinusoidal term in an O–C plot. This effect should produce a change on the order of $\Delta P/P \approx 10^{-5}$ on a time scale of decades (Applegate, 1992; Lohr et al., 2015). If the Applegate effect is short-lived, Nelson et al. (2016) suggest it may introduce a quadratic change.

Kalimeris et al. (1994a) summarises the variations as of either short-term or long-term in nature. Short-term variations include non-static long scale circulation within the eclipsing binary's common envelope, periodic changes in strong magnetic fields, as well as mass movements in the interior of either one or both of the system's components. The changes in magnetic field are mostly associated with the Applegate effect.

Long-term increases in periods are thought to be as a result of evolutionary processes such as mass-transfer from the hotter star to the cooler star, or an expansion of one of the components. If the component masses are taken to be point masses, the relationship between the orbital angular momentum J of a W UMa-type binary system and its period P, is by (Yıldız, 2014)

$$J = 1.24 \times 10^{52} (M_1 + M_2)^{\frac{5}{3}} P^{\frac{1}{3}} \frac{q}{(1+q)^2} [\mathrm{g\,cm^{-2}\,s^{-1}}], \tag{5.11}$$

with masses measured in $M_\odot$ and P measured in d. This equation shows that changes in P imply changes to the angular momentum J or mass ratio q of the system.

Conversely, under conditions of total mass and angular momentum conservation, if $dP/dt > 0$, then the more massive star, M_1, is gaining mass as given by (Nelson et al., 2014)

$$\frac{dM_1}{dt} = \left[3P \times \left(\frac{1}{M_2} - \frac{1}{M_1} \right) \right]^{-1} \times \frac{dP}{dt}. \tag{5.12}$$

5.5 Period Analysis programme

In order to perform an O–C analysis of the SuperWASP data, a Python routine developed by Ms P Skelton was used. Details of the programme and how it is used can be found in Smits & Skelton (2019).

Briefly, the HJD, the magnitude and the magnitude error of the data as described in section 5.1 were put in an input file, as well as an initial period and epoch for the star. The programme then presents minima to which parabolas can be fitted, as indicated in the left hand diagram of Fig. 5.6. An interval from 0.04 to 0.06 of the phase can be chosen to do the 2nd order fitting. The time of minimum and its uncertainty are then stored and used for the regression analysis. Once all the minima have been selected, a plot of O–C plus error bars versus cycle number is produced as, shown in the right hand diagram of Fig. 5.6. Outlying points can be removed, as indicated, before the final analysis is performed. Fits using both a linear and a quadratic ephemeris are generated. The ephemeris chosen is based on the uncertainties of the a parameter from the analysis. If the a parameter is larger than 3

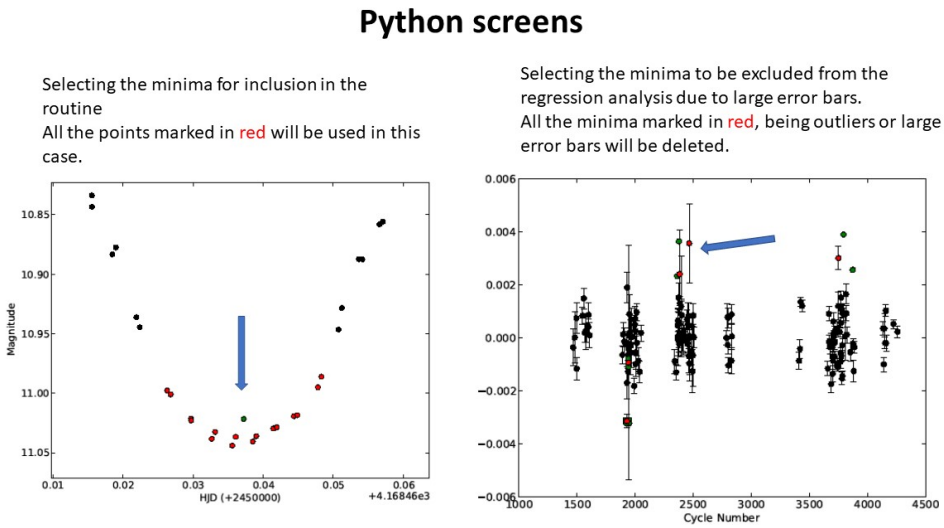

Figure 5.6: Two of the Python routine user screens for selecting appropriate data points to be included in the O–C analysis.

σ, i.e. $a > 3\Delta a$, then the second order ephemeris is used, otherwise the linear ephemeris is taken as representing the period of the system.

It is possible to add points into the various output files after the first iteration of regression analysis has been performed, and then the regression can be rerun to improve the accuracy of the O–C analysis. This scenario has been applied when suitable points from the Variable Star and Exoplanet Section of the Czech Astronomical society (B.R.N.O., 2020) have been added to the SuperWASP minima. These B.R.N.O. data points do not have error bars, so a standard value was selected to make the treatment consistent with the SuperWASP data.

The results of the O–C analysis will be discussed in the next chapter, together with a short history of the period measurements and other related facts for a small selection of stars.

Chapter 6

O–C Period Analysis

In this chapter, the results of an O–C analysis of 14 of the 46 stars from the Deb & Singh (2011) sample for which there is SuperWASP data are presented. Some properties of the stars are described, and period measurements over time discussed. Because the timeline of SuperWASP data is too short to detect any period changes, in some instances the SuperWASP times of minimum have been supplemented by timing measurements extracted from B.R.N.O. (2020). The periods and any detectable period rates of change ($a > 3\sigma_a$) determined from the O–C analysis are presented in Tables 6.1 and 6.2 respectively, in section 6.15. A short discussion on the period changes found in W-type systems is also presented because it refutes a claim in the literature.

The stars in this section are ordered according to their sequence in the Deb & Singh (2011) article. Their GCVS designation is also given.

6.1 DS6 = DY Cet

The spectral type of H16515 was determined by Houk & Smith-Moore (1988) to be F5 V. It was discovered to be variable by the *Hipparcos* mission and given its variable star name, DY Cet, and classified as EW in the 74th name list of variable stars (Kazarovets et al., 1999). Its period is listed as $P = 0.440794$ d by Pribulla et al. (2003) while Kreiner (2004a) used a linear ephemeris in an O–C analysis to get $P = 0.440790640$ d. Pribulla et al. (2009) used $P = 0.440790(6)$ d for their radial velocity study of DY Cet, from which they ascertained that this is an A-type system.

An O–C analysis of the SuperWASP data for DY Cet produced a constant period. The a coefficient in a second order model was smaller than its uncertainty so a period change could not be measured, but it is clear from the above periods and the O–C diagram presented on the Krakow Atlas of O–C diagrams[1] that the period is decreasing slowly over time. The period in Table 6.1 is compatible with the value on their website.

6.2 DS7 = EE Cet

Radial Velocity studies yielded a period $P = 0.339917$ d for EE Cet with $q = 0.315$ (Rucinski et al., 2002). It has been reported as a contact double-lined spectroscopic binary with spectral classification F8 V and that its light variability was first discovered in 1997 by the *Hipparcos* satellite mission.

[1] https://www.as.ap.krakow.pl/ephem/CET.HTM

Pribulla & Rucinski (2006) commented that EE Cet is the southern element of a visual spectroscopic system, ADS 2163, in which the northern-part is an unpublished David Dunlap Observatory spectroscopic binary, implying this is a quadrupole system, of $V_{\max} = 8.64$ mag. The northern and southern systems are separated by 5.6". It is implied that EE Cet is gravitationally impacted upon by the northern companions.

There are not many focussed studies on this star and Rucinski et al. (2002) pointed out that at that time, there was inadequate data to allow a deeper analysis of the system. However, they did suggest that it may be a promising star for future research. No detailed study of the period has been done.

The SuperWASP data has a very short time span so no period change could be detected, but even after combining the SuperWASP data with B.R.N.O. data only about 15 years' of data were available. However, a marginal ($\sigma_a = 3.8$) quadratic ephemeris is then obtained, indicating an increasing period.

6.3 DS16 = ER Ori

ER Ori was identified as a variable star by Hoffmeister (1929). It was classified as a W UMa system in 1931 and has been the subject of numerous other studies (Binnendijk, 1962). An O-C analysis of archival data plus his own observations was made by Binnendijk (1962), who noted that the period had increased in 1952 and then decreased by 1957. He obtained a period $P = 0.4234009$ d. Rovithis & Rovithis-Livaniou (1986) determined a period of $P = 0.4233993$ d but conceded it to be variable, in line with the earlier findings of Binnendijk (1962). Another study of the period was made by Kim et al. (2003) who found $P = 0.42339947$ and mention the abrupt yet unexplained variability of the period. Elements of a third body with $P_3 = 50.6(2)$ yr cannot be excluded but the period also appears to be slowing down by $\dot{P} = 7.9(9) \times 10^{-8}$ d yr^{-1} (Kim et al., 2003).

An O–C analysis of archived SuperWASP data shows a highly significant ($\sigma_a = 18$) quadratic ephemeris for this system, even though the data spans a short interval of only 2.34 years. This parabolic trend may be a portion of a sinusoidal curve and, if so, indicative of variability with a period of approximately 5 to 6 years. Additional data with a longer time span will be needed to assess the nature of the variability in more detail. The SuperWASP period is longer than previous estimates (see Table 6.1) and undergoing a much more rapid change than that reported by Kim et al. (2003). Clearly, the period of this star needs to be monitored closely to see what it does.

6.4 DS18 = AH Aur

AH Aur was discovered by Guthnick & Prager (1928) who classified it as having a typical W UMa light curve with a period $P = 0.494157$ d. The maxima were found to have equal heights while the primary and secondary minima differed by 0.1 mag. Initially, the star was named 220.1928 Aurigae.

In SIMBAD the spectral type is listed as G1, while in the HD catalogue it is given as F8. A radial velocity study by Rucinski & Lu (1999) determined a spectral type of F7 V for AH Aur, which agrees with the *Hipparcos* colours of the star. They also determined a mass ratio $q = 0.17(6)$; a slight asymmetry in the radial velocity curve of the less massive component of the binary was noted. For their analysis, Rucinski & Lu (1999) used a period $P = 0.4942624$ d which they got from the 1985 edition of the GCVS. It is not clear where this value came from. Gazeas et al. (2005) found no asymmetries in the light curve. Pribulla & Rucinski (2006) reported that it is of type A, and spectral type F7V.

New times of minima were obtained by Vanko et al. (2001) using a photoelectric photometer and CCD. They did an O–C analysis of all extant minima from which they concluded that prior to JD

2 445 000 the star was subject to pronounced period changes which make the ephemerides unusable. Their analysis of the system parameters indicates an A-type system, but they note that the system might change between A- and W-types which has led to confusion as to whether the primary or secondary minimum is being observed. Their estimated distance to AH Aur of 282 pc is close to the GAIA EDR3 distance of 249 pc.

Vanko et al. (2001) speculated that the rapid changes in period could be due to the system being a triple system, but the broadening curves of Rucinski & Lu (1999) showed no evidence of this. Pribulla & Rucinski (2006) also explored the possibility of it being a triple system but again there was no compelling evidence to indicate that this is the case.

Kreiner (2004b) used an O–C analysis of all available timings to calculate a linear ephemeris for AH Aur, which gave them a period $P = 0.4941067$ d. This is the value listed in GCVS 5.1, the most recent edition of the catalogue.

A long term period decrease $dP/dt = -2.491 \times 10^{-7}\,\mathrm{d\,yr^{-1}}$ was reported by Yu et al. (2016), suggesting rapid mass transfer between the primary star and the secondary.

The SuperWASP data (see Table 6.1) shows an increasing period rate contradictory to the findings of Yu et al. (2016). The SuperWASP result has a fit with $\sigma = 8.55$ which is a convincing result. It is possible that Yu et al. (2016) used a shorter data set to get their result.

6.5 DS26 = XY Leo

This star has been studied extensively over the past almost 90 years since its discovery by Hoffmeister (1934) who reported it as having a short period light variation. A light curve study by Hilditch (1981) categorised XY Leo as an EW type W system having a symmetric light curve. However, subsequent studies by Hrivnak (1985) and Yakut et al. (2003) indicated that the light curve is not symmetric but varies due to cool spots, magnetic fields and chromospheric activity. The light curve shows asymmetric behaviour that may not remain consistent from one season to another (Hrivnak, 1985) with a possibility of erratic mass transfer at times from the smaller component to the larger one. The notion of a third body influencing the system approximately every 10 yr may be to blame (Hrivnak, 1985), which may be a BY Draconis type body (Barden, 1987). For a triple system Yakut et al. (2003) provides values of $a_{12} \sin i = 4.083$ AU, $P_3 = 19.59$ yr and masses for the pair of $M_3 = 0.57\,M_\odot$ and $M_4 = 0.41\,M_\odot$ acting as the "third body". Pribulla et al. (2009) pointed out that this is a quadrupole system previously reported on, and provide updated spectroscopic elements, in particular $P = 0.8047497$ d for the second non-eclipsing binaries of the system.

XY Leo has a spectral classification of K0 N (Hill et al., 1975). Radial velocity analysis was performed by Hrivnak et al. (1984) who reported $q = 0.5$ with $M_1 = 0.87\,M_\odot$ and $M_2 = 0.44\,M_\odot$, $P = 0.2841$ d, and strong Ca II H and K emission lines. The emission is associated with the more massive star 1 and with a possibly chromospheric nature. Yakut et al. (2003) used $q = 0.61$ and $M_1 = 0.82\,M_\odot$ and $M_2 = 0.50\,M_\odot$.

Hilditch (1981) determined a period $P = 0.2841091$ d, but there have been numerous other versions presented with some small variations on the period by various researchers. Several studies have been conducted that indicate that the orbital period of XY Leo is changing (Yakut et al., 2003), with $\dot{P} = 2.7 \times 10^{-8}\,\mathrm{d\,yr^{-1}}$. Pribulla & Rucinski (2006) suggested that P shows intervals of increases and decreases. A follow up O–C study by Szalai et al. (2007) reported $\dot{P} = 2.85 \times 10^{-8}\,\mathrm{d\,yr^{-1}}$, and a 14 year cycle of magnetic activity.

The period of XY Leo is complex, containing both polynomial and sinusoidal variations, as can be

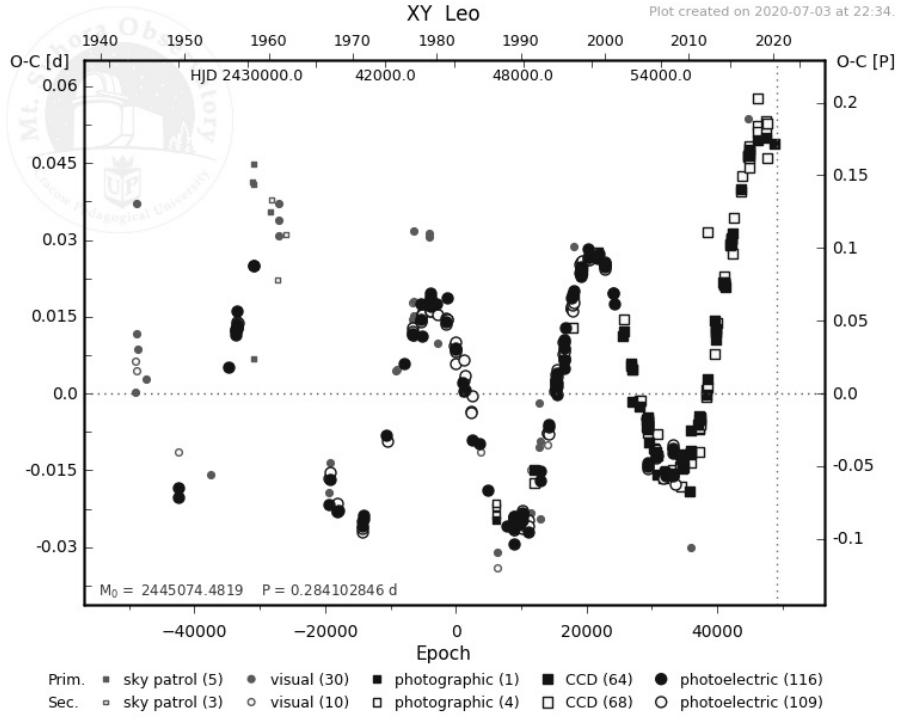

Figure 6.1: O–C analysis of XY Leo taken from Kreiner (2004a), showing the complex nature of its period.

seen from the O–C analysis shown in Fig. 6.1. The SuperWASP data of XY Leo has a short time span, but provides evidence of a changing period by virtue of the minima showing phase shifts. An O–C analysis of the SuperWASP data confirms that the period is increasing (Table 6.1), in agreement with the O–C analysis shown on the O–C Gateway webpage and in Fig. 6.1. The data span is too short to make any definitive statements about either the polynomial or sinusoidal trends in the data.

6.6 DS28 = Y Sex

Y Sex has been reported as of spectral type of F5/6 and of W UMa type A (Pribulla et al., 2009). Its variability was first observed by Hoffmeister (1934). Pribulla et al. (2009) provides an overview of the historic studies of the system. It appears to have a sinusoidal O–C variation, as can be seen in Fig. 6.2. It has been suggested that the cause of this variation is due to a third body orbiting the contact binary with a period of 57.6 yr (Wolf et al., 2000). Subsequent observations by *Hipparcos* identified the system as being part of a tight visual binary. Pribulla et al. (2009) found $q = 0.18$.

An O–C analysis of the SuperWASP data of Y Sex indicates a constant period, in disagreement with Qian & Liu (2000) who found the period decreasing. Combining SuperWASP data with B.R.N.O. points produces an increasing period (see Table 6.2). It is possible that the SuperWASP data were collected when the O–C curve is at the top of its sinusoid before turning over and starting a decreasing period. Adding the B.R.N.O points, include points on the rising section, producing an increasing period.

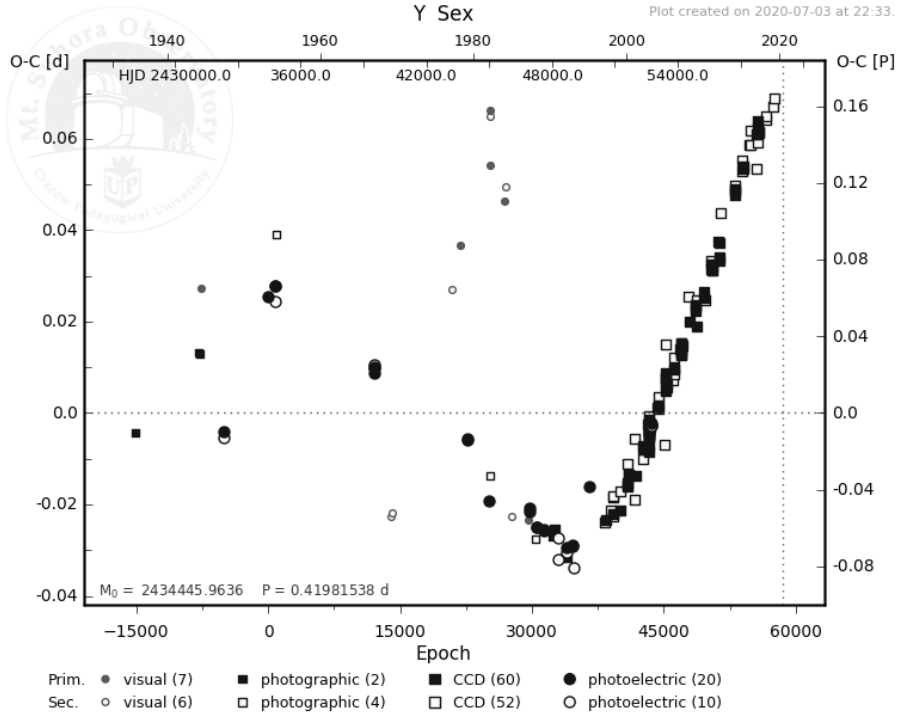

Figure 6.2: O–C diagram of Y Sex from Kreiner (2004a).

6.7 DS29 = XX Sex

XX Sex (HD 89027) was identified by Wils & Dvorak (2003) as a variable system. A period $P = 0.540110$ d was published following an O–C analysis by Pribulla et al. (2007a,b) who also classified it as spectral type F3 V system with $q = 0.100(2)$.

The period for this system was determined to be constant regardless of whether the SuperWASP data was augmented with B.R.N.O. minima.

6.8 DS31 = VY Sex

VY Sex (HD 93917) was only discovered in May 2001 by Lasala-Garcia (2001) who reported a period $P = 0.44342$ d and spectral type K0. It has been identified as having a fill-out factor $f = 0.22$ which is small, and as showing a small O'Connell effect (Gazeas et al., 2006). It was classified as of type W with $q = 0.313$ and of spectral type F9.5V by Rucinski et al. (2003). The system has not been associated with any triple nature thus far (D'Angelo et al., 2006; Pribulla & Rucinski, 2006). A radial velocity study of the system was done by Karami & Mohebi (2007).

The SuperWASP data consists of more than 139 000 points, from which 246 minima were extracted. There is a slight difference between the height of the primary and secondary maxima of $\delta m_V \sim 0.01$ mag which is consistent with the finding of Gazeas et al. (2006) of a small O'Connell effect.

To lengthen the time-line used to check for period changes, 8 B.R.N.O data-points were added to the SuperWASP minima. These points have more scatter than the SuperWASP data so the regression (see

Table 6.2) shows a less significant $\dot{P}$ than in Table 6.1, but confirms that the period of the system is slowing down.

6.9 DS32 = AM Leo

AM Leo is the brighter partner of the visual double star system ADS 8024 (Albayrak et al., 2005). It was identified as a W UMa-type binary by Worley & Eggen (1956) who determined a period $P = 0.36581$ d. Hill et al. (1975) determined a spectral type of F8 VN. A mass ratio $q = 0.43$ was estimated by Abrami (1959). Modelling by Hutchings & Hill (1973) yielded $q = 0.395$, which is similar to $q_{ph} = 0.3984$ reported from different measurements by Hiller et al. (2004) that factored in the presence of a 3$^{\rm rd}$ body.

Binnendijk (1969b) reworked the determination of the elements found earlier by Abrami (1959) and found $P = 0.36579720$ d which is approximately 0.2 s shorter than the earlier period.

Hoffmann & Hopp (1982) found that the light curve was not stable and that it appeared to change from W- to A-type. A study of the AM Leo light curve variability by Qian et al. (2005) concluded that the only plausible explanation is for the presence of a third body. They found that there is no long term variation of the period except for a cyclical change due to a third body influence that has an elliptical orbit. The mass-ratio for the system was reported as $q = 0.42$ and the period of the third body $P_3 = 51.4$ yr. The mass of the third body was found to be $M_3 = 0.175\,M_\odot$ (Albayrak et al., 2005) and the period $P = 0.3657944$ d with $P_3 = 44.82$ yr. The 3$^{\rm rd}$ body, if indeed it exists, must be very faint with $M_{\rm bol} \approx 11$ mag.

After cleaning there were approximately 100 000 SuperWASP data points concentrated over 6.3 yrs. This data on its own (see Table 6.1) indicate a decreasing period but it has only a 3.6σ significance. When combined with B.R.N.O. data the period has a significant (27σ) increase. The O–C analysis on the O–C gateway webpage shows a more complicated sequence of period changes than that of a pure sinusoid.

6.10 DS33 = AP Leo

The star BV 366 was reported as a new variable by the Dr. Karl Remeis Observatory (Strohmeier & Knigge, 1961). Spectral classification by Hill et al. (1975) found it to be of type F8 V. A mass ratio $q = 0.211$ was reported by Cristescu et al. (1979), while Brancewicz & Dworak (1980) measured $q = 0.31$, $P = 0.430358$ d and of spectral type of G0+G2. An O–C analysis of its minima by Zhang et al. (1989) determined a period $P = 0.4303572$ d. From radial velocity analysis, a spectroscopic value for the mass-ratio $q_{sp} = 0.297$ was found by Lu & Rucinski (1999), who also questioned whether the system was W- or A-type. No signatures of the presence of a third body was found during their investigations.

Li et al. (2002) report that the period and light curve show large variations and provide an ephemeris that shows the period is increasing. Following a Fourier spectrum analysis they propose that four different periodic influences are impacting on the O–C result, ranging from 35.4 to 9.2 yrs and suggest

$$\dot{P} = 8.996E \times 10^{-8}\,\mathrm{d\,yr^{-1}}\ . \tag{6.1}$$

However, Pribulla & Rucinski (2006) have not indicated that this could be a triple system.

Roughly 73 000 data points were acquired from SuperWASP, producing a set of highly concentrated minima over a period of ~ 9 yr. The O–C analysis confirms that the period is increasing, in agreement with the timing analysis on the O–C gateway webpage.

6.11 DS34 = AG Vir

The variability of this star was announced by Guthnick & Prager (1929) who classified it as a β Lyr-type variable with $P = 0.487244$ d, but this was corrected to $P = 0.64265$ d by Dugan (1933). The first radial velocity curve was obtained by Sanford (1934) who classified it as a W UMa-type with a spectral type of A0. Pribulla et al. (2006) determined a spectral type A5 V, and claim it is an A-type system that poses challenges in determining the degree of contact. Binnendijk (1969a) pointed out that most of the observed light curves had a distorted primary minimum, and the maximum following the primary minimum is brighter than the maximum preceding the primary minimum. It was also noted that the secondary minimum is a total eclipse.

Bell et al. (1990) supported a constant period for this star, whereas Hobart et al. (1998) suggested a period increase is occurring. According to the O-C gateway website, AG Vir has had a constant period for the past $\sim$55 yrs, while prior to this there might have been some small period changes (although it is difficult to be certain because these were observations made photographically or by eye).

SuperWASP data yielded $\sim$57 000 data points spanning slightly more than 4 yrs. The light curve of AG Vir is not symmetric at its primary minima and it has a flat secondary, as illustrated in Fig. 6.3. The maxima show evidence of the O'Connell effect, differing by $\Delta m \sim 0.05$ mag. There is a misalignment between the synthetic light curve and the SuperWASP data when using the model parameters of Deb & Singh (2011), suggesting that the parameters should be reviewed. No such investigation has been done for this work.

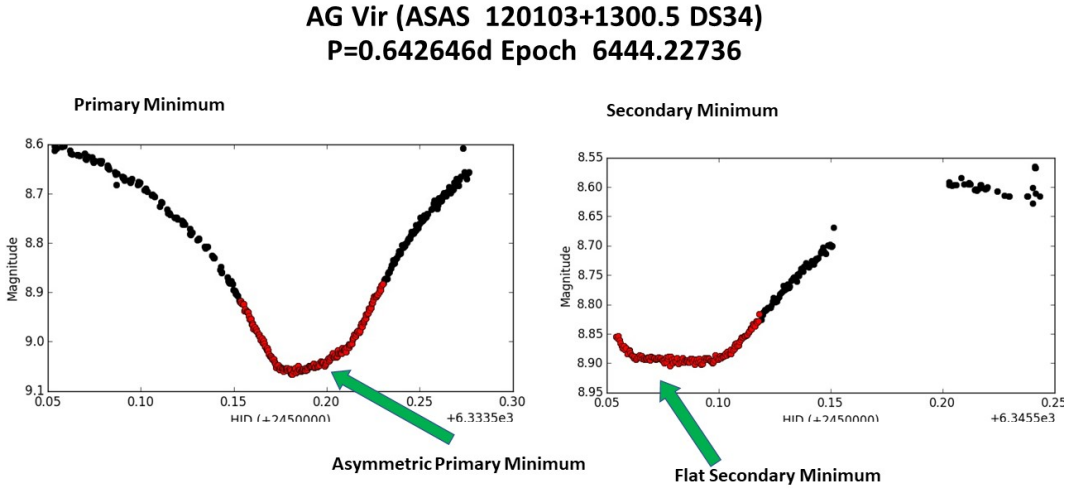

Figure 6.3: Light Curve for ASAS 120103+1300.5 (AG Vir) with $P = 0.642646(5)$ d. Note the unequal maxima, secondary minima appear flat and the primary minima are asymmetric.

The SuperWASP O–C analysis indicates a linear fit to the timing, indicating that the period of this system is constant. However, the O–C analysis for a linear fit presented in Fig. 6.4 clearly shows that the primary and secondary minima have different offsets, which means that they are not separated by 0.5 phase. Binnendijk (1969a) claimed that the secondary minimum is delayed after $\phi = 0.5$. This was confirmed by Bell et al. (1990) who suggested that this phase delay may be due to spots. Pribulla et al. (2006) could not confirm if the origin of the delay is due to spots or a third body. Given that the SuperWASP time series is only 4 yrs long, there is insufficient data to investigate a long period variability.

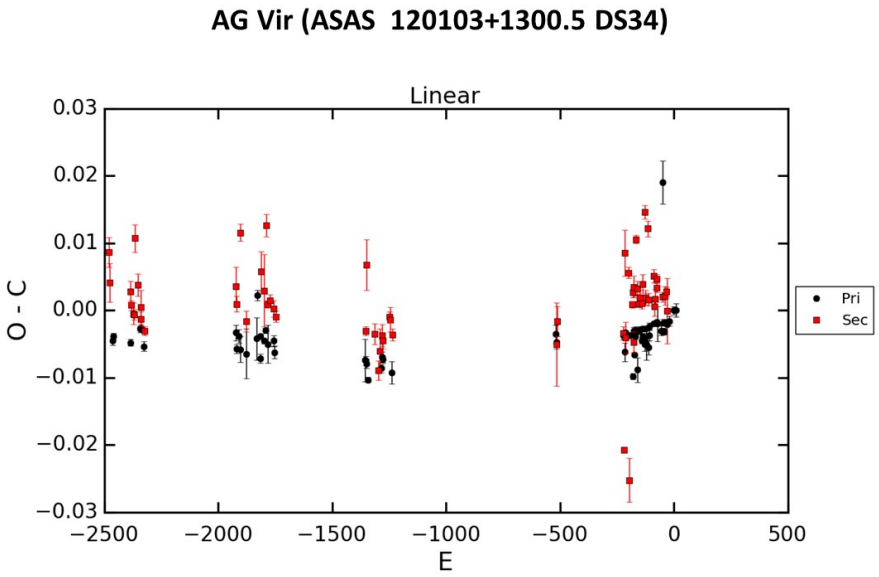

Figure 6.4: O–C results for AG Vir showing the separation of primary and secondary minima.

6.12 DS43 = OU Ser

Carney et al. (1994) suggested that G136–99 (OU Ser) might be a photometric variable and that it is a broad-lined, double-lined spectroscopic binary. However, no further observations appear to have been made of this star until it was discovered to be a variable star by the *Hipparcos* mission. Like DY Cet and EE Cet, OU Ser was given its variable star designation and classified as EW by Kazarovets et al. (1999).

Radial velocity studies by Rucinski et al. (2000) determined a spectral type of F9/G0 V for OU Ser, that it is an A-type system, and had a period $P = 0.296764$ d. Pribulla & Vanko (2002) performed *BV* photometric analysis on the system and determined $P = 0.2967645(2)$ d. These authors point out that there is something amiss with this system, noting that according to the *Hipparcos*' ephemeris the secondary minimum is the deeper one and that the system is thus of W-type. The light curve acquired by Pribulla & Vanko (2002) does not clearly show any significant difference in maxima although they noted there is a possibility of the secondary maximum being slightly brighter in *B* with $\Delta m_B = 0.027(11)$ mag.

Only about 5 years of SuperWASP data was available which is highly concentrated. The SuperWASP light curve of OU Ser clearly shows the O'Connell effect. This was not noticeable with ASAS data. A

magnitude difference of at least $\Delta V = 0.049$ mag is observed, as can be seen Fig. 6.5. This is almost double what was reported by Pribulla & Vanko (2002), but in *B*. There is a difference in the depths of the minima with the deeper at phase 0.0 in Fig. 6.5, making this an A-type system.

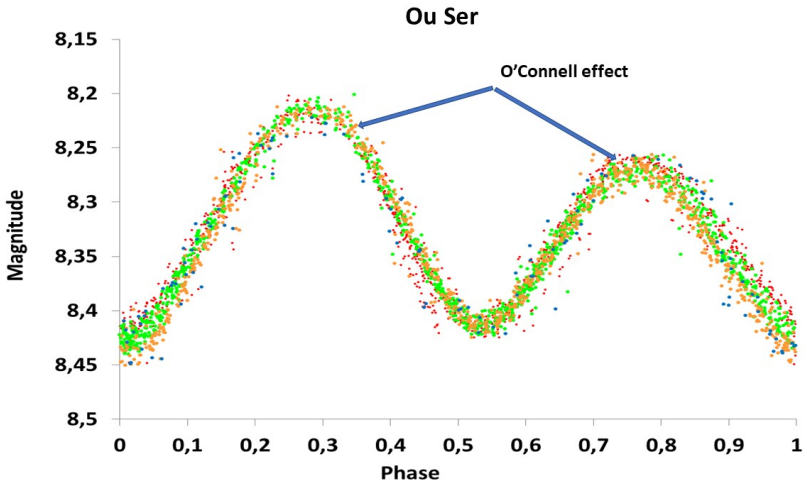

Figure 6.5: SuperWASP PMD of OU Ser showing a noticeable O'Connell effect and primary minimum at phase 0.0.

An O–C analysis of the SuperWASP data shows a clear separation of primary and secondary minima timings in Fig. 6.6. The period is constant, but the poor models and the timing separation between primary and secondary minima of this system indicates that it is clearly worth further investigation.

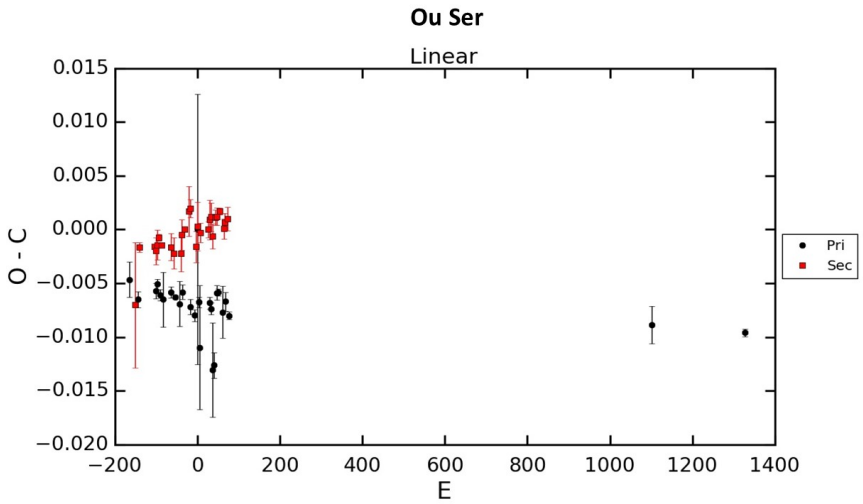

Figure 6.6: SuperWASP linear O–C results for OU Ser showing the offset between primary and secondary minima.

6.13 DS44 = VZ Lib

Hoffmeister (1933) listed VZ Lib as a short period variable star, and Tsesevich (1954) designated it as a W UMa star. Using photoelectric measurements, Claria & Lapasset (1981) reported a period $P = 0.35826334$ d following from earlier work by Tsesevich (1954).

Lu et al. (2001) conducted radial velocity measurements on the system, confirming it to be a triple system but not excluding the possibility of a fourth companion. It is an A-type system with $q = 0.237$. They found a spectroscopic companion through analysis of the broadening function, but since the system overall is faint, they qualified their results in terms of accuracy. A sharp line spike in the spectrum confirms their finding with a velocity for the third body ranging from 2.6 to 4.3 km s^{-1}.

According to Zola et al. (2004), the light curve shows an O'Connell effect. They applied a third light $L_3 = 0.2$ to get a mass-ratio $q = 0.255$.

Szalai et al. (2007) affirmed the challenges in acquiring accurate data on VZ Lib. They found $q = 0.33$ and $i = 88.4^\circ$ whereas other authors had the inclination as $i = 80.3^\circ$. No O'Connell effect was detected. They confirm changes in the O–C, indicative of phase changes. They do not offer any clear period but do recommend further studies to determine the orbital period of the tertiary companion which they suggest ranges between 1200 to 1500 d. Bonnardeau (2009) claims $P_3 = 34.8$ yr.

Qian et al. (2008) believe that VZ Lib consists of a quadrupole system. Their studies found $P = 0.35825797$ d and a cyclical variation with $P_3 = 17.1$ yr.

Liao et al. (2019) determined that the period is decreasing at a rate $\dot{P} = -2.25 \times 10^{-7}$ d yr^{-1} indicating the cause of this as a mass-transfer from the more massive star to the secondary star. A period $P = 0.358253361$ d was reported after extensive analysis. A short cyclical variation of $P_3 = 2.96(4)$ yr was found for the third body. They determined a mass-ratio $q = 0.236$ and the mass of the third companion to be $M_{3\min} = 0.52 \pm 0.07\, M_\odot$.

Yue et al. (2019) found the period to be $P = 0.35825647$ d following an O–C analysis and $P_3 = 48.69 \pm 0.06$ yr for the third companion. From the various studies that have been done, it is clear that there is no common agreement on what P_3 should be.

There are ∼57 000 SuperWASP data points for VZ Lib, spanning a time of ∼6.2 yr. A very small O'Connell effect is apparent in the light curve. An O–C plot of the SuperWASP data is shown in Fig. 6.7 which clearly shows a slow variation in the O–C residuals of ∼3 yr, i.e almost two cycles over the 6 yr span of the data. A Fourier analysis of the data yielded $P_3 = 2.88(2)$ yr, which is close to, but less than, the periods proposed by Szalai et al. (2007), and Liao et al. (2019). A linear ephemeris was found to fit the O–C results better than a quadratic. Unfortunately, the current routine used to analyse the timing of the minima does not include an option for a sinusoidal component, so this will have to wait for a later time to be fitted.

6.14 DS52 = V2612 Oph

The earliest reference to V2612 Oph can be found in the article of Kopff (1943), where it was mentioned as being of spectral type G2, as part of their investigations towards NGC 6633. Hiltner et al. (1958) subsequently noted a double star with $V = 9.5$ mag which did not appear to belong to NGC 6633. An ephemeris with $P = 0.375296$ d was determined by Koppelman et al. (2002), who proposed that it is associated with an X-Ray source, 1RXS J182912.6+064717. Their light curve has the maximum after primary minimum brighter than the maximum after the secondary minimum (O'Connell effect).

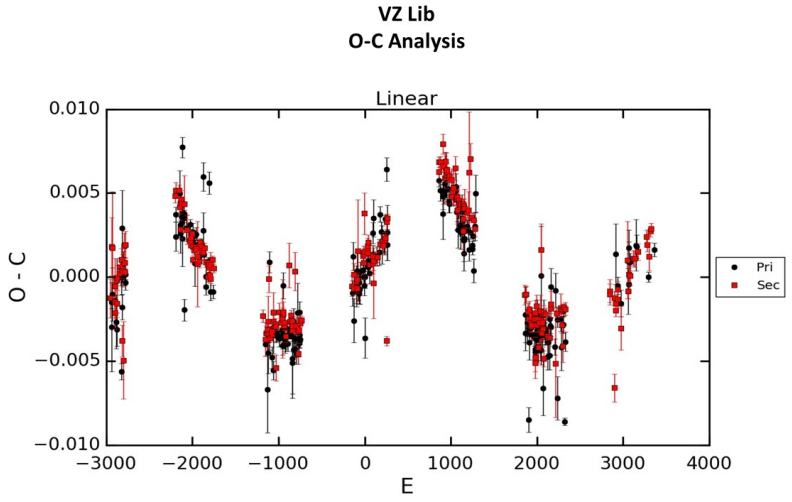

Figure 6.7: A linear ephemeris gave the above O–C residuals for the SuperWASP dataof VZ Lib, showing a clear ~ 3 yr cyclical residual which is taken as P_3.

Pribulla et al. (2007a) reported that V2612 Oph is of spectral type F7 V and a W-type W UMa. They found $P = 0.375307(3)$ d with a total mass $M = 1.279 \pm 0.011 M_{\odot}$ and $q = 0.286$. Çalışkan et al. (2014) proposed this to be an A-type W UMa on the grounds that the more massive component is causing the deeper minimum. They modelled the system with spots at the polar regions to create an asymmetric light curve to explain the O'Connell effect.

The SuperWASP data is strongly localised, consisting of only two seasons of data, containing ~ 2800 points, of which most were from season one. The light curve generated from SuperWASP data does not display the O'Connell effect; the two maxima have the same amplitude.

From the O–C analysis of the SuperWASP data the period appears to be constant, but this is over a fairly short time interval. The period is consistent with that found by Pribulla et al. (2007a). Including B.R.N.O. data in the analysis indicates a slowly decreasing period, consistent with the O–C Gateway timing data.

6.15 Summary Table of Period analysis results

In this section the results of various O–C analyses are tabulated. In all tables the a coefficients have been converted to $\dot{P}$ values. Uncertainties are presented in brackets after each number and refer to the least significant figures.

The results of the O–C analysis done on the SuperWASP data of 14 selected stars are presented in Table 6.1. Three stars show increasing periods, while two stars have decreasing periods. Nine stars have constant periods. AM Leo has the smallest $\dot{P}$ in this sample. Note that because the SuperWASP data only span a time interval of less than 10 yr, cyclical periods exceeding 10 years might not be detected.

After adding some data from B.R.N.O. to extend the time span of the timing results, the O–C results of SuperWASP + B.R.N.O. data are presented in Table 6.2. Only seven sources were subjected to this extended analysis. OU Ser had a constant period regardless of whether only the SuperWASP data

Table 6.1: O–C results using SuperWASP data only.

Star No.	Star Name	Type	P_{ME} (d)	T_0 (K)	P_{O-C} (d)	$\dot{P}$ (d yr^{-1})
6	DY Cet	A	0.440 790	6245.39142(19)	0.440 789 07(13)	
7	EE Cet	W	0.379 925	5556.4771(19)	0.379 927 2(4)	
16	ER Ori	W	0.423 406	4804.3499 (2)	0.423 413 0(1)	–3.11(17) x10^{-6}
18	AH Aur	A	0.494 106	4067.6836(6)	0.494 101 7(3)	2.13(25) x10^{-6}
26	XY Leo	W	0.284 101	4556.3984(3)	0.284 103 9(3)	2.9(5) x10^{-6}
28	Y Sex	A	0.487 736	6328.4624(4)	0.419 817 2(3)	
29	XX Sex	A	0.540 108	5997.281(2)	0.540 111 9(8)	
31	VY Sex	W	0.443 433	6362.4217(4)	0.443 435 1(8)	
32	AM Leo	W	0.365 799	6330.4208(3)	0.365 797 5(3)	–5.8(1.6) x10^{-7}
33	AP Leo	A	0.430 356	6745.4534(3)	0.430 366 9(2)	1.60(10) x10^{-6}
34	AG Vir	A	0.642 648	6444.2274(6)	0.642 646 1(5)	
43	OU Ser	A	0.296 768	4955.6760(13)	0.296 773(6)	
44	VZ Lib	A	0.358 256	5680.4950(6)	0.358 254 02(8)	
52	V2612 Oph	W	0.375 309	4298.6021(5)	0.375 307 81(9)	

were used, or the B.R.N.O. data were included. The linear period obtained from the different data sets showed a slight change, but within their uncertainties. The period rates of change are about an order of magnitude smaller than those found using only the SuperWASP data, and explains why they could not be determined from the SuperWASP data on its own.

Table 6.2: O–C results using SuperWASP + BRNO data for a selection of stars.

Star No.	Star Name	Type	P_{O-C} (d)	$\dot{P}$ (d yr^{-1})
7	EE Cet	W	0.379 9244(2)	3.7(1.0) x10^{-7}
26	XY Leo	W	0.284 10322(13)	1.16(18) x10^{-7}
28	Y Sex	A	0.419 8258(4)	2.1(3) x10^{-7}
31	VY Sex	W	0.443 43389(10)	–3.7(3) x10^{-7}
32	AM Leo	W	0.365 79759(1)	2.76(10) x10^{-8}
43	OU Ser	A	0.296 76895(7)	
52	V2612 Oph	W	0.375 3084(3)	–3.9(6) x10^{-7}

Qian (2001a) has claimed, based on a list of 30 stars he studied, that all W-type W UMa stars with mass-ratios $q > 0.4$ have increasing periods, i.e. that $dP/dE > 0$. From the sample of 49 stars in this study, an O–C analysis was done on 14 of these stars, of which 6 were of W-type. Period changes with a significance of more than 3σ were found in all six of these stars, none of which are in the Qian (2001a) sample.

In Table 6.3 the six W-type stars from this study are listed in order of increasing mass ratio q. Their period rate of change is also listed. As can be seen from the data listed, ER Ori has a $q > 0.4$ and has a $\dot{P}$ that is decreasing, in disagreement with Qian (2001a). Note that the period rate of change for this

star was determined from the SuperWASP data only (see Table 6.1). V2612 Oph and VY Sex also have decreasing periods but their mass ratios are less than 0.4.

Table 6.3: Period changes for W-type contact stars showing the relationship with q.

Star No.	Star Name	Type	$P_{\text{O–C}}$ (d)	q	Incr /Decr	$\dot{P}$ (d yr^{-1})
52	V2612 Oph	W	0.375 3084(3)	0.286	Decreasing	–3.9(6) x10^{-7}
31	VY Sex	W	0.443 43389(10)	0.313	Decreasing	–3.7(3) x10^{-7}
7	EE Cet	W	0.379 925	0.315	Increasing	3.7(1.0) x10^{-7}
32	AM Leo	W	0.365 79759(1)	0.459	Increasing	2.76(10) x10^{-8}
16	ER Ori	W	0.423 4103(1)	0.656	Decreasing	–3.11(17) x10^{-6}
26	XY Leo	W	0.284 10322(13)	0.729	Increasing	1.16(18) x10^{-7}

6.16 Conclusion

As can be seen from the 14 stars that have been subjected to an O–C analysis making use of SuperWASP data, the periods, and the variability there of the stars could be refined, along with details for P_3 in some instances. The highly concentrated SuperWASP data indeed is useful for confirming shorter period changes to a higher degree of accuracy, but longer term variability cannot be reliably detected as a longer baseline of good quality data is necessary.

Certain light curve information that would not be noticeable on the ASAS-data due to the few data points, were also extracted and led to findings that would not otherwise have been apparent.

Chapter 7

Key Findings and Future Research

W UMa stars offer many opportunities to study the structure of stars, although their own evolution is still an outstanding problem. In this dissertation, different aspects of some W UMa stars have been looked at to try and get a better understanding of the parameters describing them, and how the binary systems are evolving. A sample of binary stars with known spectroscopic mass ratios q that have modelled parameters and are bright enough to be found in the ASAS data base were identified by Deb & Singh (2011). Of their sample of 62 stars, only the A- and W-type W UMa stars were selected, which amounted to a sample of 49 systems. The parameters for these stars were used to investigate under what conditions total eclipses can occur when using the modelling code BM3. A theoretical explanation for the criteria observed from modelling is provided here. Data for a further sub-sample of 14 of these stars were extracted from the SuperWASP data base and used to determine O–C minimum timing measurements. The results of these investigations will be discussed below, and future work that can be done.

7.1 Total Eclipse Modelling

Before the modelling commenced, the parameters of the 49 stars selected were checked against ASAS data for compatibility. Deb & Singh (2011) based all of their findings on the ASAS data but used the WD code rather than BM3 for their modelling. Some discrepancies were found between the parameters provided by Deb & Singh (2011) and the modelled fits to the data which are discussed in section 4.1. In some cases, it was found that the provided parameters did not give the best fits to the data, so improved values have been suggested.

Secondary Minima

Total eclipsing binaries provide additional constraints when modelling the system parameters that give more reliable values than for systems that only show partial eclipses. Therefore, it is useful if total eclipsing can be identified and modelled. Using the modelled parameters from the 49 selected stars, the values of inclination i were varied to investigate under what conditions flat minima could occur. As shown in section 4.3, flat minima, which are an indication of total eclipses, occur more noticeably in the secondary minima than in the primary minima.

A set of conditions under which the secondary minima were found to be flat when modelled using BM3, are presented in Figs. 4.4 to 4.7 and summarized in Table 4.5. For convenience, this table is

repeated in Table 7.1, while a combined plot of Figs. 4.4 to 4.7 is shown in Fig. 7.1. This result does not depend on whether these are W- or A-type W UMa systems, or on the relative temperature differences between the two companion stars.

Table 7.1: The values for i and q that lead to the appearance of flat secondary minima in the sample of 49 W UMa stars.

q	Range of i	Appearance of Secondary Minimum	Relevant Figures
All q	$< 75°$	Rounded	A.1 to A.49
$q \leq 0.21$	$75° - 90°$	Flat	A.1 to A.8
$q \leq 0.37$	$80° - 90°$	Flat	A.1 to A.28
$q \leq 0.63$	$85° - 90°$	Flat	A.1 to A.44
$q > 0.63$	$0° - 90°$	Rounded	A.45 to A.49

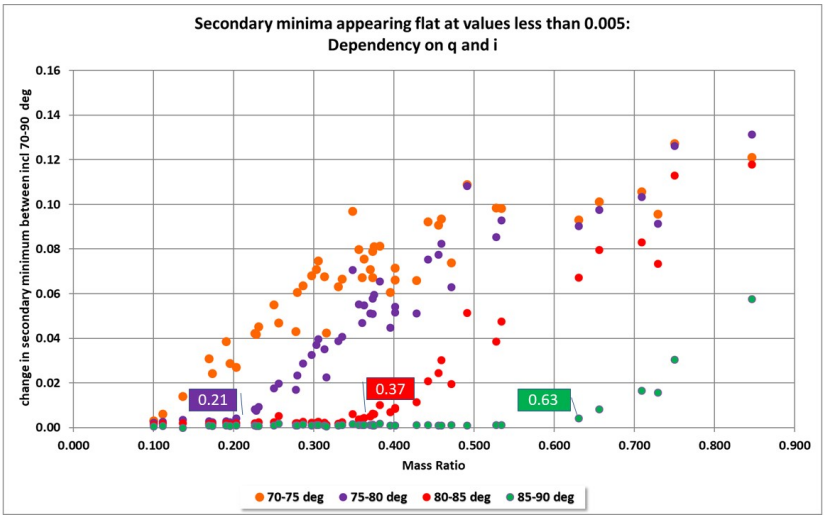

Figure 7.1: Dependency of flat secondary minima on the values of q and i.

Primary Minima

Primary minima can also appear flat but under a much more restricted set of conditions. This is partly due to the limb darkening effect on the primary star when the secondary moves in front of it. A flat eclipse will only occur when the secondary star is small enough to cover the central section of the primary star away from the effects of limb darkening. This means that the inclination must be close to 90° and the secondary star should be much smaller than the primary. As illustrated in Fig. 7.2, primary minima will only have a flat appearance with inclination angles $i \geq 85°$ and this will be limited to occur when $q < 0.34$. Note that although the two graphs for primary and secondary minima have a similar appearance, the Y-axis values are almost double between the two figures, proving that the secondary minimum is a more robust indicator of a total eclipse than the primary minimum.

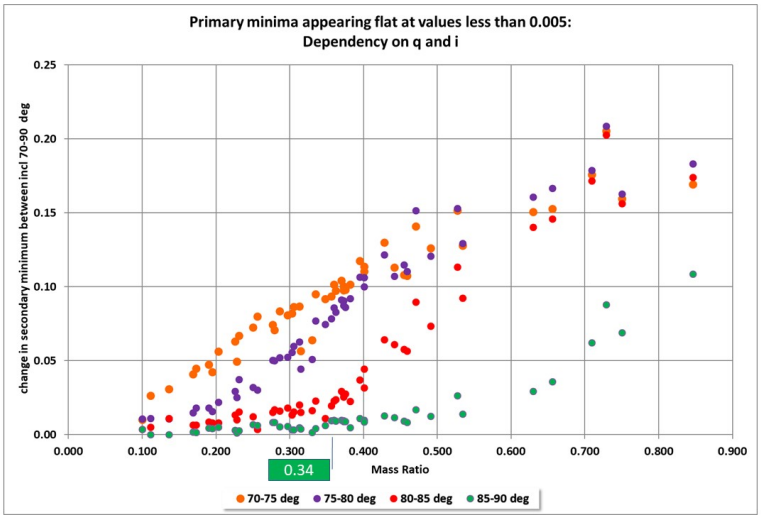

Figure 7.2: Conditions under which the primary minimum will appear flat are limited to $i \geq 85^\circ$ and systems having mass ratios $q < 0.34$.

Theoretical Considerations

Support for the empirical results using a limited set of 49 stars described in the previous sections, is provided by conditions for total eclipses in binary systems derived by Prša (2011). He shows that if a quantity Δ defined by

$$\Delta^2 = a^2(\sin^2\phi + \cos^2\phi\cos^2 i) \tag{7.1}$$

where a is the length of the semi-major axis of the orbit, i is the inclination of the orbit and ϕ the phase of the system (relative to primary minimum at phase 0), then a total eclipse will occur when

$$\Delta < R_1 - R_2 \tag{7.2}$$

where R_1 and R_2 are the radii of the orbits of each component of the binary.

The parameters as provided by Deb & Singh (2011) for the sample stars modelled in Chapter 4 can be used to determine a minimum value of i for which a total eclipse will occur. For the secondary minimum to be in eclipse the phase is set to $\phi = 0.5$.

The results of this analysis are set out in Table 7.2. The theoretical determination of when a flat secondary minimum occurs, agrees very well with the results presented in Table 7.1. The rather limited sample of 49 stars used in the modelling shows that the BM3 models agree well with theoretical considerations.

At this stage, only q and i have been investigated with regards to flat minima. Other factors, such as the fillout factor and a third body, might also have some influence, which can be explored at a later stage. This study shows that q and i have the strongest influence.

Table 7.2: Values of R_1, R_2 and a as provided by Deb & Singh (2011) for the 49 W UMa stars used in Chapter 4 arranged in order of increasing mass ratio q. The minimum value of i required for a total eclipse of the secondary minimum to occur is shown in column 7.

Serial No.	ASAS ID	q	type	$(R_1 - R_2)/R_\odot$	$a/R_\odot$	Min i in degrees
29	101602-0618.5	0.1	A	1.174	3.148	68.1032
41	143504+0906.8	0.111	A	0.883	2.55	69.7404
1	003628+2132.3	0.136	A	0.795	2.49	71.3808
18	062605+2759.9	0.169	A	0.961	3.289	73.0111
43	152243+1615.7	0.173	A	0.611	2.093	73.0267
22	073338-5007.4	0.19	A	0.756	2.746	74.0195
28	100248+0105.7	0.195	A	0.773	2.85	74.2626
62	234718-0805.2	0.203	A	0.866	3.254	74.5657
3	012104+0736.3	0.226	A	0.817	3.253	75.4543
57	204628-7157.0	0.228	A	1.179	4.45	74.6364
47	165717+1059.8	0.231	A	0.681	2.641	75.0571
21	073246-2047.5	0.25	A	1.2	4.396	74.1586
60	233655+1548.1	0.256	A	0.66	4.182	80.9197
48	171358+1621.0	0.277	A	0.597	2.711	77.2784
10	033459+1742.6	0.279	W	-0.609	2.779	77.3413
52	182913+0647.3	0.286	W	-0.553	2.598	77.7102
33	110505+0509.1	0.297	A	0.614	2.954	78.0034
30	104033+1334.0	0.303	A	0.847	4.212	78.3992
51	180921+0909.1	0.305	A	0.591	2.984	78.5767
31	105030-0241.7	0.313	W	-0.598	3.004	78.5175
7	024952+0856.3	0.315	W	-0.592	2.948	78.4154
44	153152-1541.1	0.33	A	0.453	2.384	79.0462
46	164121+0030.4	0.335	W	-0.592	3.15	79.1676
27	100234+1702.8	0.348	A	0.627	3.505	79.695
6	023833-1417.9	0.356	A	0.542	3.046	79.7503
59	222257+1619.4	0.36	W	-0.463	2.63	79.8605
54	193524+0550.3	0.362	W	-0.475	2.699	79.8637
2	011638-3942.S	0.37	W	-0.446	2.592	80.0919
9	030953-0653.6	0.373	W	-0.525	3.069	80.1502
23	073905-0239.1	0.373	A	0.744	4.453	80.382
58	205710+1939.0	0.375	W	-0.438	2.573	80.1988
34	120103+1300.5	0.382	A	0.743	4.501	80.4984
49	173356+0810.0	0.395	W	-0.436	2.695	80.6897
14	041209-1028.2	0.401	W	-0.323	2.257	81.7721
61	234535+2528.3	0.401	A	0.87	3.92	77.1771
39	141726+1234.1	0.428	A	0.345	2.348	81.5507
11	034814+2218.9	0.442	A	0.355	2.5	81.8364
24	084002+1900.0	0.455	W	-0.379	2.762	82.113
32	110211+0953.7	0.459	W	-0.377	2.77	82.1777
36	123300+2642.9	0.471	W	-0.225	1.723	82.4965
40	141937+0553.8	0.491	A	0.429	3.574	83.106
35	121206+2232.0	0.527	W	-0.177	1.58	83.5679
12	034928+1254.7	0.534	W	-0.258	2.349	83.6943
17	051832-6813.6	0.63	W	-0.164	2.02	85.3431
16	051114-0833.4	0.656	W	-0.231	3.159	85.8065
45	155649+2216.0	0.709	A	0.249	2.572	84.4444
26	100141+1724.5	0.729	W	-0.114	2.071	86.8445
5	014854-2053.6	0.75	A	-0.119	2.329	87.0712
55	194813+0918.5	0.846	A	0.098	3.355	88.3261

7.1.1 SuperWASP data and Period Analysis

In general, SuperWASP data contain many more data points per star than does the ASAS data. ASAS typically contains ~ 500 points per star, whereas SuperWASP has thousands of points. This concentration of data allows better averages of PMDs to be formed, showing details such as the O'Connell effect more accurately than can be achieved with ASAS data. Many minima in the SuperWASP data set contain several points around the minimum which can be used to determine accurate times of minimum, and thereby facilitating accurate determinations of periods and period rates of change. However, one limitation of the SuperWASP data is that it covers a limited time span.

Of the 49 stars analysed in Chapter 4, only 46 of them were found in the SuperWASP database. Because of the enormous number of SuperWASP data points for each star, cleaning and analysing the data is much more time consuming than when dealing with the ASAS data. Hence, only 14 out of the 46 stars for which there is SuperWASP have been analysed here. The stars chosen were representative of the sample, although as the results show, there are often unexpected surprises discovered when subjecting the data to close scrutiny.

As was done with the ASAS data, synthesized light curves (or more accurately, PMDs), generated using BM3, were fitted to the SuperWASP data. Instances where the synthesized data did not fit the observed data properly are listed in section 5.2. In particular, AP Leo, AG Vir and OU Ser did not align well with the synthetic curves. All these systems need to be examined in more detail at some stage, to see if the modelled parameters can be improved, or if there is a problem with the data. It is important to bear in mind that the synthesized data is produced assuming a V-band filter is being used when collecting the data. The SuperWASP telescopes use a wider band filter than the standard V-band, which could be influencing the PMDs. It is also possible that the BM3 code has limitations which could be investigated by producing synthesized light curves through other models such as the PHysics of Eclipsing binariEs (PHOEBE) or the Wilson-Devinney code.

Timings of a new set of minima for the 14 stars in the SuperWASP data set have been obtained which have a high density of points although over a limited time span. These new minima are more accurate than many of the other minima scattered around the literature and provide a valuable complement to these other measurements. These minima will be made available to other members of the variable star community to improve their models of periods and period changes.

Period determinations using only the SuperWASP data are presented in Table 6.1. The O–C model used to analyse the times of minimum analysed both linear and quadratic timing models. As displayed in Table 6.1, 5 out of the 14 systems showed period variations, while the other 9 systems had constant periods. The periods determined are more accurate than most other values listed in the literature. The limited time spans covered by the SuperWASP data precludes detecting long term trends due to evolutionary changes, or cyclical variations caused by third bodies.

By extending the time span of the timing data by using data from other sources, period rates of change for 6 out of the 14 stars were found (see Table 6.2).

Although the time span of the SuperWASP data is limited, there were nevertheless some interesting results that came out of the O–C analysis.

ER Ori is a W-type system with a mass ratio $q = 0.656$ which has been a challenging source to analyse. The timing residuals from the SuperWASP data show a highly significant $\dot{P}$. Its period rate of change is higher than previously reported, indicating a period that is decreasing. This is in disagreement with the claim made by Qian (2001a) that all W-type W UMa systems with $q > 0.4$ have increasing periods.

The high concentration of data for AG Vir confirms that the light curve has an asymmetric primary

minimum, and that the secondary is flat and therefore totally eclipsed. The O–C residuals for this star show that the primary and secondary minima have different time delays, suggesting a spot on one of the stars at either phase 0 or 0.5. This anomaly clearly needs to be investigated further.

Similarly, the primary and secondary minima of OU Ser show a separation which also suggests a spot on one of the stars. It does display an O'Connell effect which is also usually attributed to spots.

A particularly interesting finding related to the timing residuals in V2612 Oph, is that they clearly show a cyclical pattern with a period $P_3 \sim 2.88$ yr. This system has long been suspected of having a third body, but the periods associated with this third body have usually been set at periods of tens of years rather than the period discovered here. Although the SuperWASP data is seasonal, two full cycles can be seen in the 6.2 yr time span of the data. Clearly, this period needs to be refined with more observations and the O–C analysis routine needs to be able to determine the parameters using more than just a linear or quadratic model.

Based on the results presented above, it appears that it would be a worthwhile exercise to perform an O–C timing analysis on the remaining 32 stars from the Deb & Singh (2011) sample for which there is SuperWASP data to see if any more anomalous or interesting results can be found. Clearly, there is no shortage of work ahead, and results that need to be presented to the wider community via publications.

Appendix A

Synthetic Light curves

The plots are ordered according to the value of mass ratio q from smallest to largest as done in Tables 4.3 and 4.4. Each plot is labelled with its DS serial number, ASAS identifier and variable star designation. The mass ratio q and inclination i from Table 4.3 are also given.

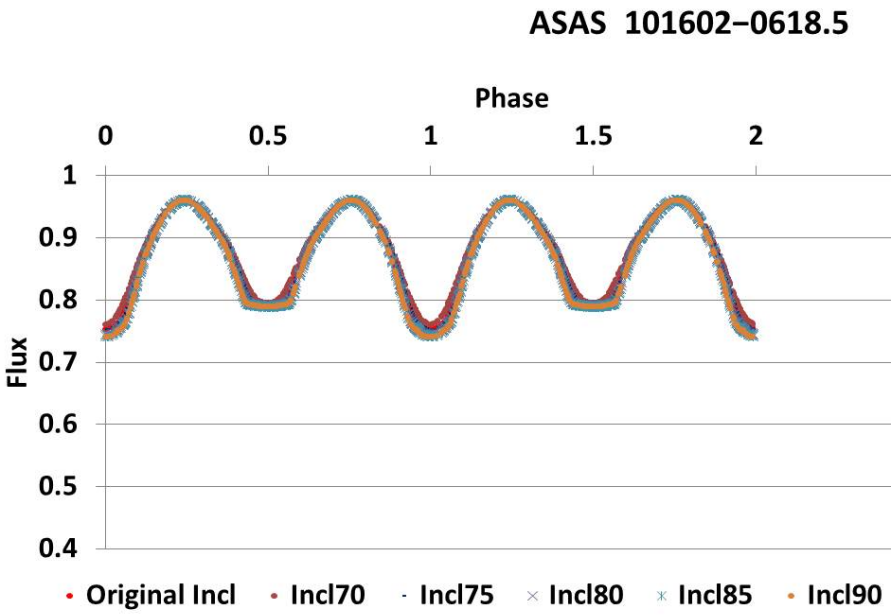

Figure A.1: DS29 = ASAS 101602–0618.5 = XX Sex. Initial values: $q = 0.100$ and $i = 74.88°$.

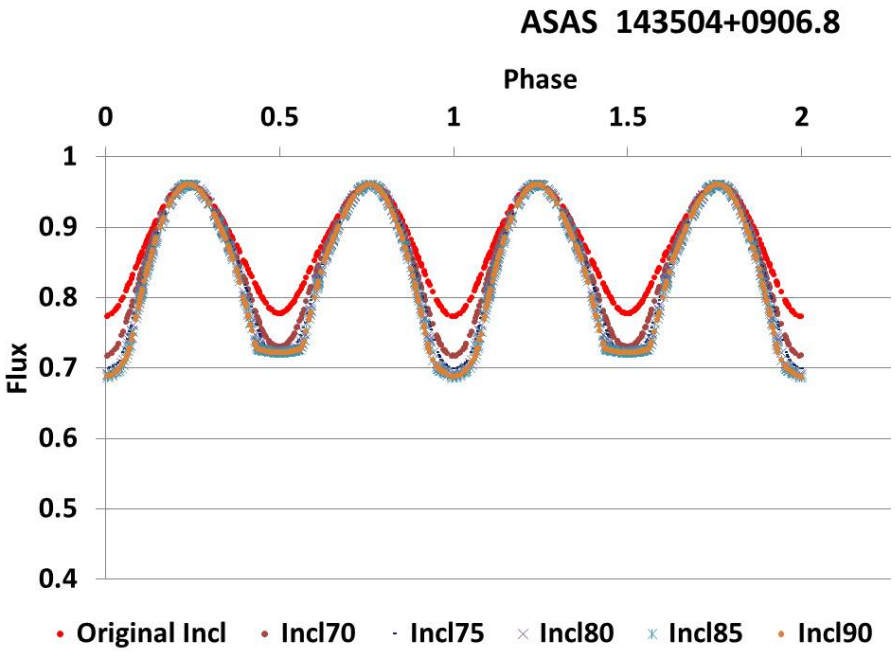

Figure A.2: DS41 = ASAS 143504+0906.8 = CK Boo. Initial values: $q = 0.111$ and $i = 60.87°$.

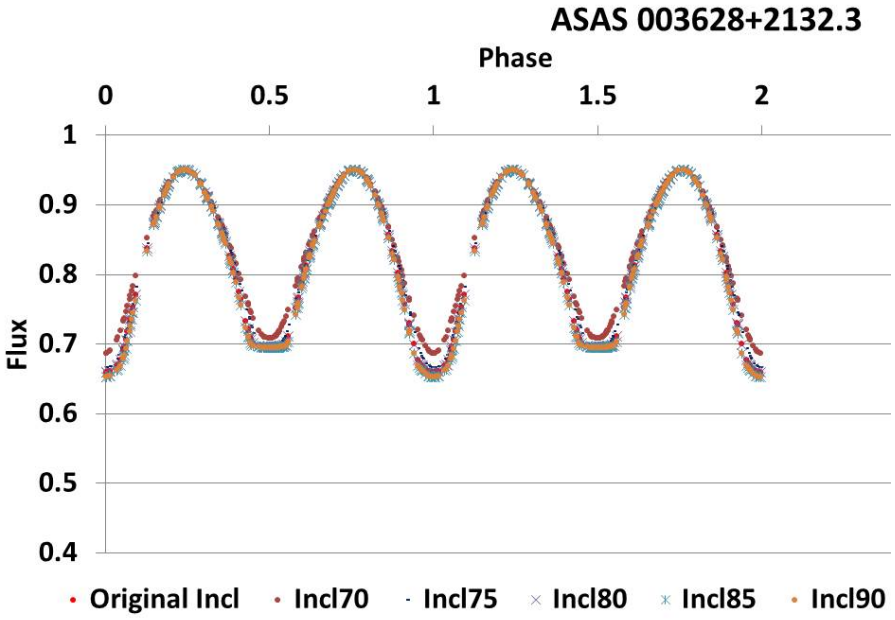

Figure A.3: DS1 = ASAS 003628+2132.3 = DZ Psc. Initial values: $q = 0.136$ and $i = 79.88°$.

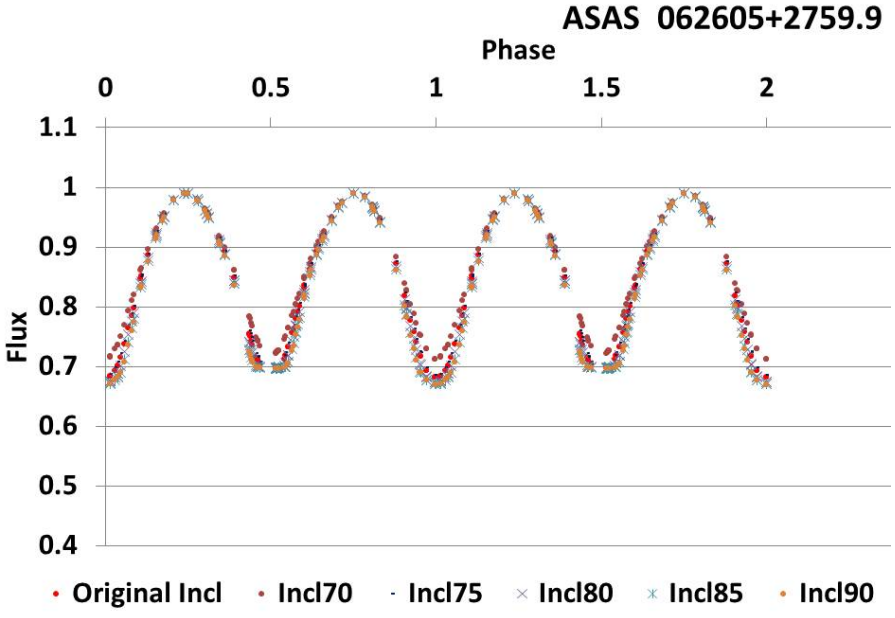

Figure A.4: DS18 = ASAS 062605+2759.9 = AH Aur. Initial values: $q = 0.169$ and $i = 76.28°$.

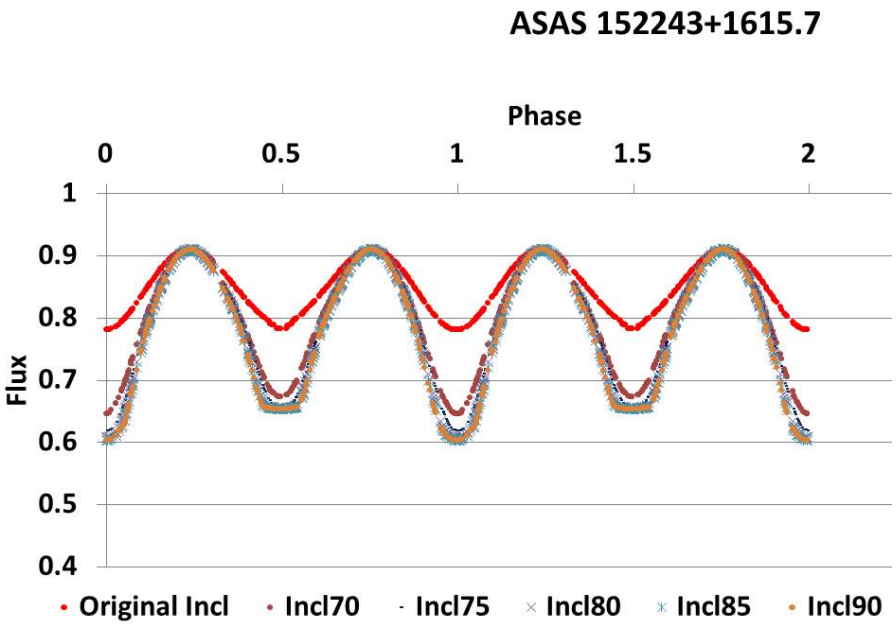

Figure A.5: DS43 = ASAS 152243+1615.7 = OU Ser. Initial values: $q = 0.173$ and $i = 50.47°$.

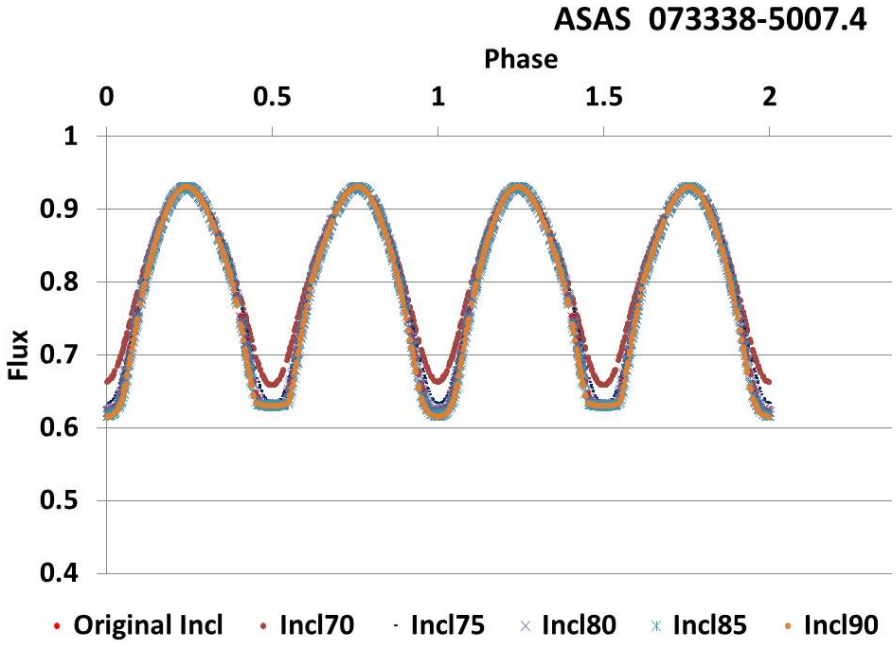

Figure A.6: DS22 = ASAS 073338–5007.4 = HI Pup. Initial values: $q = 0.19$ and $i = 79.47°$.

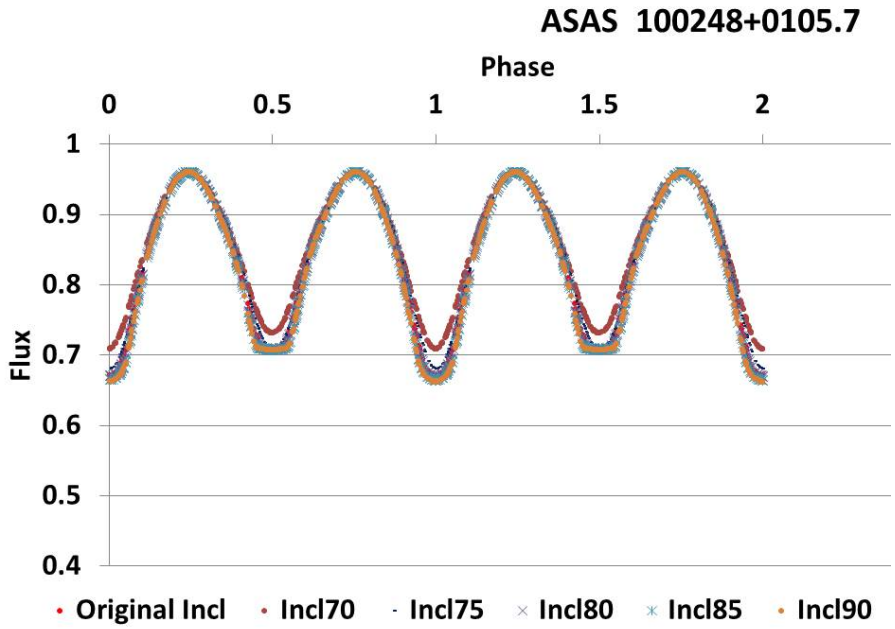

Figure A.7: SS28 = ASAS 100248+0105.7 = Y Sex. Initial values: $q = 0.0.195$ and $i = 79.12°$.

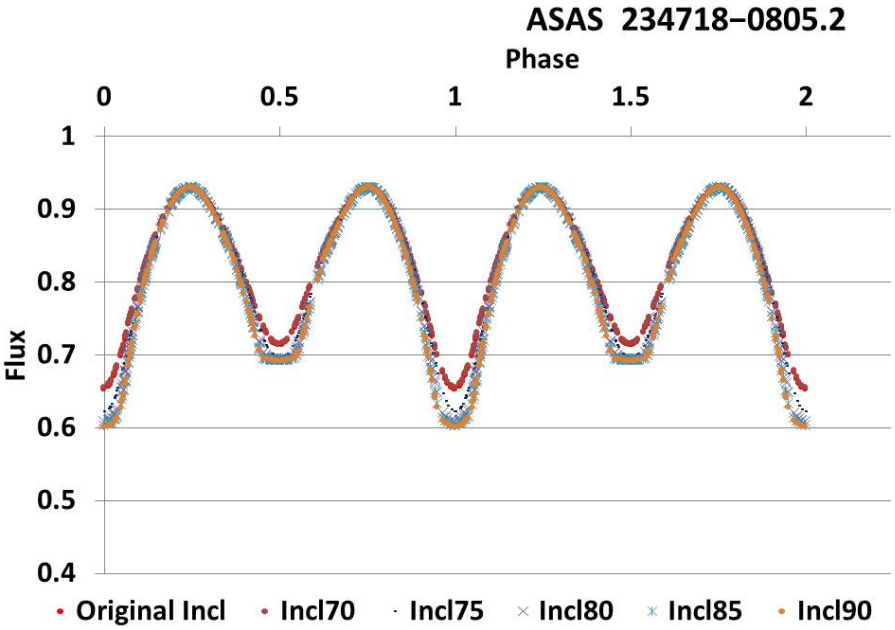

Figure A.8: DS62 = ASAS 234718–0805.2 = EL Aqr. Initial values: $q = 0.203$ and $i = 70.36°$.

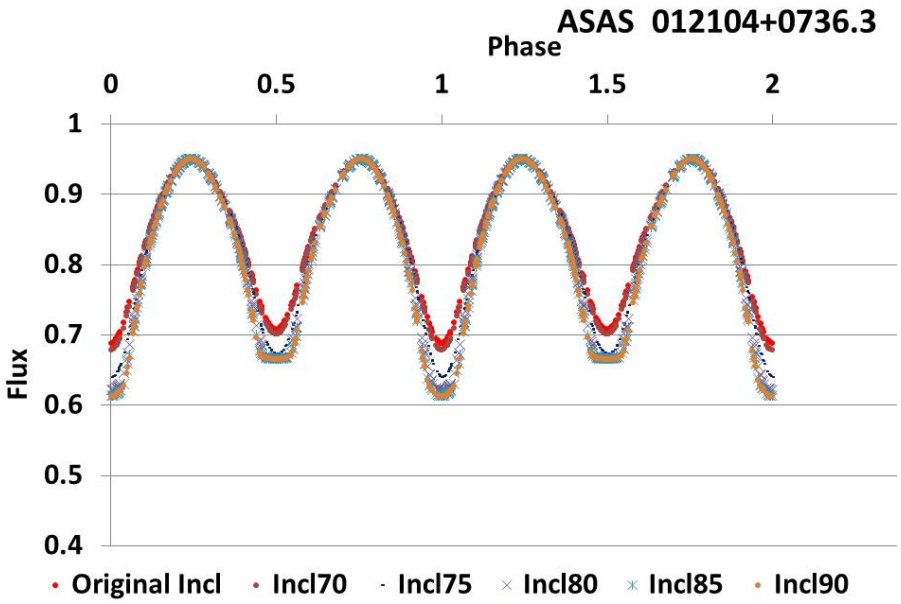

Figure A.9: DS3 = ASAS 012104+0736.3 = AQ Psc. Initial values: $q = 0.226$ and $i = 69.06°$.

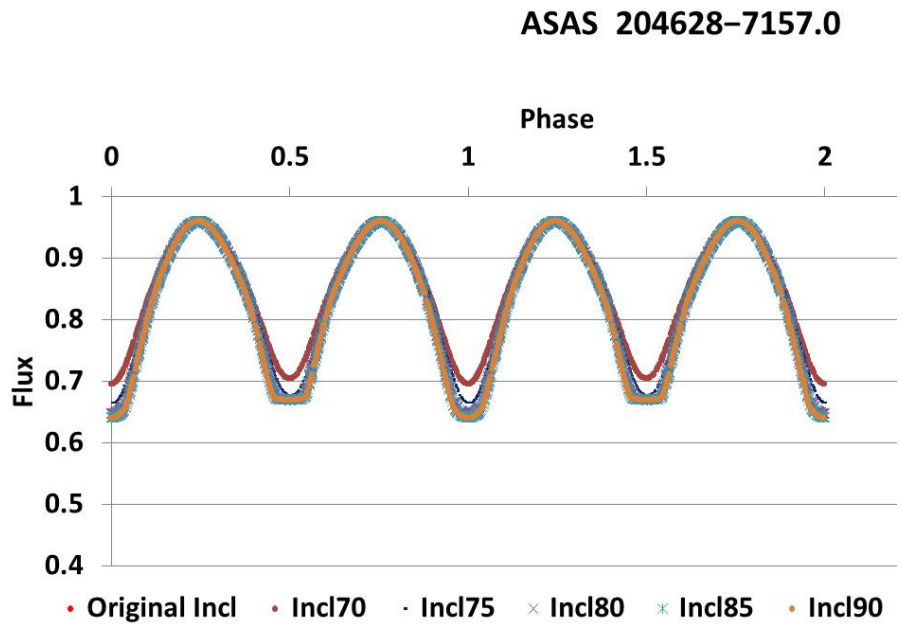

Figure A.10: DS57 = ASAS 204628–7157.0 = MW Pav. Initial values: $q = 0.228$ and $i = 84.81°$.

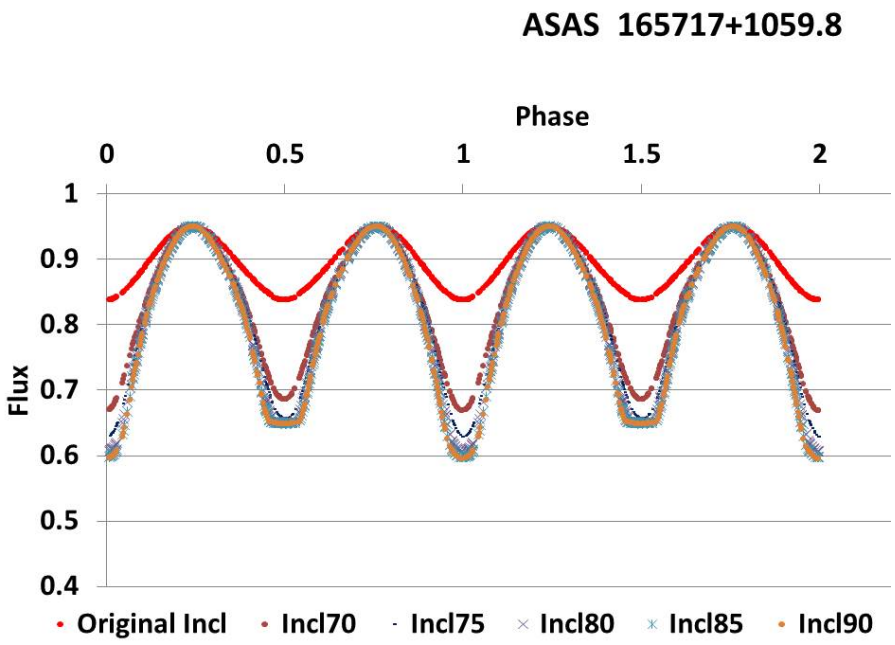

Figure A.11: DS47 = ASAS 165717+1059.8 = V2357 Oph. Initial values: $q = 0.231$ and $i = 47.05°$.

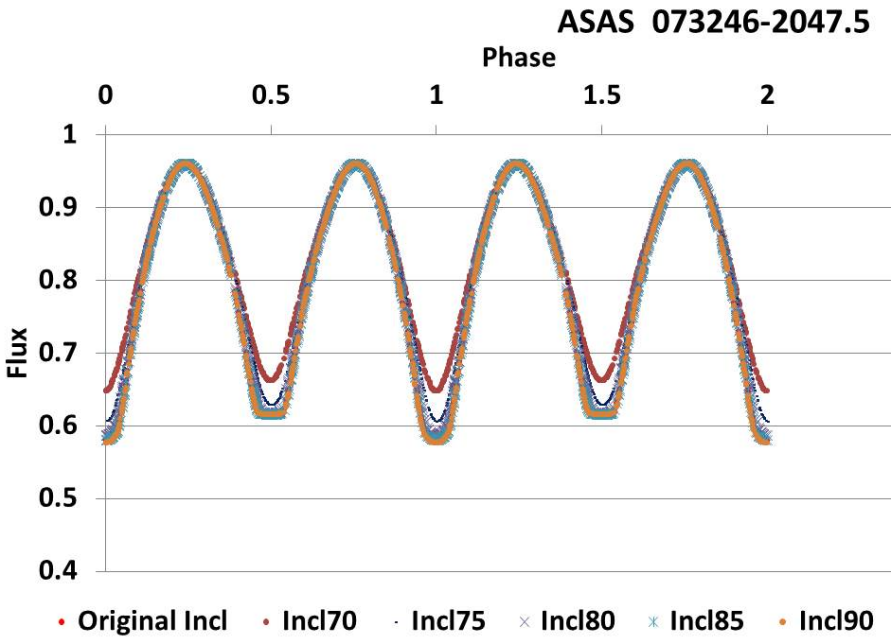

Figure A.12: DS21 = ASAS 073246–2047.5 = TY Pup. Initial values: $q = 0.25$ and $i = 84.47°$.

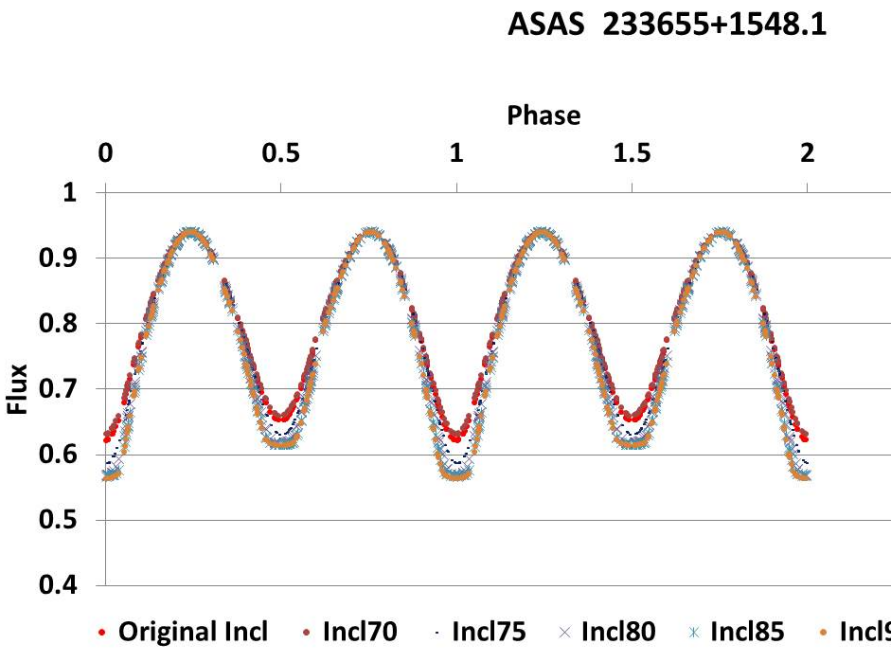

Figure A.13: DS60 = ASAS 233655+1548.1 = V407 Peg. Initial values: $q = 0.256$ and $i = 71.11°$.

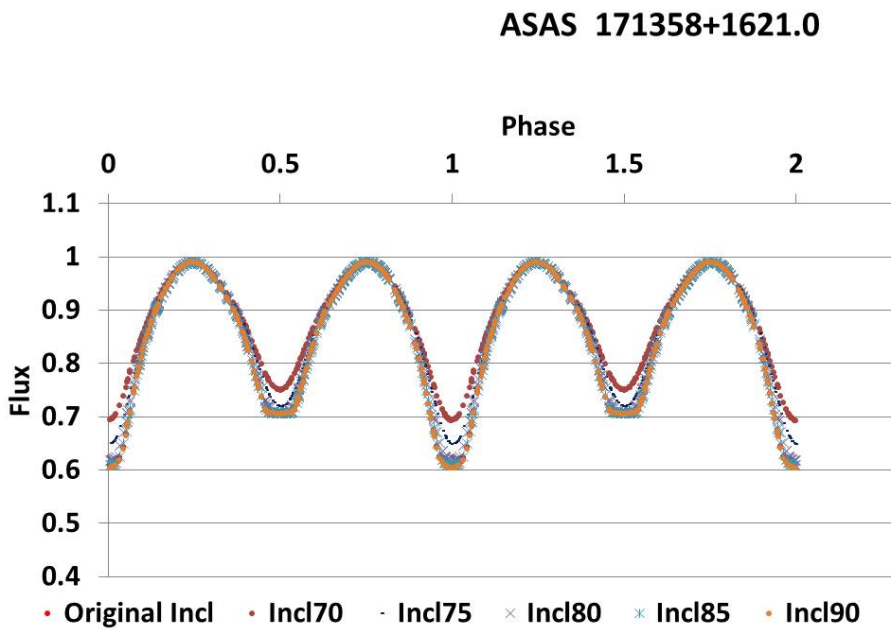

Figure A.14: DS48 = ASAS 171358+1621.0 = AK Her. Initial values: $q = 0.277$ and $i = 88.69°$.

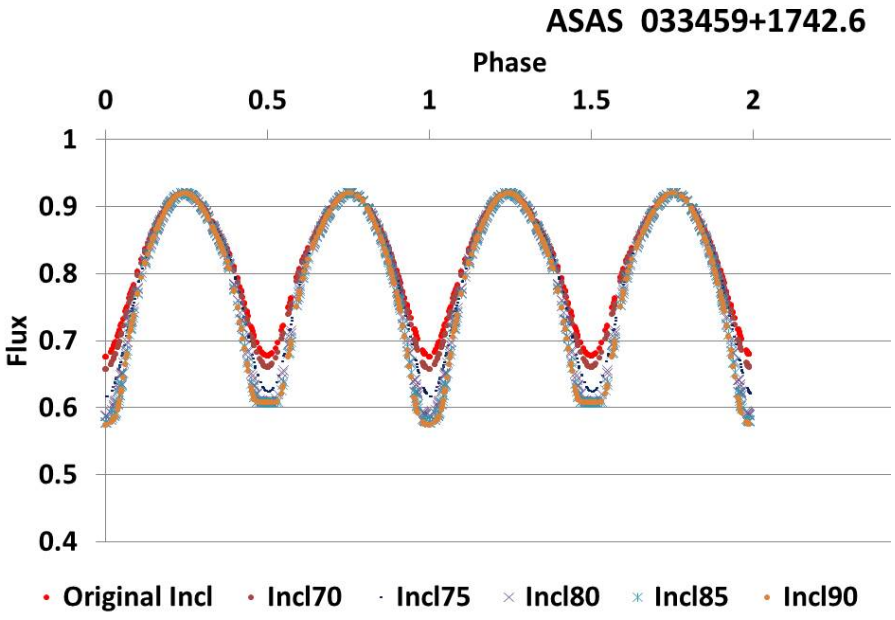

Figure A.15: DS10 = ASAS 033459+1742.6 = V1123 Tau. Initial values: $q = 0.279$ and $i = 68.10°$.

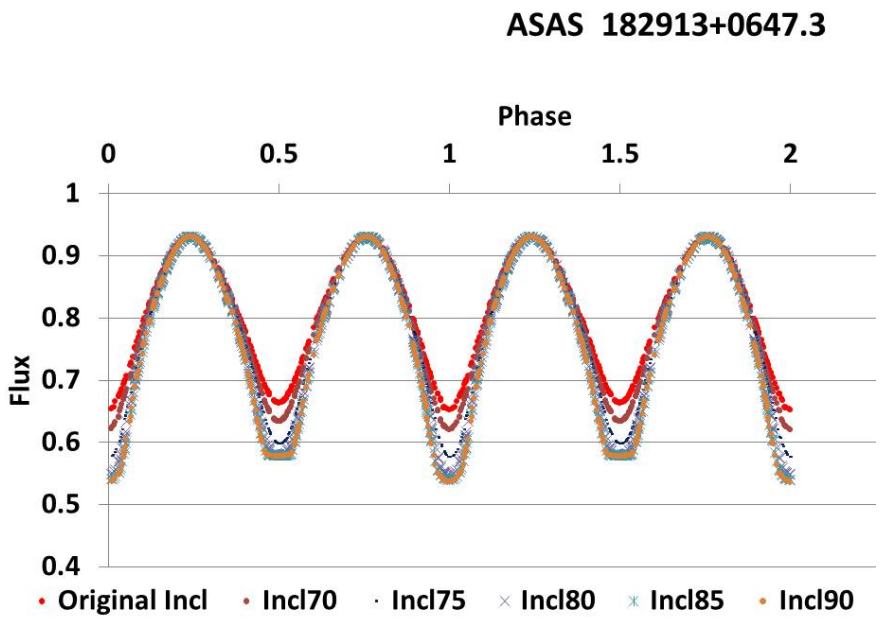

Figure A.16: DS52 = ASAS 182913+0647.3 = V2612 Oph. Initial values: $q = 0.286$ and $i = 66.36°$.

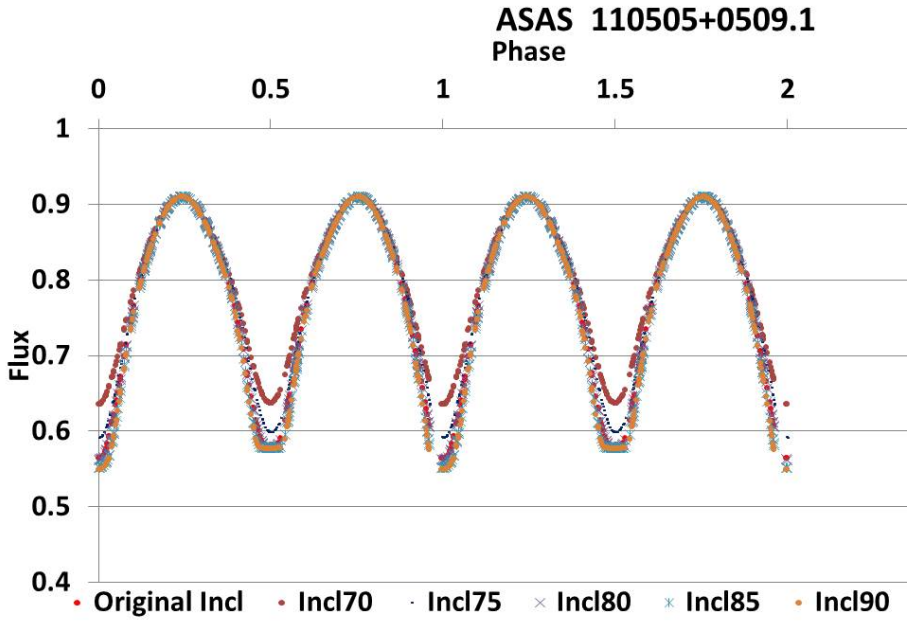

Figure A.17: DS33 = ASAS 110505+0509.1 = AP Leo. Initial values: $q = 0.297$ and $i = 79.66°$.

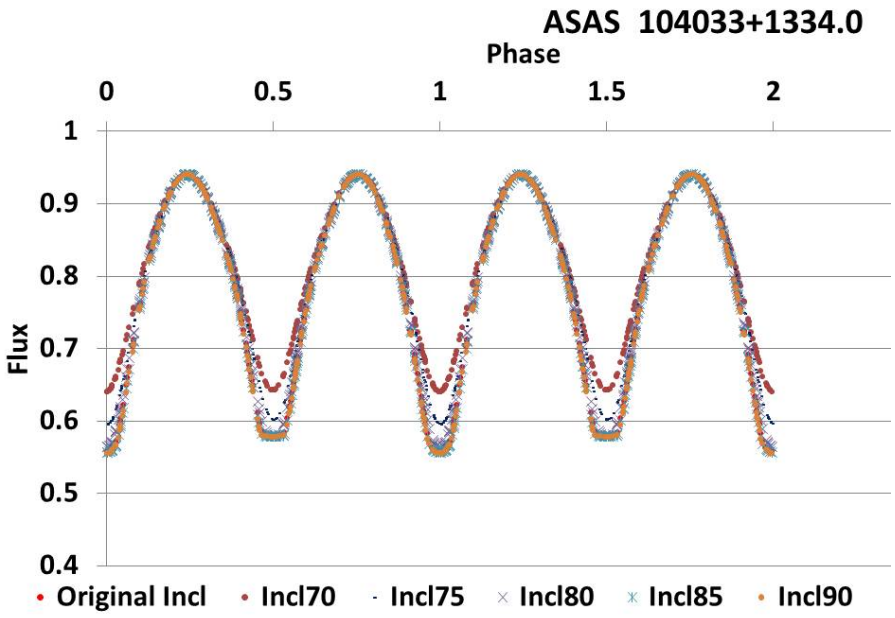

Figure A.18: DS30 = ASAS 104033+1334.0 = UZ Leo. Initial values: $q = 0.303$ and $i = 84.05°$.

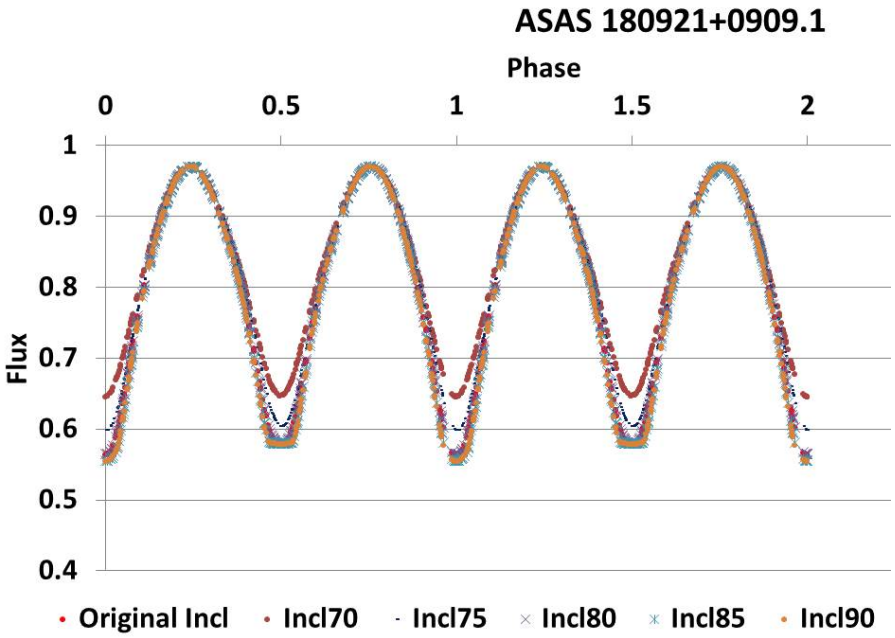

Figure A.19: DS51 = ASAS 180921+0909.1 V839 Oph. Initial values: $q = 0.305$ and $i = 80.19°$.

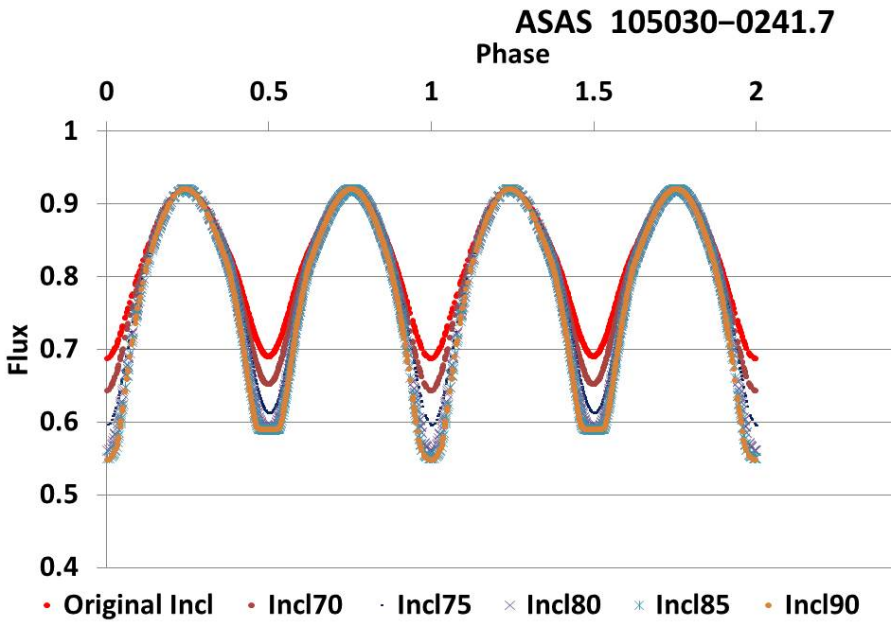

Figure A.20: DS31 = ASAS 105030–0241.7 = VY Sex. Initial values: $q = 0.313$ and $i = 65.53°$.

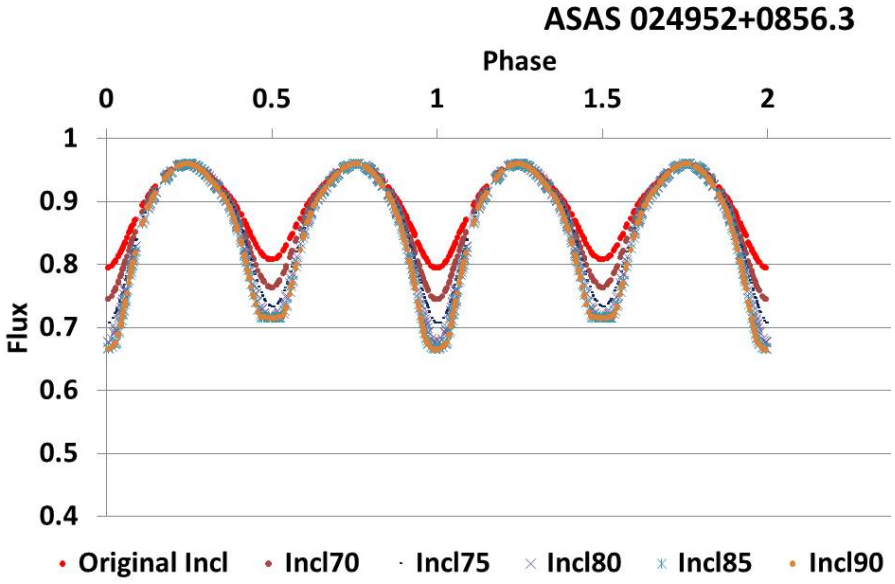

Figure A.21: DS7 = ASAS 024952+0856.3 = EE Cet. Initial values: $q = 0.315$ and $i = 63.50°$.

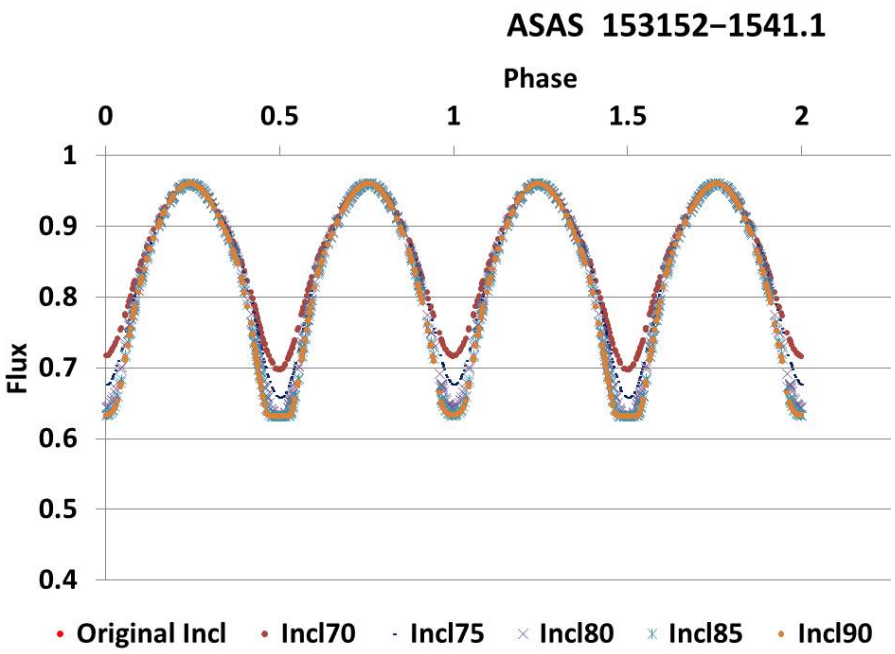

Figure A.22: DS44 = ASAS 153152–1541.1 = VZ Lib. Initial values: $q = 0.33$ and $i = 90.35°$.

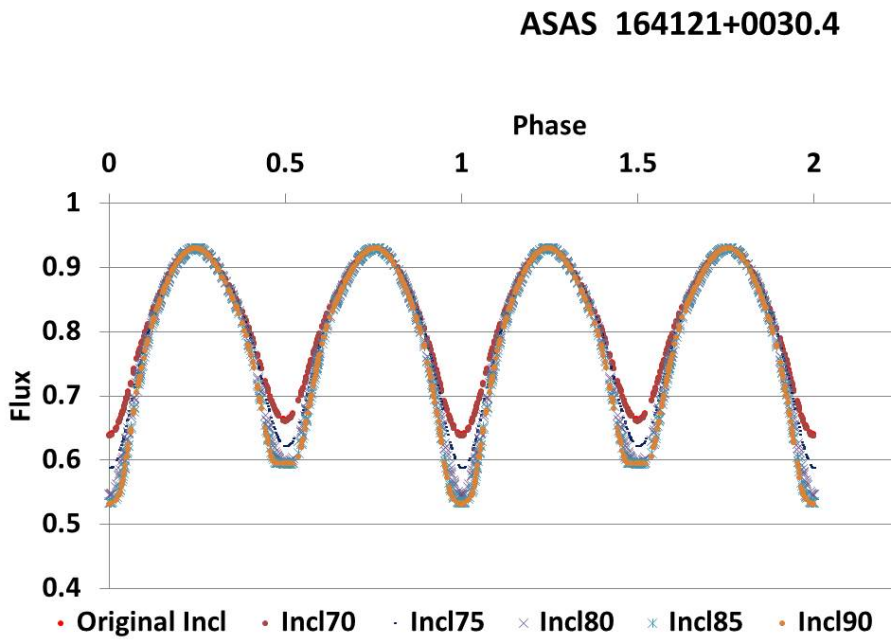

Figure A.23: DS46 = ASAS 164121+0030.4 = V502 Oph. Initial values: $q = 0.335$ and $i = 69.77°$.

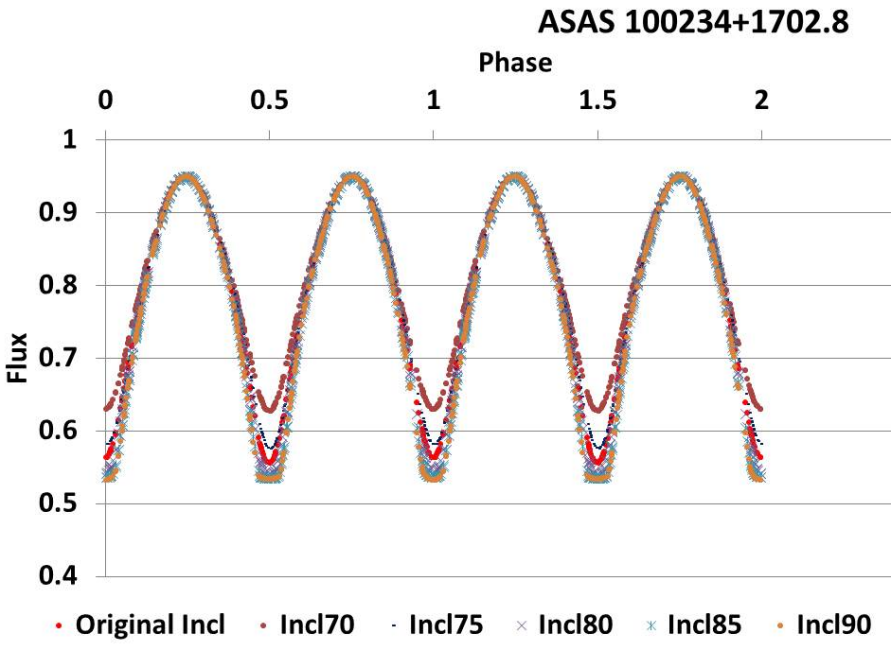

Figure A.24: DS27 = ASAS 100234+1702.8 = XZ Leo. Initial values: $q = 0.348$ and $i = 77.16°$.

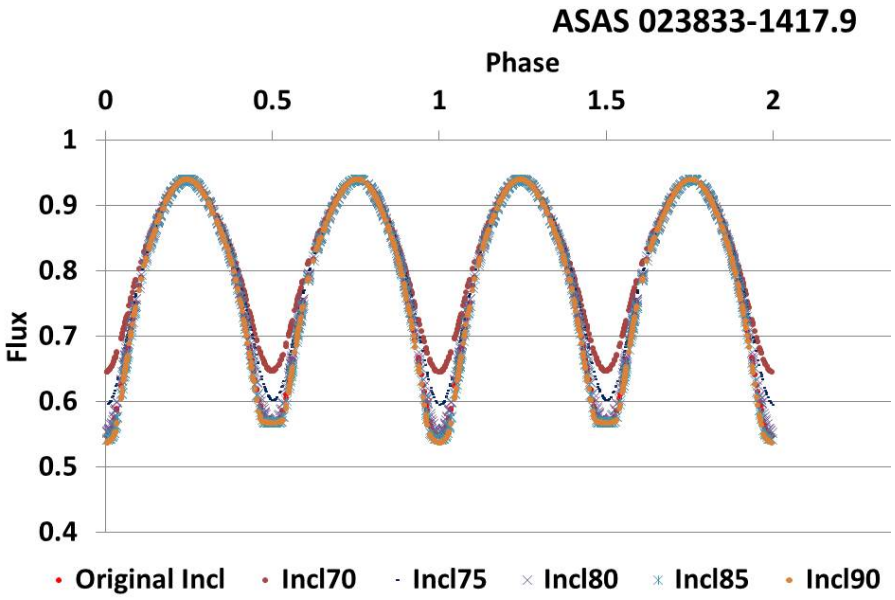

Figure A.25: DS6 = ASAS 023833–1417.9 = DY Cet. Initial values: $q = 0.356$ and $i = 82.48°$.

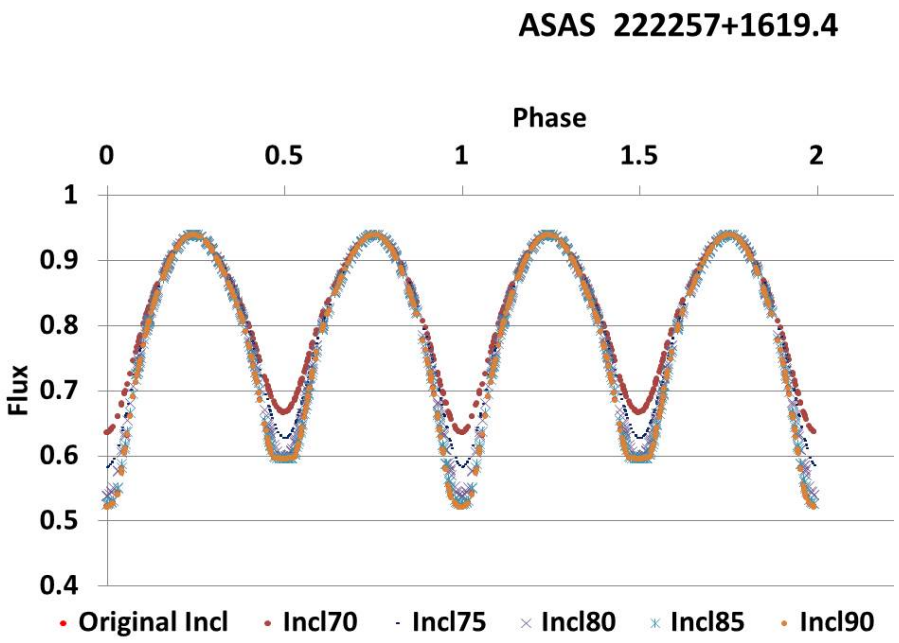

Figure A.26: DS59 = ASAS 222257+1619.4 = BB Peg. Initial values: $q = 0.360$ and $i = 87.96°$.

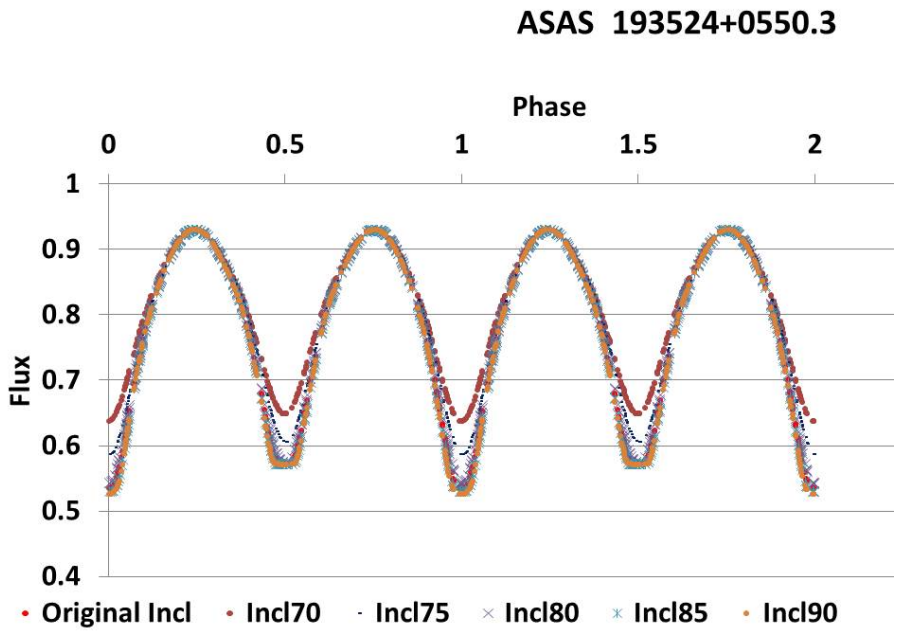

Figure A.27: DS54 = ASAS 193524+0550.3 = V417 Aql. Initial values: $q = 0.362$ and $i = 82.47°$.

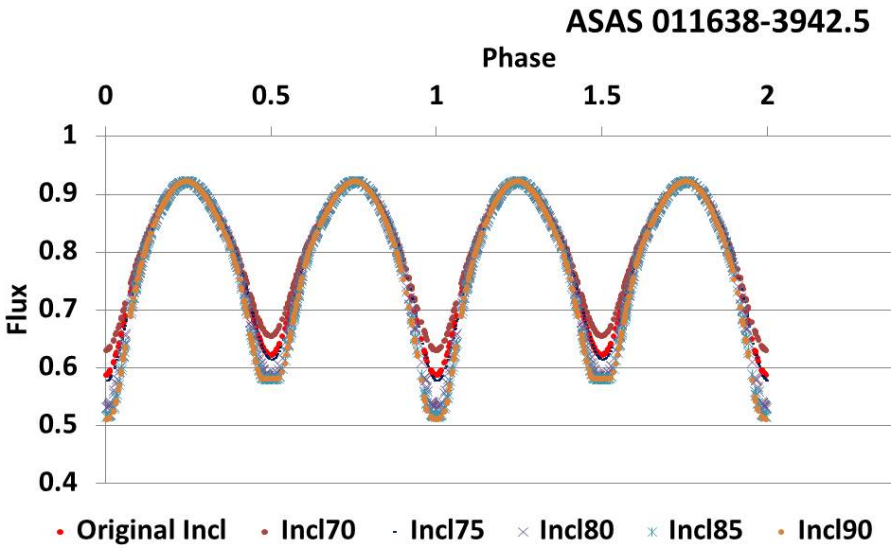

Figure A.28: DS2 = ASAS 011638–3942.5 = AD Phe. Initial values: $q = 0.370$ and $i = 74.00°$.

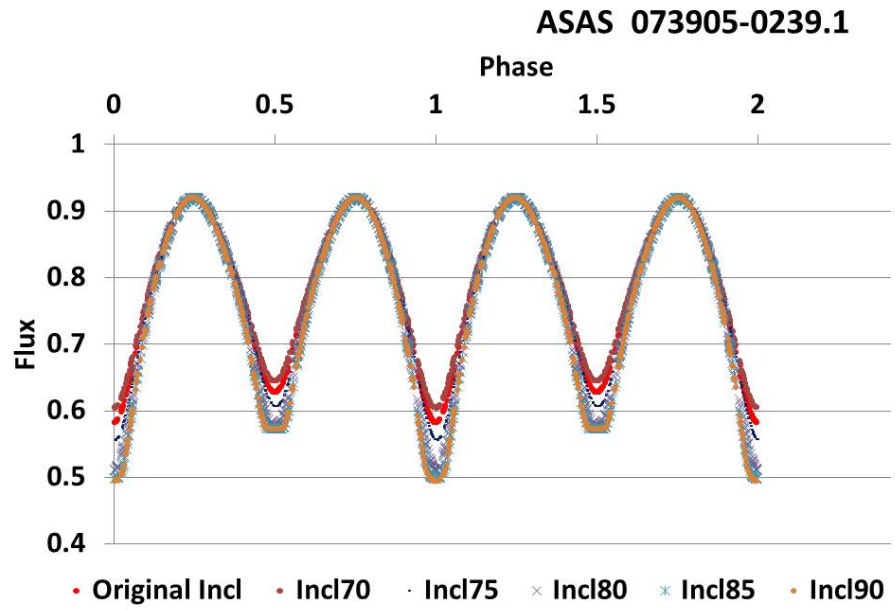

Figure A.29: DS23 = ASAS 073905–0239.1 = V868 Mon. Initial values: $q = 0.373$ and $i = 72.14°$.

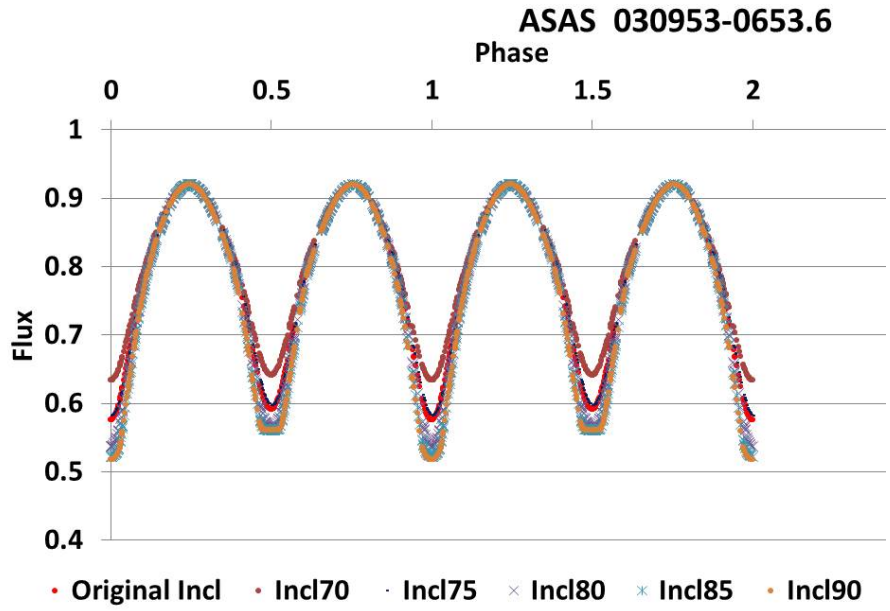

Figure A.30: DS9 = ASAS 030953–0653.6 UX Eri. Initial values: $q = 0.373$ and $i = 75.70°$.

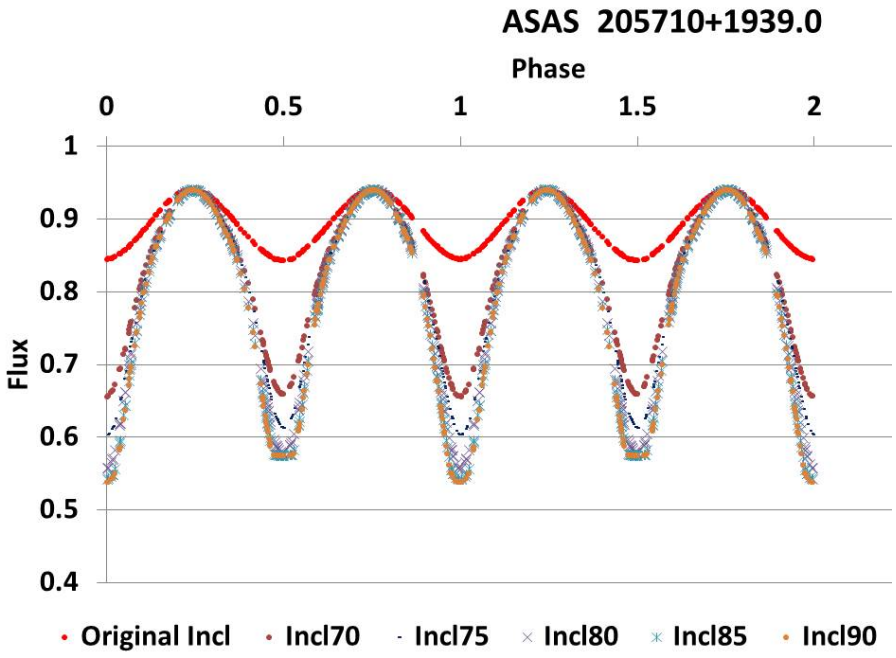

Figure A.31: DS58 = ASAS 205710+1939.0 = LS Del. Initial values: $q = 0.375$ and $i = 45.25°$.

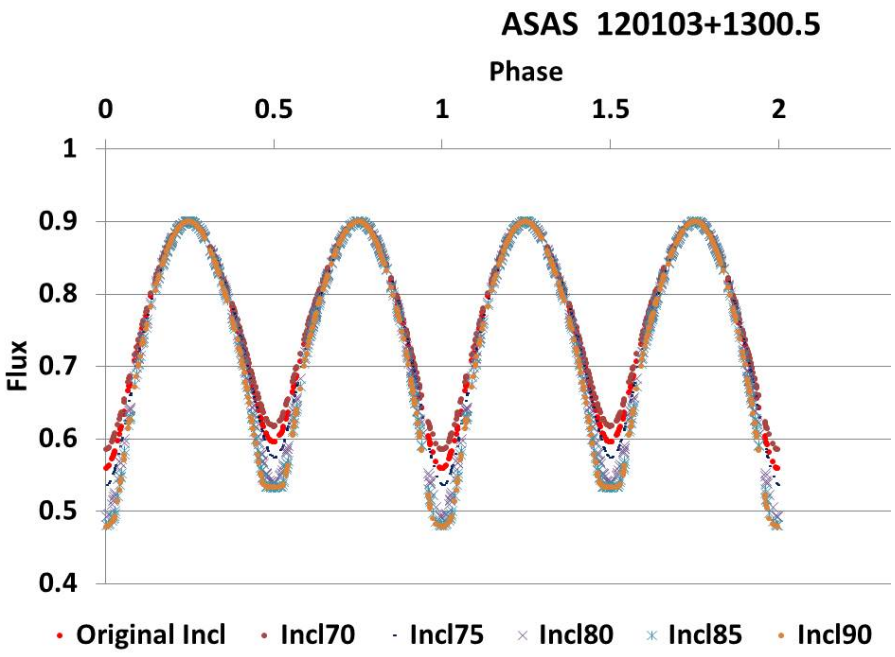

Figure A.32: DS34 = ASAS 120103+1300.5 = AG Vir. Initial values: $q = 0.382$ and $i = 72.54°$.

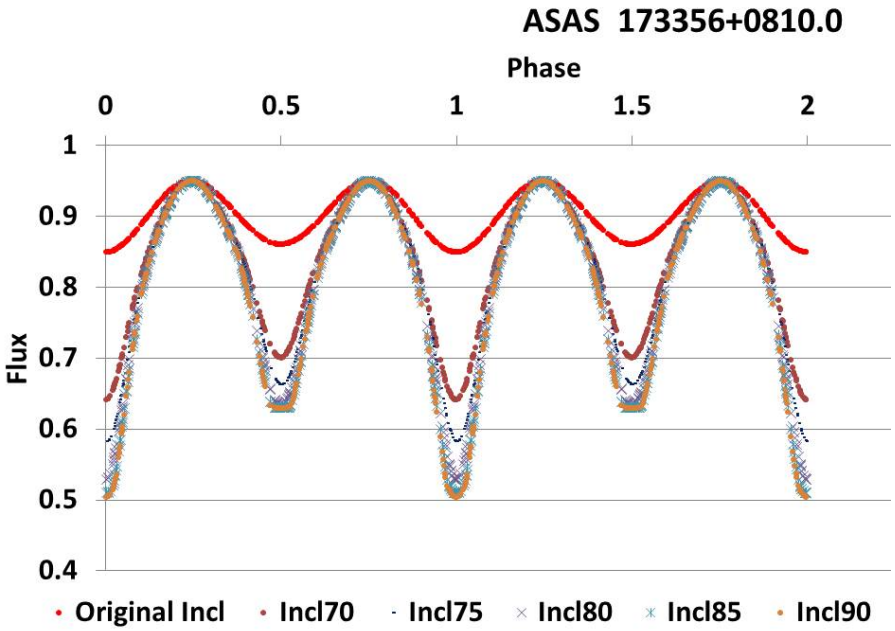

Figure A.33: DS49 = ASAS 173356+0810.0 =V2377 Oph. Initial values: $q = 0.395$ and $i = 44.06°$.

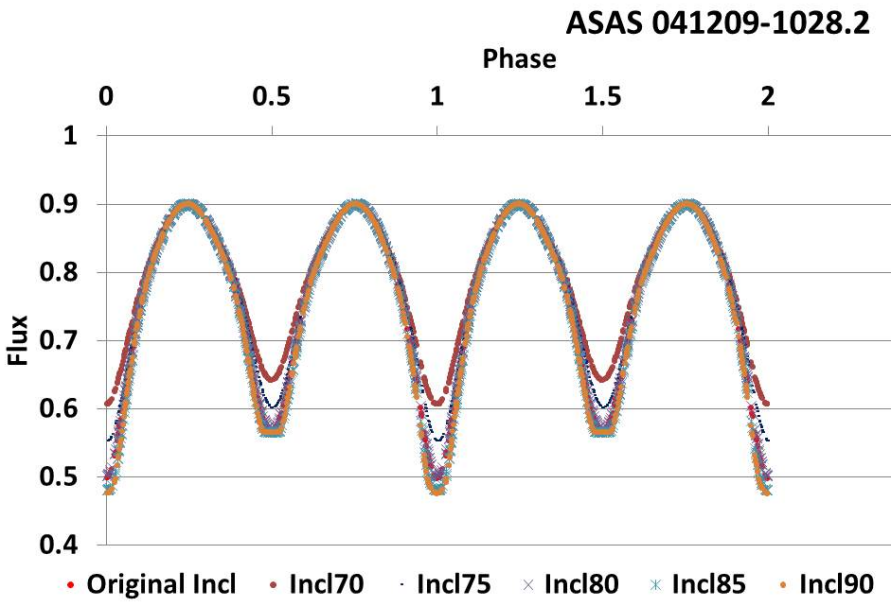

Figure A.34: DS14 = ASAS 041209–1028.2 =YY Eri. Initial values: $q = 0.401$ and $i = 80.44°$.

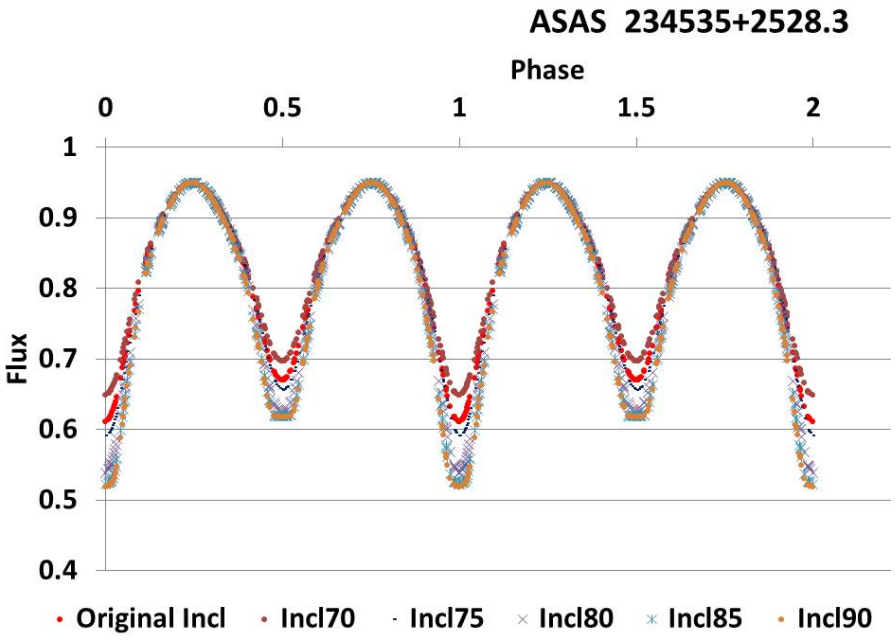

Figure A.35: DS61 = ASAS 234535+2528.3 =V357 Peg. Initial values: $q = 0.401$ and $i = 73.23°$.

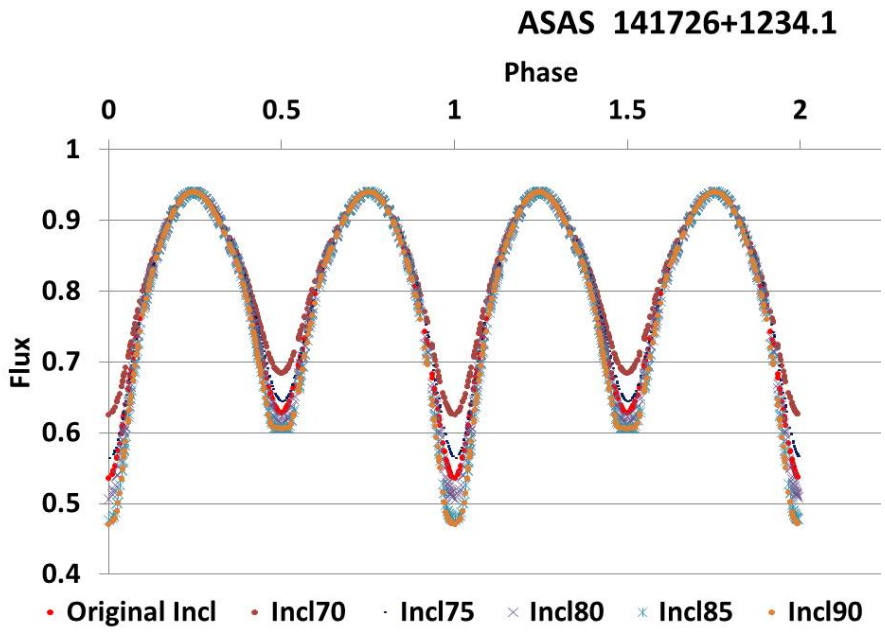

Figure A.36: DS39 = ASAS 141726+1234.1 = VW Boo. Initial values: $q = 0.428$ and $i = 77.29°$.

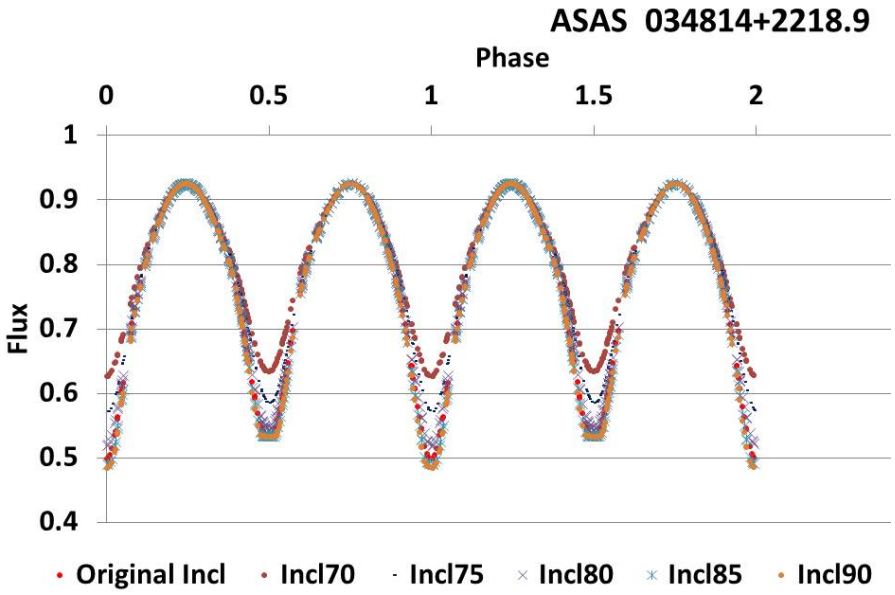

Figure A.37: DS11 = ASAS 034814+2218.9 = EQ Tau. Initial values: $q = 0.442$ and $i = 82.33°$.

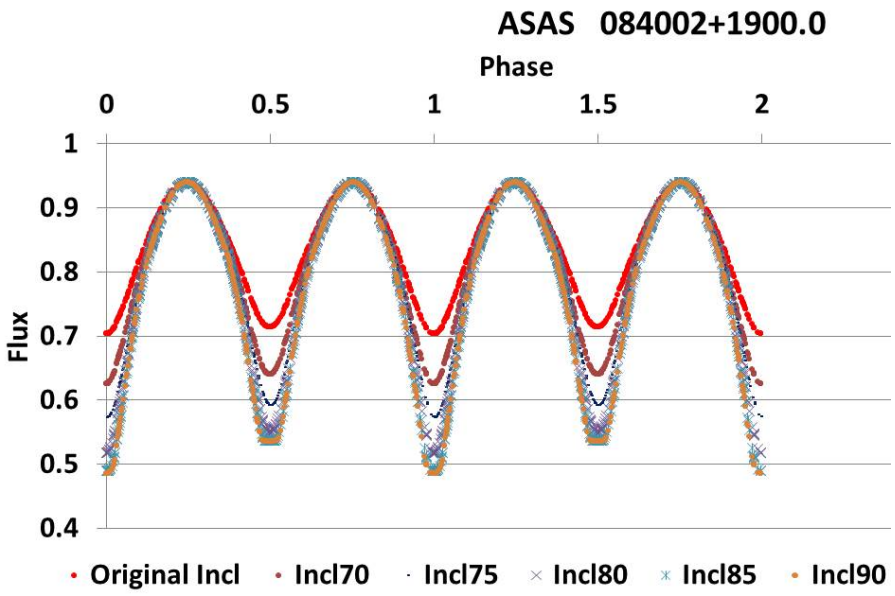

Figure A.38: DS24 = ASAS 084002+1900.0 = TX Cnc. Initial values: $q = 0.455$ and $i = 62.19°$.

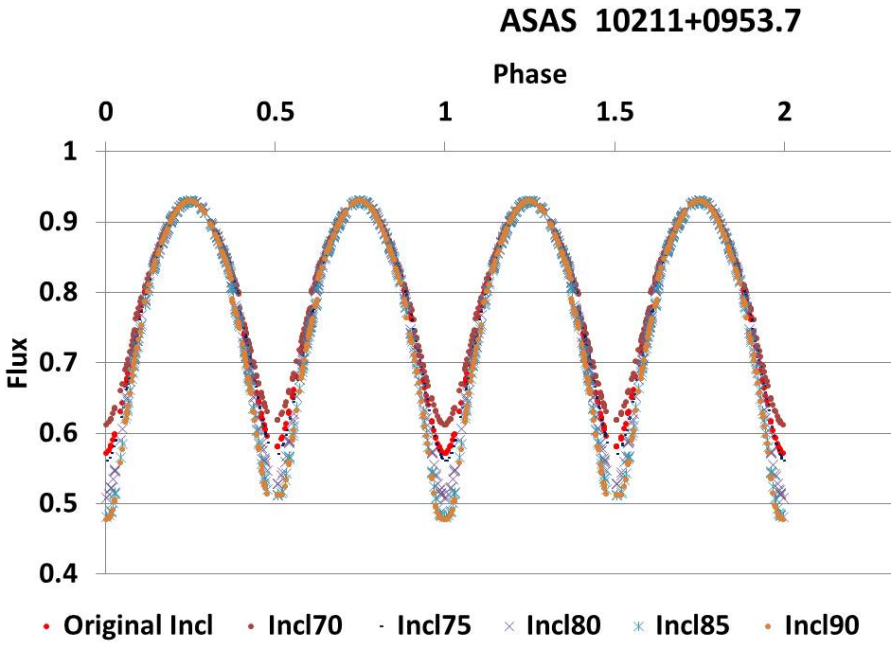

Figure A.39: DS32 = ASAS 10211+0953.7 = AM Leo. Initial values: $q = 0.459$ and $i = 73.85°$.

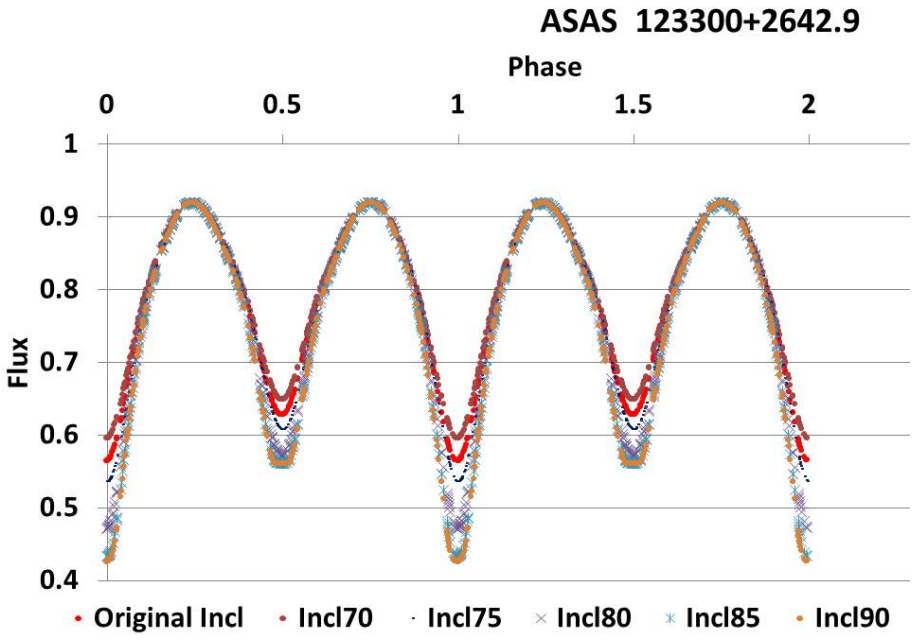

Figure A.40: DS36 = ASAS 123300+2642.9 = RW Com. Initial values: $q = 0.471$ and $i = 72.43°$.

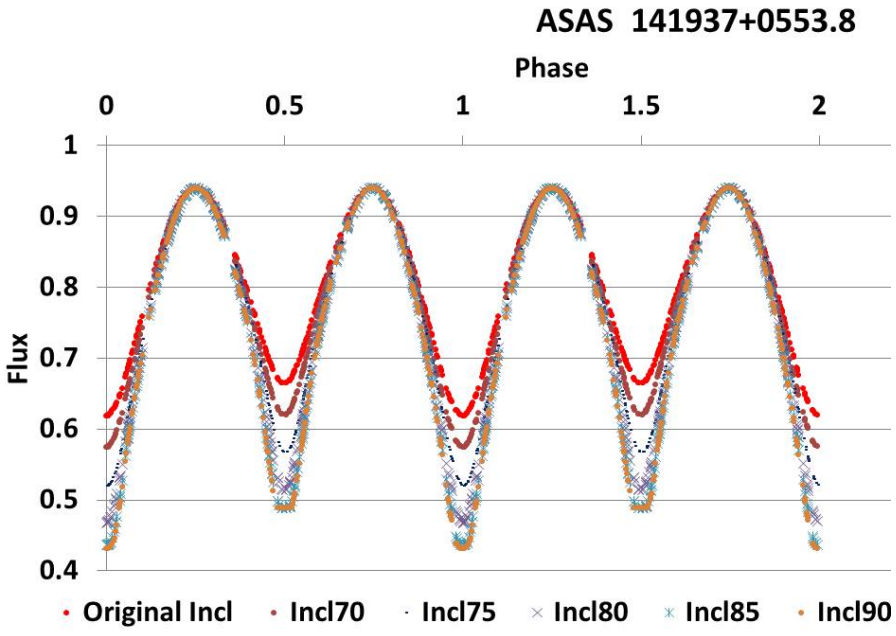

Figure A.41: DS40 = ASAS 141937+0553.8 = NN Vir. Initial values: $q = 0.491$ and $i = 65.52°$.

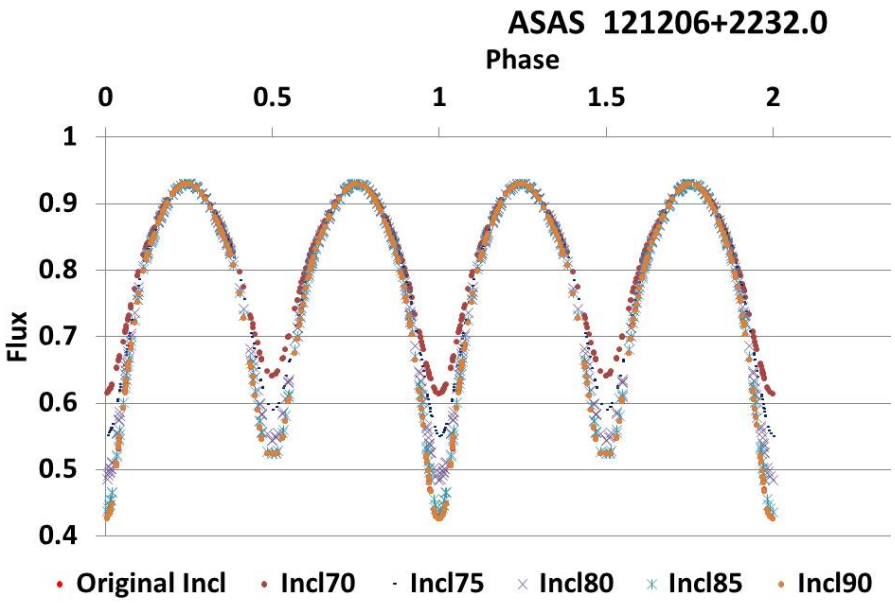

Figure A.42: DS35 = ASAS 121206+2232.0 = CC Com. Initial values: $q = 0.527$ and $i = 90.58°$.

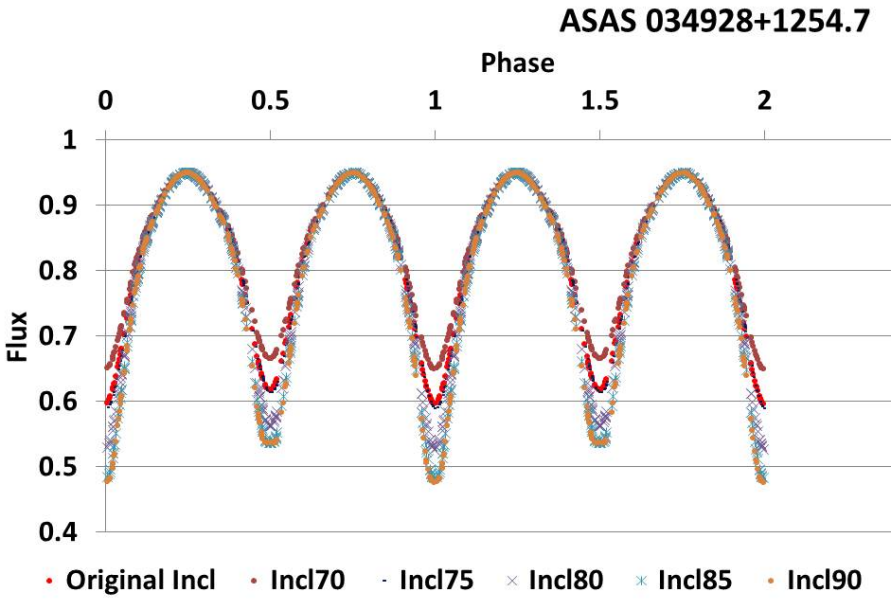

Figure A.43: DS12 = ASAS 034928+1254.7 =V1128 Tau. Initial values: $q = 0.534$ and $i = 74.50°$.

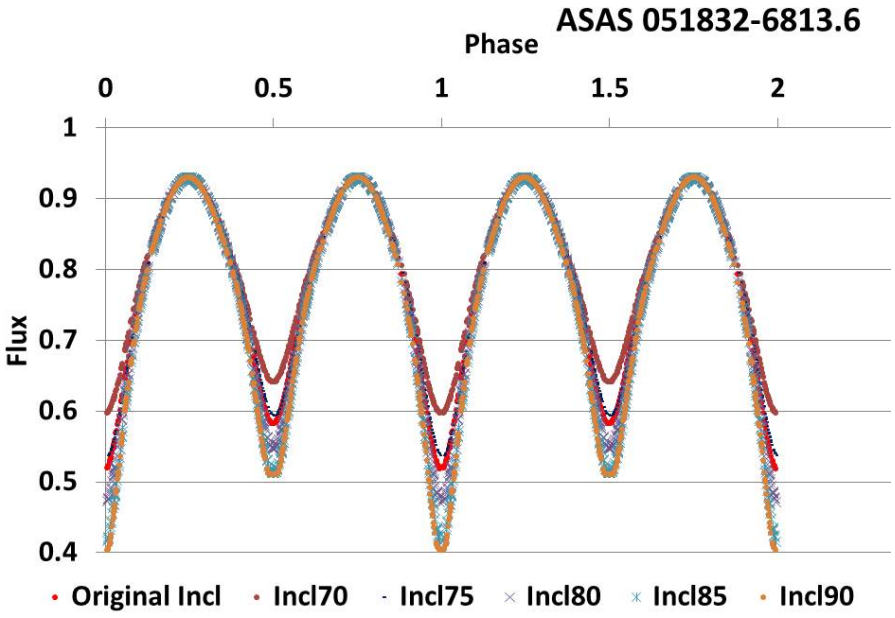

Figure A.44: DS17 = ASAS 051832–6813.6 = RW Dor. Initial values: $q = 0.63$ and $i = 76.32°$.

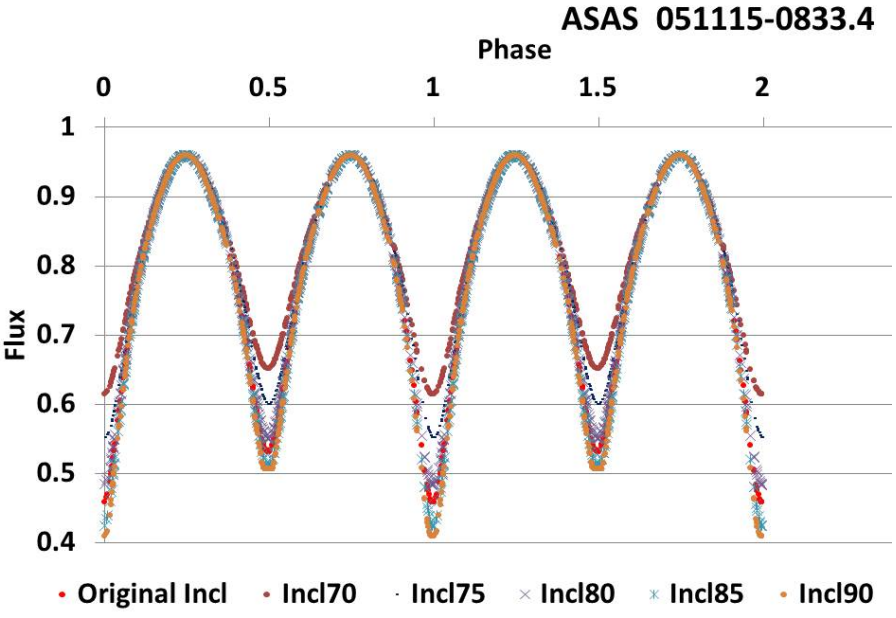

Figure A.45: DS16 = ASAS 051115–0833.4 =ER Ori. Initial values: $q = 0.656$ and $i = 82.08°$.

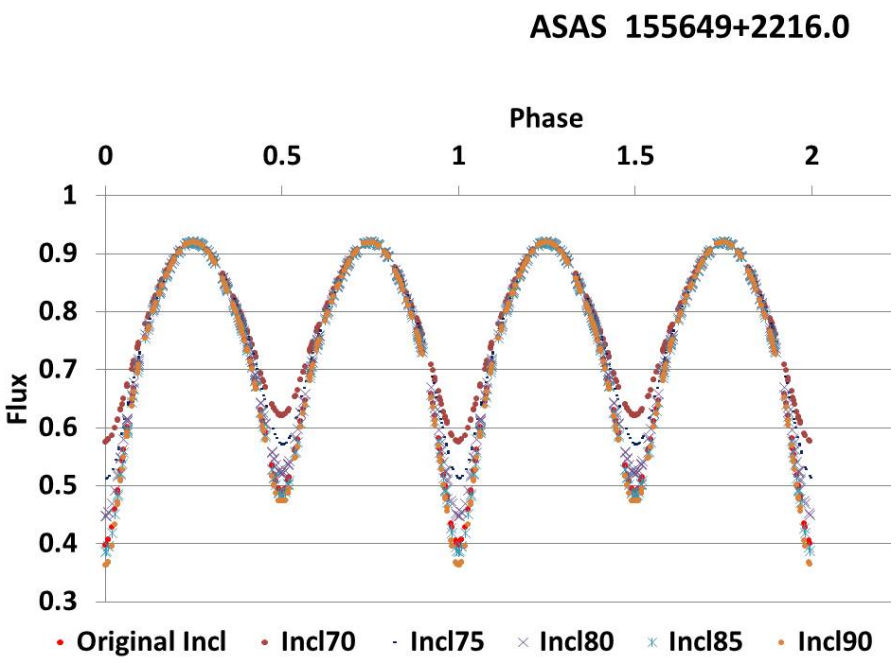

Figure A.46: DS45 = ASAS 155649+2216.0 =AU Ser. Initial values: $q = 0.709$ and $i = 83.85°$.

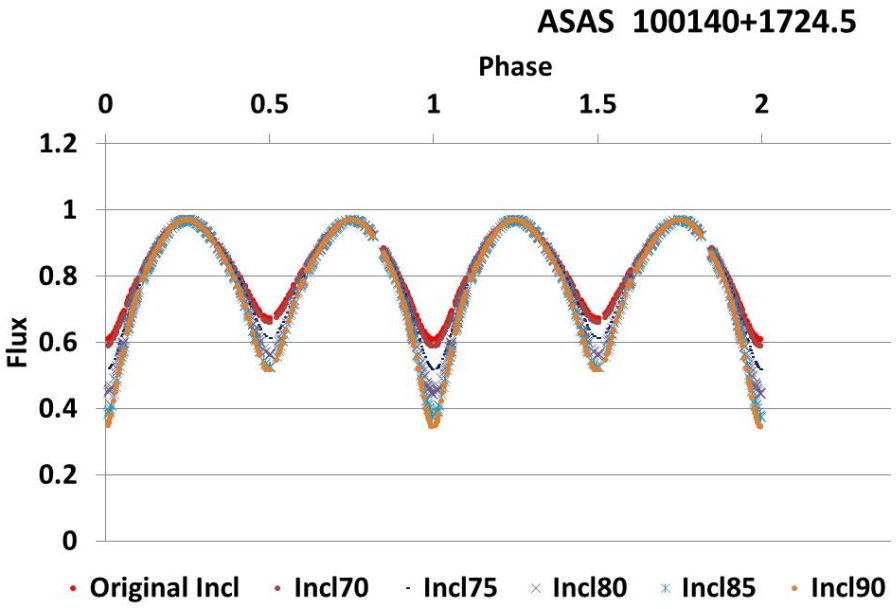

Figure A.47: DS26 = ASAS 100140+1724.5 =XY Leo. Initial values: $q = 0.729$ and $i = 68.63°$.

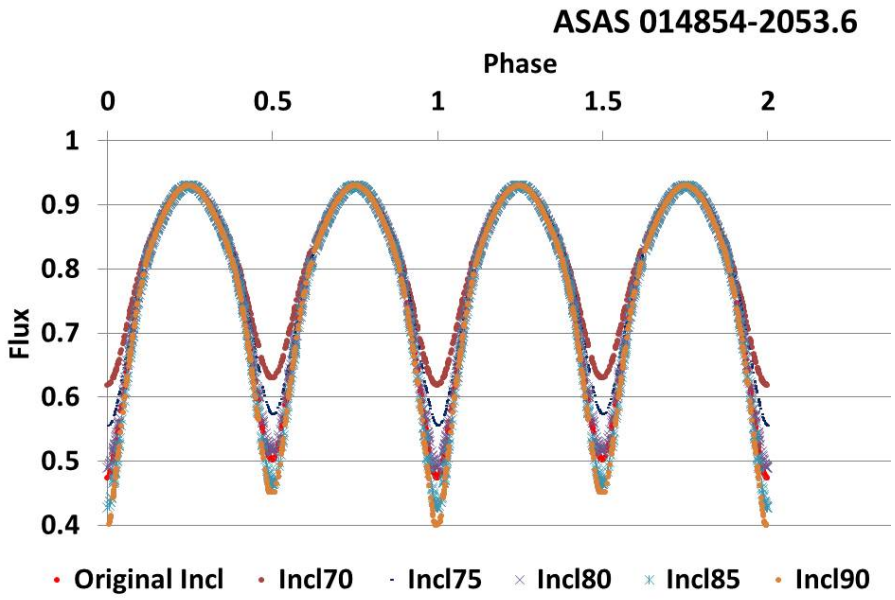

Figure A.48: DS5 = ASAS 014854–2053.6 =TW Cet. Initial values: $q = 0.75$ and $i = 81.18°$.

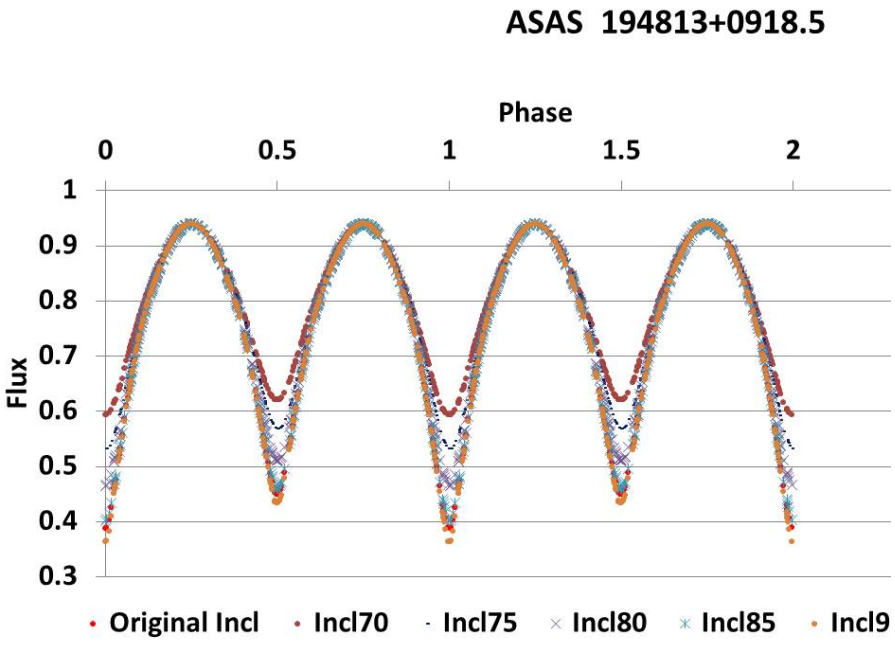

Figure A.49: DS55 = ASAS 194813+0918.5 = OO Aql. Initial values: $q = 0.846$ and $i = 93.81°$.

Bibliography

ASAS 2005, http://www.astrouw.edu.pl/asas/?page=acvs

Abrami A., 1959, Mem. Soc. Astron. Italiana, 30, 303

Albayrak B., Selam S. O., Ak T., Elmasli A., Özavci İ., 2005, Astronomische Nachrichten, 326, 122

Applegate J. H., 1992, ApJ, 385, 621

Avvakumova E. A., Malkov O. Y., 2014, MNRAS, 444, 1982

B.R.N.O. 2020, http://var2.astro.cz/ocgate/index.php?lang=en

Barden S. C., 1987, ApJ, 317, 333

Bell S. A., Rainger P. P., Hilditch R. W., 1990, MNRAS, 247, 632

Binnendijk L., 1960, Properties of double stars; a survey of parallaxes and orbits.. University of Pennsylvania Press

Binnendijk L., 1962, AJ, 67, 86

Binnendijk L., 1969a, AJ, 74, 1024

Binnendijk L., 1969b, AJ, 74, 1031

Binnendijk L., 1970, Vistas in Astronomy, 12, 217

Bonnardeau M., 2009, Journal of the American Association of Variable Star Observers (JAAVSO), 37, 137

Bowers R. L., Deeming T., 1984, Astrophysics. Vol. I: Stars. Vol. II: Interstellar matter and galaxies.. Jones and Bartlett

Bradstreet D. H., Steelman D. P., 2002, in American Astronomical Society Meeting Abstracts. p. 75.02

Brancewicz H. K., Dworak T. Z., 1980, Acta Astron., 30, 501

Carney B. W., Latham D. W., Laird J. B., Aguilar L. A., 1994, AJ, 107, 2240

Claria J. J., Lapasset E., 1981, Information Bulletin on Variable Stars, 2035, 1

Cristescu C., Oprescu G., Suran M. D., 1979, Information Bulletin on Variable Stars, 1688, 1

Csizmadia S., Klagyivik P., 2004, A&A, 426, 1001

D'Angelo C., van Kerkwijk M., Rucinski S. M., 2006, AJ, 132, 650

Deb S., Singh H. P., 2011, MNRAS, 412, 1787

Dryomova G. N., Svechnikov M. A., 2006, Astrophysics, 49, 358

Duerbeck H. W., Rucinski S. M., 2007, AJ, 133, 169

Dugan 1933, Astronomische Nachrichten, 247, 357

Eaton J. A., 1983, ApJ, 268, 800

Eggleton P. P., 1983, ApJ, 268, 368

Eggleton P. P., Kiseleva-Eggleton L., 2001, ApJ, 562, 1012

GCVS 2020, `http://www.sai.msu.su/gcvs/gcvs/iii/vartype.txt`

Gazeas K., Stępień K., 2008, MNRAS, 390, 1577

Gazeas K. D., et al., 2005, Acta Astron., 55, 123

Gazeas K. D., Niarchos P. G., Zola S., Kreiner J. M., Rucinski S. M., 2006, Acta Astron., 56, 127

Guthnick P., Prager R., 1928, Astronomische Nachrichten, 233, 35

Guthnick P., Prager R., 1929, Astronomische Nachrichten, 237, 169

Hambálek Ľ., Pribulla T., 2013, Contributions of the Astronomical Observatory Skalnate Pleso, 43, 27

Hilditch R. W., 1981, MNRAS, 196, 305

Hilditch R. W., 2001, An Introduction to Close Binary Stars. Cambridge

Hill G., Hilditch R. W., Younger F., Fisher W. A., 1975, MmRAS, 79, 131

Hiller M. E., Osborn W., Terrell D., 2004, PASP, 116, 337

Hiltner W. A., Iriarte B., Johnson H. L., 1958, ApJ, 127, 539

Hobart M. A., Peña J. H., de La Cruz C., 1998, Ap&SS, 260, 375

Hoffmann M., Hopp U., 1982, Ap&SS, 83, 391

Hoffmeister C., 1929, Astronomische Nachrichten, 236, 233

Hoffmeister C., 1933, Astronomische Nachrichten, 247, 281

Hoffmeister C., 1934, Astronomische Nachrichten, 253, 195

Houk N., Smith-Moore M., 1988, Michigan Catalogue of Two-dimensional Spectral Types for the HD Stars. Volume 4, Declinations -26°.0 to -12°.0.

Hrivnak B. J., 1985, ApJ, 290, 696

Hrivnak B. J., Milone E. F., Hill G., Fisher W. A., 1984, ApJ, 285, 683

Hutchings J. B., Hill G., 1973, ApJ, 179, 539

Kalimeris A., Rovithis-Livaniou H., Rovithis P., 1994a, A&A, 282, 775

Kalimeris A., Rovithis-Livaniou H., Rovithis P., Oprescu G., Dumitrescu A., Suran M. D., 1994b, A&A, 291, 765

Karami K., Mohebi R., 2007, Chinese J. Astron. Astrophys., 7, 558

Kazarovets E. V., Samus N. N., Durlevich O. V., Frolov M. S., Antipin S. V., Kireeva N. N., Pastukhova E. N., 1999, Information Bulletin on Variable Stars, 4659, 1

Kim C.-H., Jeong J. H., Demircan O., Muyesseroglu Z., Budding E., 1997, AJ, 114, 2753

Kim C.-H., Lee J. W., Kim H.-I., Kyung J.-M., Koch R. H., 2003, AJ, 126, 1555

Kopal Z., 1955, Annales d'Astrophysique, 18, 379

Kopal Z., 1959, Close binary systems. Wiley New York

Kopff E., 1943, Astronomische Nachrichten, 274, 69

Koppelman M. D., West D., Price A., 2002, Information Bulletin on Variable Stars, 5327, 1

Kreiner J., 2004a, Up-to-date linear elements of eclipsing binaries, `http://www.as.up.krakow.pl/minicalc/LEOXY.HTM`

Kreiner J. M., 2004b, Acta Astron., 54, 207

Kuiper G. P., 1941, ApJ, 93, 133

Lame'E M. M., Javanmardi B., Riazi N., 2010, Journal of Astrophysics and Astronomy, 31, 97

Lanza A. F., Rodonò M., 1999, A&A, 349, 887

Lasala-Garcia A., 2001, Information Bulletin on Variable Stars, 5075, 1

Li L., Zhang F., Han Z., 2002, PASJ, 54, 73

Li L., Zhang F., Han Z., Jiang D., Jiang T., 2008, MNRAS, 387, 97

Liao W. P., Qian S. B., Sarotsakulchai T., 2019, AJ, 157, 207

Liu Q.-Y., Yang Y.-L., 2003, Chinese J. Astron. Astrophys., 3, 142

Liu L., Qian S. B., Xiong X., 2018, MNRAS, 474, 5199

Lohr M. E., Norton A. J., Payne S. G., West R. G., Wheatley P. J., 2015, A&A, 578, A136

Lu W., Rucinski S. M., 1999, AJ, 118, 515

Lu W., Rucinski S. M., Ogłoza W., 2001, AJ, 122, 402

Lucy L. B., 1967, ZAp, 65, 89

Lucy L. B., 1968a, ApJ, 151, 1123

Lucy L. B., 1968b, ApJ, 153, 877

Lucy L. B., 1976, ApJ, 205, 208

Lucy L. B., Wilson R. E., 1979, ApJ, 231, 502

Maceroni C., van't Veer F., 1996, A&A, 311, 523

McLean B. J., 1981, MNRAS, 195, 931

Mochnacki S. W., 1972, in Bulletin of the American Astronomical Society. p. 399

Muller G., Kempf P., 1903, ApJ, 17, 201

Nelson R. H., Terrell D., Milone E. F., 2014, New A Rev., 59, 1

Nelson R. H., Terrell D., Milone E. F., 2016, New A Rev., 70, 1

O'Connell D. J. K., 1951, Publications of the Riverview College Observatory, 2, 85

Ogloza W., 1997, International Amateur-Professional Photoelectric Photometry Communications, 67, 51

Paczyński B., Szczygieł D. M., Pilecki B., Pojmański G., 2006, MNRAS, 368, 1311

Parkhurst J. A., Jordan F. C., 1906, ApJ, 23, 79

Percy J. R., 2007, Understanding Variable Stars. Cambridge

Podsiadlowski P., ed. 2001, Evolution of Binary and Multiple Star Systems; A Meeting in Celebration of Peter Eggleton's 60th Birthday Astronomical Society of the Pacific Conference Series Vol. 229

Pojmanski G., Geyer E. H., 1990, Acta Astron., 40, 245

Pojmanski G., Maciejewski G., 2004, Acta Astron., 54, 153

Pollacco D. L., et al., 2006, PASP, 118, 1407

Pribulla T., Rucinski S. M., 2006, AJ, 131, 2986

Pribulla T., Vanko M., 2002, Contributions of the Astronomical Observatory Skalnate Pleso, 32, 79

Pribulla T., Kreiner J. M., Tremko J., 2003, Contributions of the Astronomical Observatory Skalnate Pleso, 33, 38

Pribulla T., et al., 2006, AJ, 132, 769

Pribulla T., Rucinski S. M., Conidis G., DeBond H., Thomson J. R., Gazeas K., Ogłoza W., 2007a, AJ, 133, 1977

Pribulla T., Rucinski S. M., Conidis G., DeBond H., Thomson J. R., Gazeas K., Ogłoza W., 2007b, AJ, 133, 1977

Pribulla T., et al., 2009, AJ, 137, 3655

Prša A., 2011, PHOEBE Scientific Reference, PHOEBE Version 3.0. Villanova University, `http://phoebe-project.org/1.0/docs`

Qian S., 2001a, MNRAS, 328, 635

Qian S., 2001b, MNRAS, 328, 914

Qian S., Liu Q., 2000, A&A, 355, 171

Qian S.-B., He J., Xiang F., Ding X., Boonrucksar S., 2005, AJ, 129, 1686

Qian S. B., Liao W. P., Liu L., Yuan J. Z., He J. J., Zhu L. Y., Dai Z. B., Zhang J., 2008, New A, 13, 98

Robertson J. A., Eggleton P. P., 1977, MNRAS, 179, 359

Rovithis P., Rovithis-Livaniou H., 1986, A&A, 155, 46

Rovithis-Livaniou H., 2006, Publications de l'Observatoire Astronomique de Beograd, 80, 107

Rovithis-Livaniou H., Kalimeris A., Rovithis P., 2003, in Sterken C., ed., Astronomical Society of the Pacific Conference Series Vol. 292, Interplay of Periodic, Cyclic and Stochastic Variability in Selected Areas of the H-R Diagram. p. 163

Ruciński S. M., 1969, Acta Astron., 19, 245

Rucinski S. M., 1993, PASP, 105, 1433

Rucinski S. M., 1997, AJ, 113, 1112

Rucinski S. M., Duerbeck H. W., 1997, PASP, 109, 1340

Rucinski S. M., Lu W., 1999, AJ, 118, 2451

Rucinski S. M., Maceroni C., 2001, AJ, 121, 254

Rucinski S. M., Lu W. X., Shi J., 1993, AJ, 106, 1174

Rucinski S. M., Lu W., Mochnacki S. W., 2000, AJ, 120, 1133

Rucinski S. M., Lu W., Capobianco C. C., Mochnacki S. W., Blake R. M., Thomson J. R., Ogłoza W., Stachowski G., 2002, AJ, 124, 1738

Rucinski S. M., et al., 2003, AJ, 125, 3258

Russell H. N., 1912, ApJ, 36, 133

Sanford R. F., 1934, ApJ, 79, 89

Sarotsakulchai T., et al., 2018, AJ, 156, 199

Shu F., 1982, The Physical Universe An Introduction to Astronomy. University Science Books

Smith A. M. S., WASP Consortium 2014, Contributions of the Astronomical Observatory Skalnate Pleso, 43, 500

Smits D. P., Skelton P. L., 2019, New A, 67, 53

Sterken C., 2005, in Sterken C., ed., Astronomical Society of the Pacific Conference Series Vol. 335, The Light-Time Effect in Astrophysics: Causes and cures of the O-C diagram. p. 3

Strohmeier W., Knigge R., 1961, Astronomische Nachrichten, 286, 133

Struve O., Horak H. G., 1950, ApJ, 112, 178

SuperWASP 2018, `http://wasp.warwick.ac.uk/vsi2/vsi2.php?`

Szalai T., Kiss L. L., Mészáros S., Vinkó J., Csizmadia S., 2007, A&A, 465, 943

Tsesevich B. P., 1954, Izvestia Astronomical Observatory, 4, 196

Vanko M., Pribulla T., Chochol D., Parimucha S., Kim C. H., Lee J. W., Han J. Y., 2001, Contributions of the Astronomical Observatory Skalnate Pleso, 31, 129

Walker R. L., 1993, AJ, 106, 2051

Watson C. A., Dhillon V. S., 2004, MNRAS, 351, 110

Webbink R. F., 2003, in Turcotte S., Keller S. C., Cavallo R. M., eds, Astronomical Society of the Pacific Conference Series Vol. 293, 3D Stellar Evolution. p. 76 (`arXiv:astro-ph/0304420`)

Whelan J., Mochnacki S. W., Worden S. P., 1974, MNRAS, 168, 31

Wils P., Dvorak S. W., 2003, Information Bulletin on Variable Stars, 5425, 1

Wilson R. E., 1994, PASP, 106, 921

Wolf M., Molík P., Hornoch K., Šarounová L., 2000, A&AS, 147, 243

Worley C. E., Eggen O. J., 1956, PASP, 68, 452

Yakut K., Eggleton P. P., 2005, ApJ, 629, 1055

Yakut K., İbanoğlu C., Kalomeni B., Değirmenci Ö. L., 2003, A&A, 401, 1095

Yang Y., Liu Q., 1999, A&AS, 136, 139

Yıldız M., 2014, MNRAS, 437, 185

Yıldız M., Doğan T., 2013, MNRAS, 430, 2029

Yu Y.-X., Xiang F.-Y., Hu K., 2016, PASP, 128, 044202

Yue Q., Zhang L.-Y., Han X.-M. L., Lu H.-P., Long L., Yan Y., 2019, Research in Astronomy and Astrophysics, 19, 097

Zhang J.-T., Zhang R.-X., Zhai D.-S., Li Q.-S., Jin T.-L., 1989, Information Bulletin on Variable Stars, 3302, 1

Zhang X.-D., Qian S.-B., Liao W.-P., 2020, MNRAS, 492, 4112

Zhou X., Qian S., He J., Zhang J., Jiag L., 2015, PASJ, 67, 98

Zola S., et al., 2004, Acta Astron., 54, 299

Çalışkan Ş., et al., 2014, AJ, 148, 126

van Hamme W., 1982, A&A, 105, 389

van Hamme W., 1993, AJ, 106, 2096

van't Veer F., Maceroni C., 1989, A&A, 220, 128

von Zeipel H., 1924, MNRAS, 84, 665